Synthesis of dispersants to generate fillers for composites designed to have an enhanced echogenic response

Amy Stimpson, MSci

Thesis submitted to the University of Nottingham for the degree of Doctor of Philosophy

May 2020



University of Nottingham
UK | CHINA | MALAYSIA

Declaration

Except where specific reference has been made to other sources, the worked presented in this thesis is the original work of the author. It has not been submitted, in whole, or in part, for any other degree or professional qualification.

Signed……Date……

Amy Stimpson

Acknowledgements

Firstly, I would like to thank my supervisor Prof. Derek Irvine for giving me the opportunity to carry out this PhD project. His endless patience and help throughout the past few years has been invaluable and I am grateful for all the support. Who would have known back in 2009 when I first met Derek at my UoN undergrad admission interview that I would still be here 10 years later? Special thanks also go to my special advisor Dr Abby Whittington for project supervision, especially during my Summers in Virginia, and allowing me to be a part of this project, in addition to Jerry Contreras and the IRES programme for funding. Thanks must also go to secondary supervisors at UoN; Prof. Steve Howdle, Prof. Ifty Ahmed and Prof. Ed Lester. Particularly to Steve for allowing me to work in B10 as part of a great research group who made day-to-day life a little more entertaining.

A special mention has to go to Alice Haddleton, Olivia Monaghan & Rachel Atkinson for being the ultimate coffee crew, I mean it when I say I couldn't have got through these last few years without you girls.

Finally, last but by no means least, the biggest thank you goes to my parents for always being my number 1 supporters.

Abstract

Ultrasound (US) imaging was identified as an advantageous imaging modality over the typically used X-ray. Thus, composites comprising of dispersed US-visible contrast agents embedded in a thermoplastic polyurethane matrix were made. To form the composite device, a commercially available material was used as a dispersant for microparticles. These coated phosphate-based glass microspheres were used as ultrasound visible contrast agents, in a medical grade polymer matrix. Ultrasound images of hollow tubes were obtained by Children's National Medical Center (Washington DC, USA), which proved to show promising initial results. Imaging artefacts attributed to poor dispersion were observed, thus optimisation of device focussed on dispersant design. To optimise the dispersion of contrast agent throughout medical devices, bespoke dispersants were designed and synthesised to be more compatible with the matrix polymer. The first technique was to employ a thiol chain transfer agent (CTA) which was a one-pot, high yielding reaction to produce oligomers. The other method was catalytic chain transfer polymerisation (CCTP) followed by post-functionalisation of the vinyl-terminated oligomeric product *via* thiol-ene click chemistry. It was found that carboxylic acid containing thiols were excellent CTAs for monomers detailed.

The synthesis of various iron-α-diimine complexes as potential alternatives to commercially available cobalt-based complexes that are typically used as control agents in catalytic chain transfer polymerisation (CCTP) was carried out. Their efficiency as chain transfer agents was investigated and related to the catalyst generation method, concentration and heating type. Although they did not exhibit high efficiencies as catalytic chain transfer agents under the conditions described, chain transfer behaviour was observed for these complexes. It was noted that molecular

weight and dispersity of polymer products were lower than products obtained from uncontrolled free radical polymerisations. The differential effects of utilising microwave heating (MWH) on the rate and molecular composition of final products obtained compared to when conventionally heating (CH) was applied was also investigated. The differences were found to be related to an increase in the rate of propagation in the case of MWH conditions, which was attributed to the selective heating of particular radical species. Higher molecular weight polymers were obtained from MWH reactions, with the dispersity remaining relatively equivalent to those of the products obtained from analogous CH reactions. This suggests the selective heating of the propagating polymer radical dominated in this CCTP system rather than additional heating of the iron complex. The latter having been proposed as a potential route that electromagnetic waves may have increased the efficiencies of the iron-based catalysts due to their ferromagnetic centre in comparison to the paramagnetic cobalt complexes.

Index of figures

Figure 1-1. Kinetic profiles of different polymerisation mechanisms. 1-2

Figure 1-2. Thermal decomposition of AIBN. 1-4

Figure 1-3. Termination mechanisms a) combination and b) disproportionation for polymerisation of methyl methacrylate (R = CO_2Me). 1-5

Figure 1-4. Polymer structures. 1-7

Figure 1-5. The Trommsdorff-Norrish effect. 1-11

Figure 2-1. Synthetic scheme for ring opening of DDSA with water. 2-4

Figure 2-2. Procedure for the extrusion of composites. 2-6

Figure 2-3. Synthesis of MMA_2 *via* PhCoBF mediated CCTP of MMA. 2-6

Figure 2-4. ^{1}H NMR spectra of MMA_2. 2-7

Figure 2-5. Thiol-ene reaction between MMA_2 and 3MPA. 2-8

Figure 2-6. Synthetic route to ligands [RN=CH-CH=NR] where R = a) 2,6-diisopropylphenyl (DIPP) - L1 and b) 2,4,6-trimethylphenyl (TMP) - L2. 2-9

Figure 3-1. Structures of various phosphates. 3-5

Figure 3-2. Structures of a) DDSA and b) DDSD. 3-10

Figure 3-3. Biphasic suspension test. 3-11

Figure 3-4. Thermogram of DDSD. 3-12

Figure 3-5. Thermogram of P40 microspheres. 3-13

Figure 3-6. Example thermogram for P40-DDSD. 3-14

Figure 3-7. Thermogram of polyurethane. 3-15

Figure 3-8. SEM images of P40 at varying magnification with arrows indicating non spherical particles. 3-16

Figure 3-9. SEM image of P40-DDSD. 3-17

Figure 3-10. Example wide scan XPS spectra of uncoated P40. 3-18

Figure 3-11. Example wide scan spectra of P40-DDSD with peaks assigned to elements. 3-19

Figure 3-12. High-resolution C 1s scan P40-DDSD. 3-21

Figure 3-14. C 1s high-resolution scan P40-DDSD with environments fitted 3-22

Figure 3-13. Structure of DDSD with carbon environments labelled in accordance to Table 3-3. 3-22

Figure 3-15. Backscatter ESEM images of extruded tube samples showing common defects. A – cross section of tube after cryofracture, showing fractured particles. B – inner lumen of tube after blade sectioning, showing shear defects. C – tube sample

after sectioning, showing air pockets in the wall. Data collected by Jerry Contreras (Virginia Tech) and used with permission. 3-25
Figure 3-16. Backscatter ESEM images of optimal extrusion sample. a) - cross section and b) - lengthwise views of sample after cryofracture. Data collected by Jerry Contreras (Virginia Tech) and used with permission. 3-26
Figure 3-17. Sectioning of extruded tubes for analysis. 3-27
Figure 3-18. Example thermogram for extruded PU tube sample. 3-28
Figure 3-19. B-mode ultrasound images of a) commercially available catheter and b) extruded polyurethane tube. 3-30
Figure 3-20. B-Mode US images of tubes with varying wt% of P40 microspheres. a, b, c - 1 wt%. d, e, f – 3 wt%. g, h, i – 5 wt%. 3-31
Figure 3-21. B-mode US images of extruded tubes containing P40-DDSD at a) 1 wt%, b) 5 wt% and c) 10 wt%. 3-33
Figure 4-1. General thiol-ene scheme. 4-2
Figure 4-2. Thiol-ene reaction between MMA_2 and 3MPA. 4-4
Figure 4-5. Structures of thiol CTAs a) 3-mercaptopropionoic acid and b) mercaptosuccinic acid. 4-9
Figure 4-4. Structures of oligomers used as second-generation dispersants. 4-16
Figure 4-5. High resolution C 1s scan P40-(MMA_2-3MPA). 4-19
Figure 4-6. High-resolution C1s scan with components fitted. Red – original spectra, blue – aliphatic component, green – OCH_3 component, black – COOH component. 4-20
Figure 4-7. Structure of MMA_2-3MPA with different carbon environments labelled in accordance with Table 4-14. 4-21

Figure 5-1. Structure of cobalt-porphyrin CCTP catalyst. Axial ligands are not shown in structures as there are a variety of groups available that form active catalysts. ..4-3
Figure 5-2. Structure of cobalt-phthalocyanine. 4-4
Figure 5-3. General structure of cobaloxime CCT agent.[12] 4-5
Figure 5-4. Structure of bis[(difluoroboryl) diphenylglyoximato] cobalt (II) (PhCoBF). 4-6
Figure 5-5. Mechanism of CCTP cycle of MMA mediated by PhCoBF. 4-7
Figure 5-6. Proposed termination schemes of a) methyl acrylate and b) methyl methacrylate.[22] 4-9
Figure 5-7. Comparison of heat dissipation between CH (RHS) and MWH (LHS).[32].4-12
Figure 5-8. The electromagnetic spectrum. 4-13
Figure 5-9. Mechanisms of microwave heating methods: a) dipolar polarisation and b) ionic conduction. 4-14
Figure 5-10. Structures of FeX_2L.....4-18

Index of Tables

Table 2-1. Quantities of reagents used to form FeX_2L complexes. 2-10
Table 3-1. Elemental composition of P40 samples determined by XPS. 3-18
Table 3-2. Elemental composition of P40 and P40-DDSD samples determined by XPS. 3-20
Table 3-3. High-resolution C 1s scan data and comparison with theoretical composition. 3-23
Table 3-4. TGA results of extruded tube samples. 3-28

Table 4-1. Thiol-ene reactions of MMA_2 (3 mmol) and 3MPA (3 mmol) with AIBN (0.6 mmol) in 1,4-dioxane (10 mL) at varying temperatures. 4-4
Table 4-2. Thiol-ene reactions of MMA_2 (3 mmol) and 3MPA (3 mmol) with AIBN (0.6 mmol) in 1,4-dioxane (10 mL) at varying temperatures using microwave heating. ..4-5
Table 4-3. Bulk (no solvent) thiol-ene reactions between MMA2 (11 mmol) and 3MPA (11 mmol) with varying AIBN concentration and reaction time. 4-6
Table 4-4. Thiol-ene reactions between MMA2 (10 mmol) and 3MPA (10 mmol). ..4-7
Table 4-5. Polymerisation of MMA using varying concentrations of 3MPA as CTA. 4-9
Table 4-6. Polymerisation of MMA using varying concentrations of MSA as CTA. 4-10
Table 4-7. Polymerisation of DEGMA using varying concentrations of 3MPA as CTA. 4-11
Table 4-8. Polymerisation of DEGMA using varying concentrations of MSA as CTA. 4-12
Table 4-9. Polymerisation of PEGMA using thiols as CTA. 4-13
Table 4-10. Polymerisation of EGDPEA using varying concentrations of 3MPA as a CTA. 4-14
Table 4-11. Polymerisation of EGDPEMA using varying concentrations of 3MPA as CTA. 4-15
Table 4-12. Overview of second-generation dispersants. 4-17
Table 4-13. Elemental composition of P40-(MMA_2-3MPA) and P40 for comparison determined by XPS. 4-19
Table 4-14. High-resolution C 1s scan data and theoretical composition. 4-21
Table 5-1. Comparison of reduction in molecular weight obtained in PhCoBF mediated polymerisations of MMA. 4-17
Table 5-2. Iron-mediated polymerisation of MMA. 4-19

Table 5-3. Effect of catalyst generation method on polymerisation of MMA with $FeCl_2L2$ as CTA. 4-21

Table 5-4. Effect of catalyst generation method on polymerisation of MMA with $FeCl_2L1$ as CTA. 4-23

Table 5-5. Effect of catalyst generation method on polymerisation of MMA with $FeBr_2L1$ as CTA. 4-23

Table 5-6. Polymerisation of MMA with $FeBr_2L2$ as CTA.....4-25

Table 5-7. Effect of heating method on polymerisation of MMA with $FeBr_2$ based CTAs. 4-27

Table 5-8. Effect of CTA generation method and concentration on polymerisation of MA with $FeBr_2L1$ as CTA. 4-28

Table 5-9. Gel point determination. 4-30

Abbreviations

AIBN	2,2-azobis(isobutyronitrile)
ATRP	Reversible Atom Transfer Radical Polymerisation
CCTP	Catalytic Chain Transfer Polymerisation
CH	Conventional Heating
CIRP	Catalytic Inhibition of Radical Polymerisation
CRP	Controlled Radical Polymerisation
C_S	Chain Transfer Constant
CTA	Chain Transfer Agent
Đ	Dispersity
DDSA	Dodecenylsuccinic anhydride
DDSD	Dodecenylsuccinic diacid
DP	Degree of Polymerisation
FRP	Free Radical Polymerisation

GPC	Gel Permeation Chromatography
MA	Methyl acrylate
MMA	Methyl methacrylate
M_n	Number Average Molecular Weight
M_W	Weight Average Molecular Weight
MWH	Microwave Heating
MWt	Molecular Weight
NMP	Nitroxide Mediated Polymerisation
NMR	Nuclear Magnetic Resonance
PBG	Phosphate Based Glass
PhCoBF	bis-[(difluoroboryl)diphenylglyoximato] cobalt (II)
PMMA	Poly(methyl methacrylate)
PU	Polyurethane
RAFT	Reversible Addition-Fragmentation Chain Transfer
TGA	Thermogravimetric Analysis
US	Ultrasound
XPS	X-ray photoelectron spectroscopy
SEM	Scanning electron microscopy
TMP	2,4,6-trimethylphenyl
DIPP	2,6-diisopropylphenyl
THF	Tetrahydofuran
DCM	Dichloromethane

Declaration ii

Acknowledgements iii

Abstract iv

Abbreviations x

Chapter 1 - Introduction 1-1

1.1 Polymers & oligomers 1-1

1.2 Polymerisation 1-1

1.2.1 Initiation 1-3

1.2.2 Propagation 1-4

1.2.3 Termination 1-5

1.3 Molecular weight 1-5

1.4 Polymer architecture 1-7

1.5 Chain transfer 1-8

1.5.1 Conventional chain transfer 1-9

1.5.2 Catalytic chain transfer 1-9

1.5.3 C_s value 1-9

1.6 The Trommsdorff-Norrish effect 1-10

1.7 Polymer characterisation 1-11

1.7.1 Size exclusion chromatography (SEC) 1-11

1.7.2 Nuclear magnetic resonance (NMR) 1-12

1.7.3 Thermogravimetric analysis (TGA) 1-12

1.8 Thesis overview 1-13

1.9 References 1-13

Chapter 2 - Experimental 2-1

2.1 Materials used in Chapter 3 and Chapter 4 2-1

2.1.1 Commercially available dispersants 2-1

2.1.2 Dispersant synthesis 2-1

2.1.3 Phosphate based glass 2-2

2.1.4 Composite fabrication 2-2

2.2 Materials used in Chapter 5 2-2

2.2.1 Iron complexes 2-2

2.3 Characterisation 2-2

2.3.1 ^{1}H nuclear magnetic resonance (NMR) 2-3

2.3.2 Gel permeation chromatography (GPC) 2-3

2.3.3 Scanning electron microscopy (SEM) 2-3

2.3.4 X-ray photoelectron spectroscopy (XPS) 2-4

2.3.5 Thermogravimetric analysis (TGA) 2-4

2.4 Experimental procedures for Chapter 3 2-4

2.4.1 Ring opening of dodecenylsuccinic anhydride 2-4

2.4.2 Generation of dispersant coated fillers for composites 2-5

2.4.3 Fabrication of composites 2-5

2.5 Experimental procedures for Chapter 4 2-6

2.5.1 Synthesis of MMA dimer (MMA_2) 2-6

2.5.2 Synthesis of dispersants....2-7

2.5.3 Generation of dispersant coated fillers for composites....2-9

2.6 Experimental procedures for Chapter 5....2-9

2.6.1 Ligand and catalyst synthesis....2-9

2.6.2 General polymerisation technique – conventional heating....2-10

2.6.3 General polymerisation technique – microwave heating....2-11

2.7 References....2-12

Chapter 3 - The design and fabrication of novel composites for the improved monitoring of medical devices.....3-1

3.1 Aims and objectives....3-1

3.2 Introduction....3-2

3.2.1 Medical devices....3-2

3.2.2 Dispersants....3-4

3.2.3 Phosphate based glass....3-4

3.2.4 X-ray photoelectron spectroscopy (XPS)....3-6

3.2.5 Ultrasound imaging....3-7

3.3 Results and discussion....3-9

3.3.1 Dispersants for contrast agents....3-9

3.3.2 Biphasic suspension test....3-10

3.3.3 Thermogravimetric analysis (TGA)....3-12

3.3.4 Scanning electron microscopy (SEM)....3-15

3.3.5 XPS....3-17

3.3.6 Extrusion of composites....3-24

3.3.7 Imaging of composites....3-29

3.4 Conclusions....3-33

3.5 References....3-34

Chapter 4 - The design and synthesis of dispersants for ultrasound visible medical devices. 4-1

4.1 Aims and objectives....4-1

4.2 Introduction....4-1

4.2.1 Thiols as chain transfer agents....4-1

4.2.2 Thiol-ene....4-2

4.2.3 Oligomers as dispersants....4-2

4.3 Results and discussion....4-3

4.3.1 MMA_2-3MPA....4-3

4.3.2 Synthesis of oligomers....4-8

4.3.3 Coating of P40....4-17

4.3.4 XPS....4-18

4.3.5 Extrusion of tubes....4-22

4.3.6 Imaging of composites....4-22

4.4 Conclusions....4-23

4.5 References....4-24

Chapter 5 - An investigation into the use of iron-α-diimine complexes as catalytic chain transfer agents and alternative routes to functional materials 4-1

5.1 Aims and objectives 4-1

5.2 Introduction 4-1

5.2.1 Catalytic chain transfer polymerisation 4-2

5.2.2 Alternatives to cobalt catalysts for CCTP 4-9

5.2.3 Fundamentals of microwaves 4-11

5.3 Results and discussion 4-16

5.3.1 PhCoBF mediated polymerisations 4-16

5.3.2 Iron mediated polymerisations 4-17

5.3.3 Effect of catalyst generation method 4-20

5.3.4 The effect of MWH on MMA polymerisations 4-26

5.3.5 Iron-mediated polymerisation of methyl acrylate 4-28

5.3.6 Iron mediated hyperbranched polymer synthesis 4-30

5.4 Conclusions 4-32

5.5 Future work 4-33

5.6 References 4-34

Chapter 6 - Conclusions and future work 6-1

6.1 Chapter 3 – the design and synthesis of novel composite for the improved monitoring of medical devices 6-1

6.2 Chapter 4 – the design and synthesis of dispersants for ultrasound visible medical devices 6-2

6.2.1 Future work.....6-2

6.3 Chapter 5 – an investigation into the use of iron-α-diimine complexes as catalytic chain transfer agents and alternative routes to functional materials 6-3

6.3.1 Future work.....6-4

Chapter 1 - Introduction

1.1 Polymers & oligomers

Polymers can be defined as macromolecules, made up of a large number of smaller repeating units. These small molecules, called monomers, are covalently bonded in a polymerisation reaction.[1,2] Until 1920, it was thought polymers consisted of aggregates of small molecules, held together with physical interactions. However, Staudinger pioneered the idea accepted today by probing the synthesis and properties of certain polymers. Further evidence for the covalently bonded macromolecular structure was provided by crystallographic studies of naturally occurring polymers.[3] Following this, research into polymers accelerated and Staudinger received a Nobel Prize in Chemistry in 1953. The academic strides in polymer research generated industrial interest and commercial production of polymers became increasingly prevalent in the 1950s. Nowadays, polymers are used in day-to-day life, and some of the largest global polymer production companies report multi-billion dollar annual sales figures.[4] Oligomers are shorter chain polymer molecules, which are made up of 10 or less repeating units. The terms dimer, trimer, tetramer and pentamer refer to oligomers with two, three, four and five repeating units respectively. Polymers composed of a single monomer are called homopolymers and those synthesised from two or more monomers are called copolymers. Polymers and oligomers have a wide range of applications and these differ vastly depending on their molecular weight.[5]

1.2 Polymerisation

Monomers must have at least one polymerisable functional group, able to react and form covalent bonds with other monomers. There are three main types of

polymerisation; chain-growth, step-growth and living. The latter technique is also referred to as controlled radical polymerisation (CRP). Figure 1-1 shows how these methods can be differentiated between by understanding the conversion vs molecular weight relationship.



Figure 1-1. Kinetic profiles of different polymerisation mechanisms.

The kinetic profile of chain-growth is characterised by a sharp increase in molecular weight at low conversion. The molecular weight plateaus as conversion reaches up to 100 %. In a step-growth polymerisation, molecular weight increases slowly, as short chain polymers are formed. Once a certain conversion is reached, these oligomers combine resulting in a rapid increase in molecular weight. Step growth polymerisation is also described as condensation polymerisation. It can include the elimination of a small molecule, such as H_2O or HCl as a by-product of the polymerisation. 'Living' polymerisation or CRP displays a linear relationship between molecular weight and conversion, which is how this technique can be used to accurately predict and control molecular weight. Some examples of this type of polymerisation include reversible addition-fragmentation chain transfer (RAFT) polymerisation, nitroxide mediated polymerisation (NMP) and reversible atom transfer radical polymerisation (ATRP).[6–10] These techniques can be utilised to form complex structures such as block copolymers

since polymer chains can be re-initiated due to the reversible end group. RAFT polymerisations use dithioester molecules as a control agents, which reversibly cap the growing polymer chains during the reaction. Metal complexes, most commonly copper-based, are utilised for ATRP control agents.[11] Due to the reversibility of end group attachment in these CRP techniques, chains grow at the same rate and as a result of this, products obtained have a narrow molecular weight distribution.[12]

Free radical polymerisation (FRP) is a chain-growth polymerisation which proceeds *via* the transfer of a propagating free radical consuming monomer, while increasing molecular weight. There are three main steps of FRP: initiation, propagation and termination.[13]

1.2.1 Initiation

The first stage of initiation is decomposition of an initiator (I), either thermally or photochemically, into initiator fragments (2R•), which possess a free radical moiety. Common free radical initiators include molecules that contain an azo or peroxide group.

$$I \rightarrow 2R\cdot$$

Figure 1-2 shows the decomposition of a common free radical initiator, 2,2-azobis(isobutyronitrile) (AIBN).

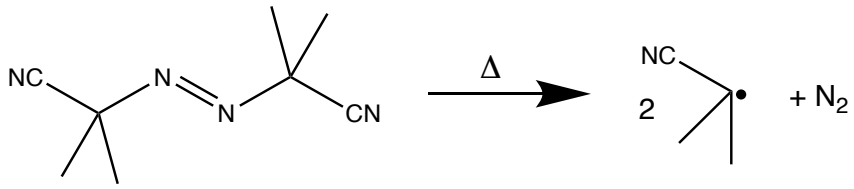


Figure 1-2. Thermal decomposition of AIBN.

The molecule splits to produce two free radical containing fragments and N_2. The radical resides on the tertiary carbon centre, which is stabilised by the neighbouring CN group.

Initiator half-life is an important factor to consider when selecting a suitable initiator for polymerisation reactions. This can be defined as the amount of time required for the original concentration of initiator to reduce by half, at a given temperature.[14] The half-life of AIBN at 80 ºC is 1 hour.[15]

In the second part of the initiation step, an initiator radical reacts with the double bond of a monomer, which forms a chain initiating radical (RM•).

$$R\cdot + M \rightarrow RM\cdot$$

1.2.2 Propagation

The next step is propagation, in which the radical-monomer species (RM_i•) reacts with another monomer, increasing the chain length by one repeat unit (RM_{i+1}•). The propagation step continues with the radical monomer species continuing to react with the double bond of further monomers, increasing the chain length and hence molecular weight. Propagation continues to occur until termination of the propagating polymer radical.

$$RM_i\cdot + M \rightarrow RM_{i+1}\cdot$$

1.2.3 Termination

Termination can occur by two mechanisms; combination and disproportionation. In a combination reaction, two propagating polymer radicals react to form the dead polymer chain by the formation of a covalent carbon-carbon bond. Disproportionation occurs when a propagating polymer chain abstracts a hydrogen atom from another growing chain to form two dead polymers, one with a double bond end group and one with a saturated end group (Figure 1-3).

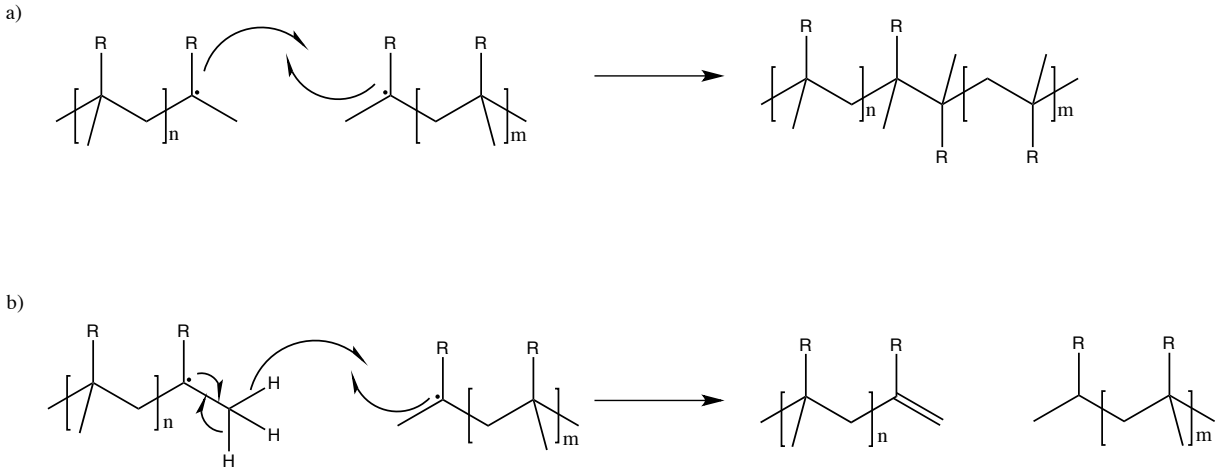


Figure 1-3. Termination mechanisms a) combination and b) disproportionation for polymerisation of methyl methacrylate (R = CO_2Me).

The tendency for one of these mechanisms to dominate the termination process is defined by the monomer type and reaction temperature.

1.3 Molecular weight

The properties and potential applications of a polymer heavily depend on its molecular weight.

The molecular weight of a polymer is not a definitive value; rather it is calculated as a statistical average of the sample. There are a number of representations of MWt, the most commonly used are number average (M_n) and weight average (M_w).

Number average molecular weight;

$$M_n = \frac{\sum M_i N_i}{\sum N_i}$$

Weight average molecular weight;

$$M_w = \frac{\sum M_i^2 N_i}{\sum M_i N_i}$$

Where; M_i = molecular weight of *i* monomer units, N_i = number of polymers with molecular weight M_i.

The number average molecular weight can be used to calculate the degree of polymerisation (DP), which is defined as the number of monomer units a polymer chain is comprised of. Weight average molecular weight takes greater account of higher molecular weights and is regularly used in industry as it provides an indication of the polymer viscosity. Dispersity (Đ) is a measure of the uniformity of the sample; a value of 1 (Đ ≥ 1) indicates the whole sample consists of polymers of one single MWt. It is calculated by the following equation.

$$Đ = \frac{M_w}{M_n}$$

Polymers with a non-linear architecture, such as hyperbranched polymers, have high dispersity values. This is due to the intrinsically random branching that leads to the structure that is formed.

1.4 Polymer architecture

Depending on the monomers and polymerisation technique, there are a number of different macromolecular structures that can be obtained.

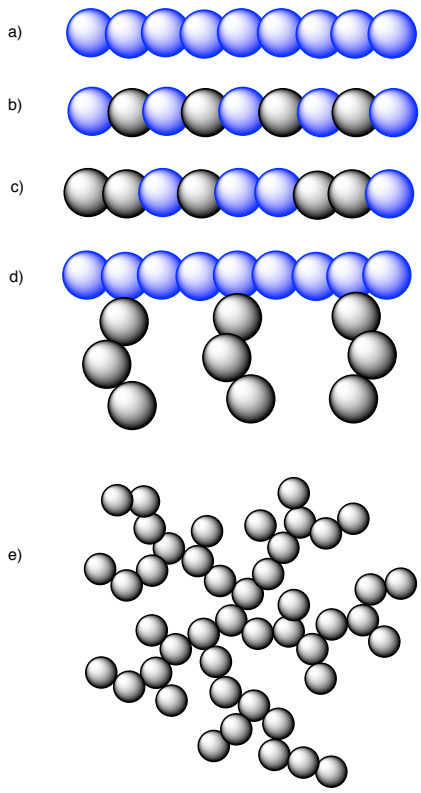


Figure 1-4. Polymer structures.

The polymers shown in Figure 1-4 are a) homopolymer, b) alternating copolymer, c) random copolymer, d) comb-graft (co)polymer, e) hyperbranched polymer. Homopolymers are synthesised from one type of monomer. Copolymers contain two or more different monomer types, and the polymerisation method can affect the monomer distribution. Comb graft polymers can be made from one monomer with a large pendent group, or by copolymerisation. Hyperbranched polymers are complex structures, which are formed using monomers with two or more functional groups,

which are polymerised creating branching points. The architecture of a polymer affects its physical properties.

1.5 Chain transfer

Chain transfer takes place in most polymerisation reactions and is the process in which the activity of a growing polymer chain is transferred to another molecule. This can be intentional, for example by the addition of a chain transfer agent (CTA), designed to reduce the molecular weight of the polymer. Chain transfer can also happen as an unwanted reaction. During chain-growth polymerisation, chain transfer can occur to any of the following:

- chain transfer agent – this process relies on a CTA with an easily abstractable group.[16]
- solvent – if reaction in conducted in solvent, the solvent can behave as a CTA.[17]
- monomer – the propagating polymer can abstract a hydrogen from a monomer.
- polymer – the propagating polymer can react inter- or intra-molecularly.

Chain transfer to any of these molecules involves the abstraction of typically a hydride (H^-) or a halide (X^-) atom. CTAs contain easily abstractable atoms, to facilitate the chain transfer process. In the case of chain transfer to polymer, intramolecular chain transfer can occur between the propagating radical and the polymer backbone. This is called ‘backbiting’. When intermolecular chain transfer to polymer events happen, a branching point is introduced as a result of abstraction from polymer back bone. This branching point is a site from which further propagation can occur.

1.5.1 Conventional chain transfer

The use of CTAs as a method of controlling molecular weight and dispersity has been widely employed since its discovery in 1937.[18] Common CTAs include thiols, disulfides, halomethanes and other molecules with a readily abstractable hydrogen atom.[13] Some of the most efficient CTAs are commercially available thiols. These molecules have a readily abstractable H^- due to their weak S-H bond.[19] The efficiency of CTAs depends on the monomer and conditions used.[20]

1.5.2 Catalytic chain transfer

Transition metal complexes can be used in catalytic quantities to reduce molecular weight in polymerisations.[21] This is called catalytic chain transfer polymerisation (CCTP) and is regarded as a very efficient method for controlling molecular weight and dispersity.[22] The mechanism of catalytic CTAs is slightly more complex than conventional chain transfer but still relies on the transfer of active radical to control molecular weight. The activity of the catalyst can be thought of as a cycle, where the catalysts goes through many transition states during the reaction and can be reformed.[23,24]

More details of CCTP can be found in Chapter 5, where development of catalyst and mechanism is discussed.

1.5.3 C_s value

The efficiency of a CTA is determined by finding its chain transfer constant (C_s) value, which is different depending on monomer and other variables.[25] The Mayo equation is used to find the C_s for a CTA in the polymerisation of a particular monomer at a certain temperature.[26]

$$\frac{1}{DP} = \frac{1}{DP_0} + C_s \frac{[CTA]}{[monomer]}$$

Where; DP = degree of polymerisation, DP_0 = degree of polymerisation with no CTA, C_s = chain transfer constant, [CTA] = concentration of CTA, [monomer] = concentration of monomer.

$$DP = \frac{M_n}{M_0}$$

Where; DP = degree of polymerisation, M_n = number average molecular weight, M_0 = mass of repeating unit.

The C_s value can be used to predict required CTA concentration to target a specific molecular weight product. The higher the C_s value, the lower the concentration of CTA required for a reduction in molecular weight.[20]

1.6 The Trommsdorff-Norrish effect

It is common to use a technique that provides control in FRP. This is most generally for targeting a desired molecular weight polymer and avoiding the Trommsdorff-Norrish effect (TN effect). The TN effect happens at the point in the polymerisation reaction where an exotherm occurs, causing the reaction become out of control because of a chain reaction of events described below (Figure 1-5), which can often be accompanied by an explosion.[27] Especially in an industrial case, it is highly important to be able to have control over polymerisation so this undesired and potentially dangerous effect does not occur.

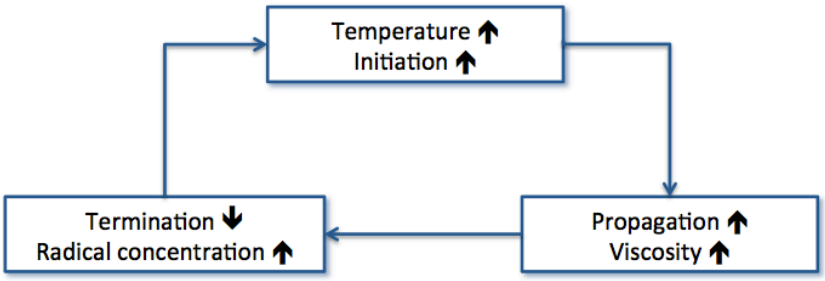


Figure 1-5. The Trommsdorff-Norrish effect.

FRP is an exothermic process; as the temperature of the reaction increases, more initiation reactions happen. As propagation occurs, the viscosity of the medium increases, which causes a decrease in termination reactions since this step is diffusion controlled. The concentration of radicals in the system is therefore also increased. Propagation reactions increase with the higher concentration of radicals, which further increases viscosity. The temperature and pressure increase within the vessel and a chain reaction of these processes can occur, which can result in an explosion. The TN effect can be avoided by stopping the polymerisation at low conversion or low molecular weight, the use of a solvent to reduce the viscosity of the reaction medium or by the addition of a CTA.

1.7 Polymer characterisation

1.7.1 Size exclusion chromatography (SEC)

Gel permeation chromatography (GPC) or SEC is a vital technique for analysing polymers. It provides information on molecular weight and dispersity of products obtained dependent on the polymer's hydrodynamic volume. During GPC, the polymer

sample in the mobile phase flows through columns, which are packed with crosslinked polymer porous beads, referred to as the stationary phase. Small molecules (i.e. low molecular weight polymers) can enter these pores as they travel through the column and are retained, which increases the path length and hence the elution time. In contrast, larger molecules are eluted quicker as these have a larger hydrodynamic volume, they cannot enter the pores. The hydrodynamic volume (sometimes referred to as Stokes radius of polymer) is dependent on solvent, polymer structure and molecular weight.

1.7.2 Nuclear magnetic resonance (NMR)

NMR is a widely used technique for determining the atomic environments present within a sample and can provide information about molecular structure. ^{1}H NMR is a technique commonly used to determine conversion of monomer to polymer in polymerisation reactions and can be used to find molecular weight in specific cases. The chemical shift of NMR active nuclei is affected by its atomic environment.

1.7.3 Thermogravimetric analysis (TGA)

TGA is a useful analysis technique for polymers. During TGA, the weight of a sample is recorded over time while temperature is increased in a controlled environment. This provides information about thermal transitions of the sample such as phase changes and decomposition.[28] For polymers, TGA can be used to determine thermal stability.[29] The decomposition or degradation temperature can be determined by finding the onset of weight loss of a polymer sample.

1.8 Thesis overview

Chapter 1 provides an introduction to polymers, including their applications and synthetic routes. Analytical techniques that are used later in the thesis are explained. Experimental information is detailed in Chapter 2, which includes general practical techniques and specific analytical equipment is described. The first results section is in Chapter 3, where commercially available materials were used to fabricate an ultrasound visible composite medical device. Chapter 4 builds on results obtained for the first composite device. Specifically, the design and synthesis of oligomeric dispersants for the contrast agent in the composite was carried out. Finally, in Chapter 5, the development of iron-based control agents is discussed. Iron mediated polymerisations were investigated in an attempt to produce oligomers *via* catalytic chain transfer polymerisation and avoiding the use of cobalt catalysts. Microwave heating was employed as an alternative to conventional heating methods, with an increase in product molecular weight observed.

1.9 References

1. Staudinger, H. Über Polymerisation. *Berichte der Dtsch. Chem. Gesellschaft (A B Ser.* **53**, 1073–1085 (1920).
2. Allcock, H. R., Lampe, F. W. & Mark, J. E. *Contemporary Polymer Chemistry*. (Pearson/Prentice Hall, 2003).
3. Introduction to Polymers - Robert J. Young, Peter A. Lovell - Google Books.
4. Top 10 Plastic Resin Producers. Available at: https://polymerdatabase.com/Polymer Brands/Plastic Manufacturers.html. (Accessed: 10th May 2020)
5. Jr., C. E. C. *Carraher's Polymer Chemistry, Ninth Edition*. (CRC Press, 2013).

6. Chiefari, J. *et al.* Chain transfer to polymer: a convenient route to macromonomers. *Macromolecules* **32**, 7700–7702 (1999).
7. Moad, G. *et al.* Living free radical polymerization with reversible addition - fragmentation chain transfer (the life of RAFT). *Polym. Int.* **49**, 993–1001 (2000).
8. Hawker, C. J., Bosman, A. W. & Harth, E. New Polymer Synthesis by Nitroxide Mediated Living Radical Polymerizations. *Chem. Rev.* **101**, 3661–3688 (2001).
9. Wang, J.-S. & Matyjaszewski, K. Controlled/"living" radical polymerization. atom transfer radical polymerization in the presence of transition-metal complexes. *J. Am. Chem. Soc.* **117**, 5614–5615 (1995).
10. Matyjaszewski, K. & Xia, J. Atom Transfer Radical Polymerization. *Chem. Rev.* **101**, 2921–2990 (2001).
11. Matyjaszewski, K. & Xia, J. Atom transfer radical polymerization. *Chem. Rev.* **101**, 2921–2990 (2001).
12. Goto, A. *et al.* Mechanism and kinetics of RAFT-based living radical polymerizations of styrène and methyl methacrylate. *Macromolecules* **34**, 402–408 (2001).
13. Matyjaszewski, K. & Davis, T. P. *Handbook of radical polymerization*. (Wiley-Interscience, 2002).
14. Brandrup, J. *et al. POLYMER HANDBOOK FOURTH EDITION A WILEY-INTERSCIENCE PUBLICATION*. (1999).
15. Smith, A. D. *et al.* Dielectric Properties of Free-Radical Polymerizations: Molecularly Symmetrical Initiators during Thermal Decomposition. doi:10.1021/ie901201h
16. Furuncuoğlu, T., Uğur, I., Degirmenci, I. & Aviyente, V. Role of chain transfer agents in free radical polymerization kinetics. *Macromolecules* **43**, 1823–1835

(2010).

17. Mayo, F. R. Chain Transfer in the Polymerization of Styrene: The Reaction of Solvents with Free Radicals 1. *J. Am. Chem. Soc.* **65**, 2324–2329 (1943).
18. Flory, P. J. The Mechanism of Vinyl Polymerizations 1. *J. Am. Chem. Soc.* **59**, 241–253 (1937).
19. Blanksby, S. J. & Ellison, G. B. Bond dissociation energies of organic molecules. *Acc. Chem. Res.* **36**, 255–263 (2003).
20. Furuncuoğlu, T., Uğur, I., Değirmenci, I. & Aviyente, V. Role of Chain Transfer Agents in Free Radical Polymerization Kinetics. *Macromolecules* **43**, 1823–1835 (2010).
21. Gridnev, A. A. & Ittel, S. D. Catalytic Chain Transfer in Free-Radical Polymerizations. *Chem. Rev.* **101**, 3611–3660 (2001).
22. Karmilova, L. V, Ponomarev, G. V, Smirnov, B. R. & Bel 'govskii, I. M. Metalloporphyrins as Catalysts of Chain Transfer in Radical Polymerisation and Stereoselective Oxidation. *Uspekhi Khimii Russ. Chem. Rev.* **53095**, (1984).
23. Poli, R. Relationship between One-Electron Transition-Metal Reactivity and Radical Polymerization Processes. *Angew. Chemie Int. Ed.* **45**, 5058–5070 (2006).
24. Gridnev, A. A., Lampeka, Y. D., Smirnov, B. R. & Yatsimirskii, K. B. Structural features of macrocyclic cobalt complexes ?catalysts of chain transfer to a monomer in radical polymerization. *Theor. Exp. Chem.* **23**, 293–297 (1987).
25. Heuts, J. P. A., Davis, T. P. & Russell, G. T. Comparison of the Mayo and Chain Length Distribution Procedures for the Measurement of Chain Transfer Constants. *Macromolecules* **32**, 6019–6030 (1999).
26. Ward, I. M. Polymers: Chemistry and Physics of Modern Materials, 3rd edition,

by J.M.G. Cowie and V. Arrighi. *Contemp. Phys.* **50**, 670–670 (2009).

27. Alger, M. S. M. *Polymer Science Dictionary*. (Springer Science & Business Media, 1997).
28. MacCallum, J. R. Thermogravimetric analysis of polymers for assessing thermal degradation. *Thermochim. Acta* **96**, 275–281 (1985).
29. A New Method for Assessing the Thermal Stability of Polymers via Single Heating Rate TGA Curve--《Journal of East China University of Science and Technology(Natural Science Edition)》2006

Chapter 2 - Experimental

This chapter describes the experimental procedures implemented throughout this thesis and explains the characterisation methods performed on the materials synthesised. Unless stated otherwise, all reagents were used as received from the supplier, without purification. Where necessary, stoichiometric quantities of reagents were calculated to take into account material purity.

2.1 Materials used in Chapter 3 and Chapter 4

2.1.1 Commercially available dispersants

Dodecenyl succinic anhydride (DDSA) and ethanol were purchased from Sigma Aldrich.

2.1.2 Dispersant synthesis

Methyl methacrylate (MMA, ProSciTech, 99 %), ethylene glycol dicyclopentenyl acrylate (EGDPEA, Sigma Aldrich), ethylene glycol dicyclopentenyl methacrylate (EDGPEMA, Aldrich), poly(ethylene glycol) methacrylate (PEGMA, average M_n = 360 g mol^{-1}, Aldrich), 3-mercaptopropionoic acid (3MPA, Acros Organics, 99 %), mercaptosuccinic acid (MSA, Aldrich, 97 %), 2,2-azobis(isobutyronitrile) (AIBN, Sigma Aldrich, 98 %), cyclohexanone (Acros Organics), hexane (Fisher Scientific), dichloromethane (Sigma Aldrich), methanol (Fisher Scientific), chloroform (Sigma Aldrich), deuterated chloroform ($CDCl_3$, Sigma Aldrich), tetrahyrofuran (THF, Fisher Scientific, HPLC Grade) were purchased and used without further purification.

2.1.3 Phosphate based glass

Phosphate based glass microspheres were manufactured in-house and provided by Dr Zakir Hossain and Dr Ifty Ahmed (Faculty of Engineering, University of Nottingham). The chemical composition was $40P_2O_5$–24MgO–16CaO–$17.5Na_2O$–$2.5TiO_2$ (referred to as P40 Ti2.5). They were prepared *via* a flame spheridoisation process.[1]

2.1.4 Composite fabrication

Texin RxT90A pellets, medical grade aromatic polyether-based thermoplastic polyurethane (TPU) with a softening point of 180 ºC, were purchased from Covestro (Pittsburgh, PA) and used as the matrix polymer.[2]

2.2 Materials used in Chapter 5

2.2.1 Iron complexes

In addition to MMA, AIBN, THF and $CDCl_3$ (materials described in section 2.1.2), methyl acrylate (MA, Sigma Aldrich, 99 %), iron(II) bromide ($FeBr_2$, Aldrich), iron (II) chloride ($FeCl_2$, Aldrich), glyoxal (40 wt% water solution, Sigma Aldrich), 2,6-diisopropylaniline (DIPP, Sigma Aldrich), 2,4,6-trimethylaniline (TMP, Merck), diethyl ether (Fisher Scientific), toluene (Fisher Scientific), divinylbenzene (DVB, Aldrich, 80 %) and bis[(difluoroboryl) diphenylglyoximato] cobalt (II) (PhCoBF, DuPont) were all purchased and used without further purification.

2.3 Characterisation

The following analytical techniques were used throughout the thesis.

2.3.1 ^{1}H nuclear magnetic resonance (NMR)

^{1}H NMR was performed on a Bruker DPX-300 spectrometer (300 MHz) at 25 ºC. Samples were prepared as 10 mg/mL solutions in deuterated chloroform ($CDCl_3$) or deuterated dimethylsulfoxide (DMSO-d_6) to which chemical shifts, measured in δ_H (ppm), were referenced to (residual $CHCl_3$ at 7.26 ppm and residual DMSO at 2.50 ppm). Analysis of spectra was carried out using Mestrelab Mnova 10.0 software.

2.3.2 Gel permeation chromatography (GPC)

GPC was performed on an Aglient 1260 Infinity system (Agilent Technologies, USA) equipped with a PL-gel 5 μm guard column and two PL-gel mixed-D (7.5 mm x 300 mm) columns in series. Tetrahydrofuran (THF, HPLC grade, Fisher Scientific) was the mobile phase at a flow rate of 1 mL/min. A Wyatt Optilab light scattering detector and a differential refractometer (DRI), were used for sample detection and analysis. The differential index of refraction value (dn /dc), 0.0816, was used to calculate the polymer molecular weight and dispersity. GPC samples were made up as 2 mg/mL solutions in HPLC grade THF which were filtered into a sample vial through a syringe filter (Whatman, 25 mm, 0.2μm). Analysis of the spectra obtained was carried out using Astra software.

2.3.3 Scanning electron microscopy (SEM)

SEM was performed to determine phosphate based glass microparticle size. Particles were mounted on an SEM stub using carbon tape and coated using a platinum coater (120 seconds, 2.2 V, Polaron SC7640), to provide a conductive surface and prevent charge build up. The particles were imaged using Phillips XL30 SEM at varying

magnifications. The average particle size of samples was determined by finding the average diameter of 100 particles using imageJ software.

2.3.4 X-ray photoelectron spectroscopy (XPS)

XPS was performed by Dr Emily Smith (NMRC, University of Nottingham) on Kratos Axis Ultra DLD. Samples were prepared on double sided sticky tape. Analysis of data was performed using Casa XPS software.

2.3.5 Thermogravimetric analysis (TGA)

TGA was performed on a TA Instrument Discovery. Samples were analysed in high temperature platinum pans in an N_2 environment, with a heating rate of 10 ºC/min from 28 ºC up to the desired maximum temperature. Analysis was carried out using TA Instruments TRIOS software.

2.4 Experimental procedures for Chapter 3

2.4.1 Ring opening of dodecenylsuccinic anhydride

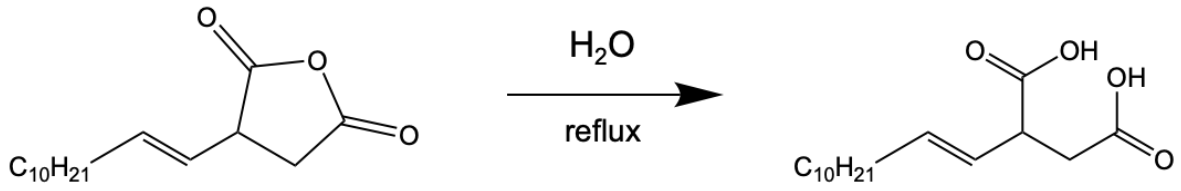


Figure 2-1. Synthetic scheme for ring opening of DDSA with water.

Deionised water (10 mL) was added to dodecenylsuccinic anhydride (DDSA) (5 g, 18.77 mmol) in a round bottom flask equipped with a magnetic stirrer bar and the

solution was refluxed overnight. The product (termed dodecenylsuccinic diacid (DDSD)) was characterised by ^{1}H NMR.

2.4.2 Generation of dispersant coated fillers for composites

DDSD (prepared from DDSA as described above) (1.27 g, 43.00 mmol) was dissolved in ethanol (50 mL). To the solution, phosphate based glass microspheres (1.5 g) were added. The microspheres were left to soak in the stirred solution for 1 hour, after which they were collected by filtration and dried at 120 ºC for 2 hours. The microspheres were added to ethanol (25 mL), which was stirred for 30 minutes in order to remove any further unattached dispersant, then collected by filtration and dried at 120 ºC for 2 hours. The dispersant-coated PBG microspheres are subsequently referred to as P40-DDSD.

2.4.3 Fabrication of composites

A Haake Minilab Micro Compounder (Thermo Fisher Scientific, Waltham, MA) with a custom die was used to extrude hollow tubes comprising of dispersant coated microspheres and TPU as shown in Figure 2-2.

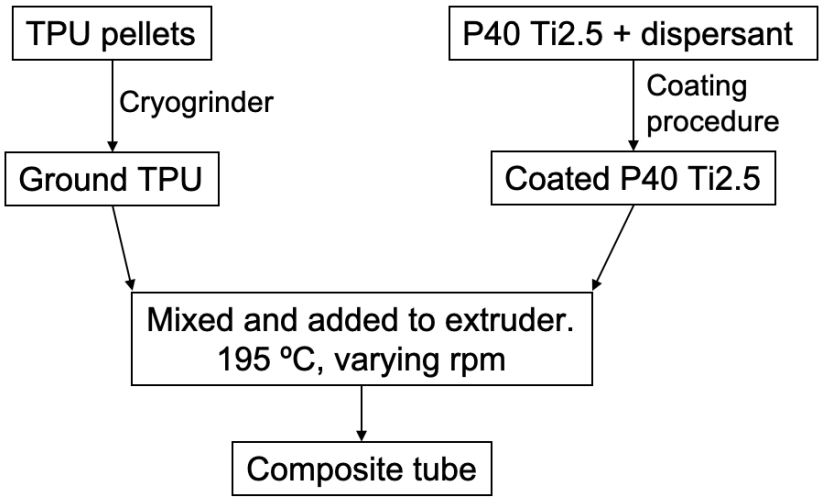


Figure 2-2. Procedure for the extrusion of composites.

The TPU pellets were grinded using a cryogrinder for 5 minutes to reduce particle size. Using a smaller particle size ensured the TPU melted faster in the extruder and prevented overheating and thus discolouration of the extrudate. A total of 5 g (ground TPU pellets and ≤ 10 wt% dispersant coated microspheres) were added to the hopper and manually pushed into the cavity. The extruder was preheated to 195 ºC and the speed of extrusion was varied.

2.5 Experimental procedures for Chapter 4

2.5.1 Synthesis of MMA dimer (MMA_2)

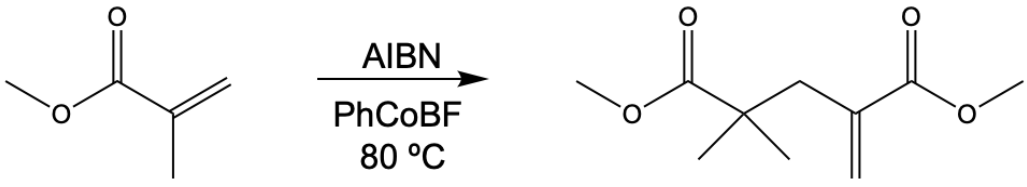


Figure 2-3. Synthesis of MMA_2 *via* PhCoBF mediated CCTP of MMA.

MMA (240 mL, 2.25 mol), AIBN (1.12 g, 0.5 wt% wrt MMA, 6.82 mmol) and PhCoBF (128 mg, 600 ppm) were placed into a reaction vessel and sealed. The solution was degassed by passing a flow of argon through the vessel for 30 minutes. The reaction vessel was then submerged into a preheated oil bath and maintained at 80 ºC for the duration of the reaction (24 hours). The progress of the reaction was monitored using ^{1}H NMR. The reaction mixture was purified *via* reduced pressure distillation to isolate unreacted monomer, MMA_2 and MMA_3. These fractions were analysed using ^{1}H NMR spectroscopy (MMA_2 example shown in Figure 2-4).

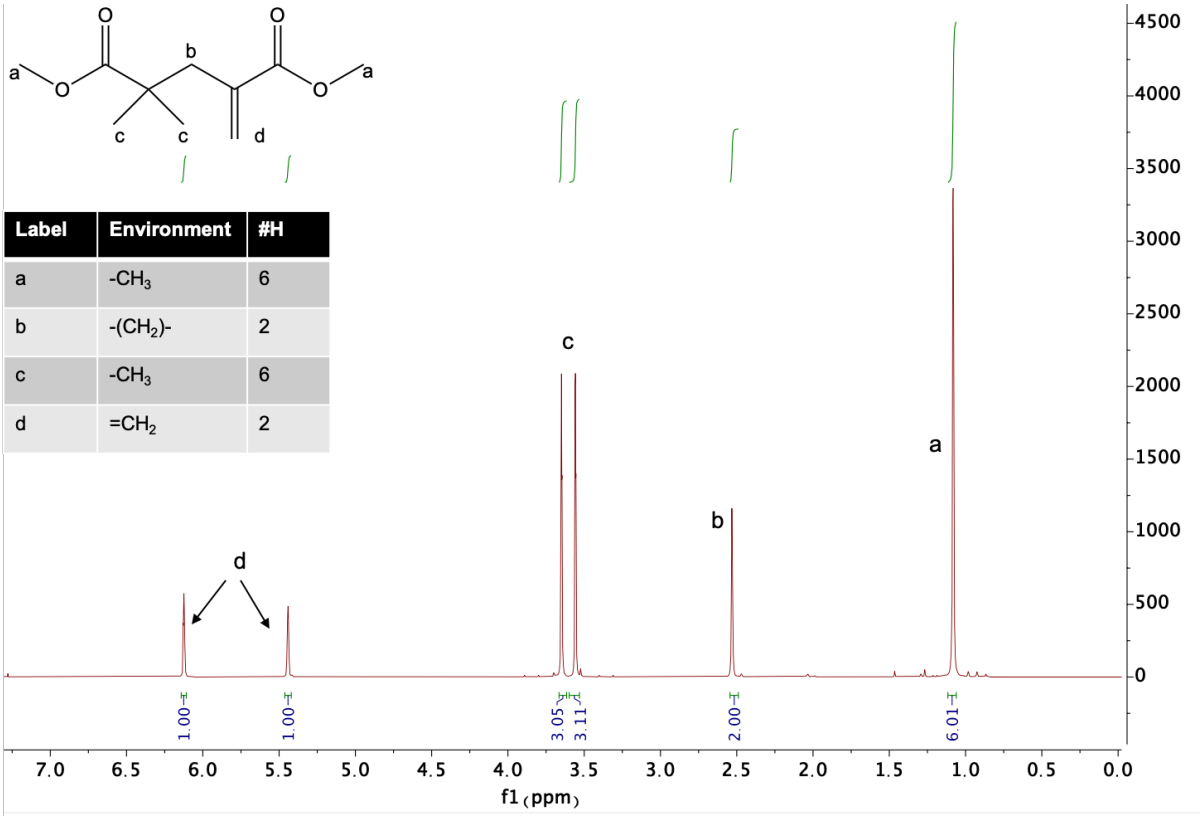


Figure 2-4. ^{1}H NMR spectra of MMA_2.

2.5.2 Synthesis of dispersants

Synthesis of dispersants was carried out using standard Schlenk line techniques.

2.5.2.1 MMA_2-3MPA *via* thiol-ene reaction

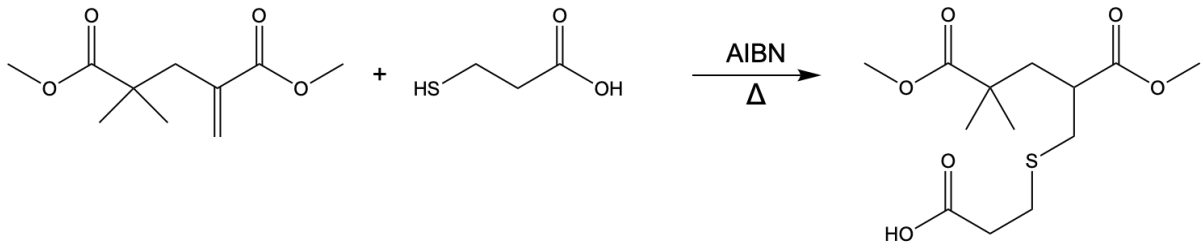


Figure 2-5. Thiol-ene reaction between MMA_2 and 3MPA.

Required quantities of MMA_2, 3MPA, AIBN and cyclohexanone were added to a reaction vessel and degassed under a flow of argon for 30 minutes. After this time, the reaction was submerged into a preheated thermostatically controlled oil bath at i) 80 ºC for 4 hours or ii) 65 ºC for 24 hours. Conversion was determined using ^{1}H NMR. The product (MMA_2-3MPA) was isolated by extraction.

2.5.2.2 Oligomers *via* the use of thiols as CTA

3MPA and MSA were chosen as CTAs for the polymerisation of MMA, DEGMA, PEGMA and EGDPE(M)A. Required quantities of reagents were added to a reaction vessel and degassed under argon for 30 minutes. The vessel was then submerged into a preheated oil bath at 80 ºC for the duration of the reaction. Reactions were quenched by exposing the contents to oxygen and cooling over ice. To determine conversion of monomer to oligo-/poly-mer, ^{1}H NMR was carried out on the crude reaction mixture before purification. The product was obtained by precipitation into an appropriate anti-solvent, collected *via* filtration and dried in a vacuum oven (25 ºC) for 24 hours. GPC and ^{1}H NMR analysis was performed on pure products. These products were termed ‘second-generation dispersants’ and used in composite production.

2.5.3 Generation of dispersant coated fillers for composites

MMA_2-3MPA and oligomeric second-generation dispersants were used to coat P40 microparticles in the same way as described above (2.4.2) but were dissolved in cyclohexanone instead of ethanol.

2.6 Experimental procedures for Chapter 5

Polymerisation reactions were conducted using standard Schlenk link techniques.

2.6.1 Ligand and catalyst synthesis

Ligand synthesis was carried out using methodology from Gibson et al.[3]

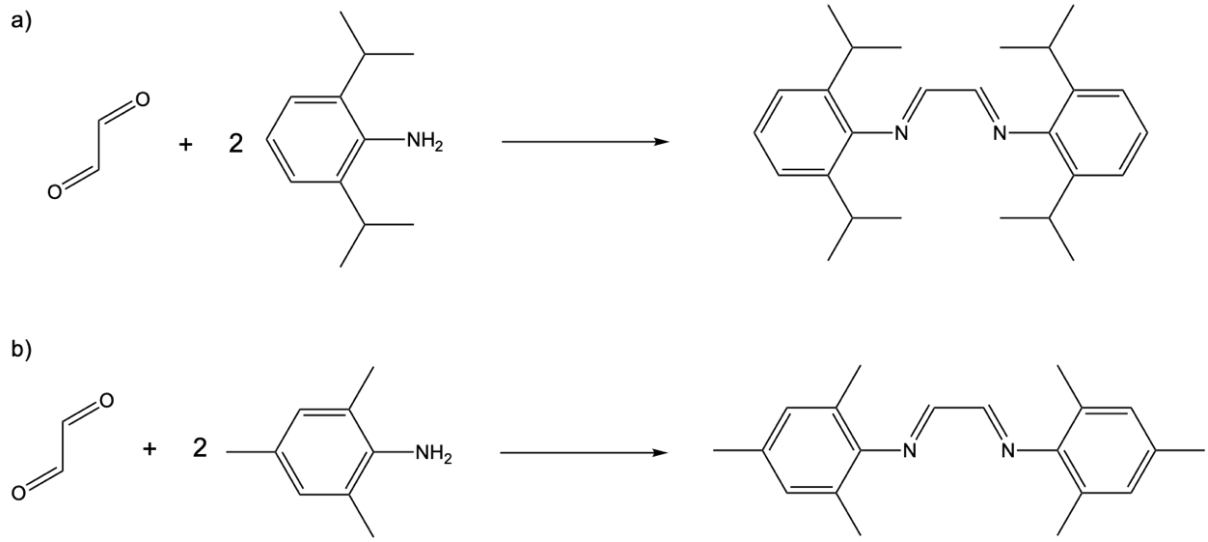


Figure 2-6. Synthetic route to ligands [RN=CH-CH=NR] where R = a) 2,6-diisopropylphenyl (DIPP) - L1 and b) 2,4,6-trimethylphenyl (TMP) - L2.

Glyoxal (10 g, 0.17 mol) was added to 2,6-diisopropylaniline (61.09 g, 0.34 mol) or 2,4,6-trimethylaniline (46.59 g, 0.34 mol) in propan-2-ol (100 mL) in a round-bottomed flask equipped with a magnetic stirrer bar. The flask was sealed and submerged in a thermostatically controlled oil bath at 70 ºC for 5 hours. After this time, 100 mL

deionised water was added, and a yellow solid precipitated out in both cases. This solid was filtered and washed with deionised water (3 x 30 mL) and the product was collected by vacuum filtration. The product was allowed to dry in a vacuum oven (25 ºC) for 24 hours and characterised by ^{1}H NMR spectroscopy.

To form the iron complexes, $FeBr_2$ or $FeCl_2$ were stirred at room temperature with 1 molar equivalent of the ligands in diethyl ether overnight according to the quantities in Table 2-1. The catalyst formed as a precipitate, the solvent was allowed to evaporate and the solid was collected.

Table 2-1. Quantities of reagents used to form FeX_2L complexes.

Iron (II) halide	L1		L2	
	Mass (g)	mmol	Mass (g)	mmol
$FeBr_2$ (1.5 g, 6.96 mmol)	2.62	6.96	2.03	6.69
$FeCl_2$ (1.5 g, 11.8 mmol)	4.45	11.80	3.44	11.80

2.6.2 General polymerisation technique – conventional heating

Solid reagents (initiator and catalyst) were placed into the reaction vessel and degassed by passing a flow of argon through the vessel for 20 minutes. In separate vessels, liquid reagents (monomer and solvent) were degassed by passing a flow of argon through them for 20 minutes. Preserving the inert atmosphere, required quantities of liquid reagents were added *via* syringe to the reaction vessel which was then submerged into a preheated, thermostatically controlled oil bath at 80 ºC for the duration of the reaction. After the required time, the reaction was quenched in ice and

exposed to air. Aliquots were taken for ^{1}H NMR and GPC analysis using techniques described above.

The crude reaction solution was added dropwise to cold hexane or methanol (typically a 20:1 v:v excess wrt polymerisation solvent) after which the polymer product was collected *via* vacuum filtration. GPC analysis was performed on the purified polymer and ^{1}H NMR was used to confirm the purity of the sample.

2.6.3 General polymerisation technique – microwave heating

The reaction solution was prepared in the same way as the CH experiment described in section 2.6.2. In this case, the rubber septum used to seal the reaction vessel had a quartz sheath in order for the fibre optic probe to be inserted into the reaction. Once the degassed reagents were in the reaction vessel, the tube was placed inside the cavity of a Sariem Miniflow 2. Prior to inserting the reaction vessel, a sacrificial sample of the reaction solution in an identical reaction vessel was placed in the cavity to optimise the frequency of the Miniflow. The sliding short and fine adjustment thread were adjusted to find the position in the waveguide that provided the least reflected power when 10 W was applied. Time and temperature parameters were then set to reaction conditions and the reaction vessel inserted into the cavity. Variable power (up to 200 W) was supplied to maintain a constant temperature of 80 ºC, monitored by a fibre optic probe for the duration of the reaction. The reaction was quenched by cooling and exposure to air and the products were analysed as previously described in section 2.6.2. During MWH reactions, the temperature of reaction and the forward and reflected power were recorded.

2.7 References

1. Ahmed, I., Ren, H. & Booth, J. Developing Unique Geometries of Phosphate-Based Glasses and their Prospective Biomedical Applications. *Johnson Matthey Technol. Rev.* **63**, 34–42 (2019).
2. Stevenson, A. T. *et al.* Fabrication and characterization of medical grade polyurethane composite catheters for near-infrared imaging. *Biomaterials* **54**, 168–76 (2015).
3. Gibson, V. C. *et al.* Four-coordinate iron complexes bearing ??-diimine ligands: efficient catalysts for Atom Transfer Radical Polymerisation (ATRP). *Chem. Commun.* 1850–1851 (2002). doi:10.1039/b204510

Chapter 3 - The design and fabrication of novel composites for the improved monitoring of medical devices.

3.1 Aims and objectives

This study aims to expand initial research conducted between the Faculty of Engineering at the University of Nottingham (UoN) and the Department of Materials Science and Engineering at Virginia Tech (VT). The objective of the section of work reported in this chapter was to design and fabricate a medical device (a catheter) capable of being imaged using ultrasound (US). The strategy to fabricate such devices was to obtain a high-level dispersion of echogenic glass spheres within the polyurethane (PU) matrix that makes up the device. The initial exploratory stage work has shown that addition of echogenic particles can increase the contrast of a catheter when inserted into the body. However, it also showed that dispersion of contrast agent was not optimal. Therefore, it was concluded that dispersants should be added to the particle surface to improve the dispersion and hence improve the contrast observed when in the body.

The need for a device capable of being imaged by US was supported by clinicians at Children's National Medical Center (Washington DC). The main reason for this is because the amount of information that can be gained from the current preferred imaging technique (X-ray) is limited due to the potential danger to patients through over-exposure of this type of radiation.

Therefore, this section of work was comprised of the following parts:

- The selection of a suitable dispersant for chosen contrast agent (essential for ultrasound imaging) to be incorporated into the medical device from commercially available reagents
- The development of deposition and characterisation methods to coat the echogenic glass spheres
- The fabrication of a prototype medical device to be analysed in comparison to currently available devices and those without dispersant coated glass spheres.

3.2 Introduction

3.2.1 Medical devices

There is a requirement to be able to monitor the placement of medical devices when implanted into the body. Catheters for example, require accurate initial positioning in order to ensure that the therapeutic treatment is delivered to the correct area. Failure to do this is a key reason for negative outcomes in hospital treatments.[1,2] This is particularly true in the case of paediatric medicine where the patients are small in stature and so the difference between correct and incorrect placement can be very small.[3] Additionally, as these devices can be used in long-term treatments, they have the tendency to migrate during use and such movement must be tracked and corrected when necessary.[4] Typically, the implemented imaging technique for checking the placement of such medical devices in hospitals and clinics is X-ray. However, too much exposure to this type of radiation can have significant negative health impacts, especially for sensitive patient populations, such as paediatric or geriatric cases.[5,6]

Furthermore, exposure to X-ray radiation is a prolonged issue that extends beyond the current treatment strategy, as it is known to increase the risk of developing cancer in later life.[7] Thus, less harmful options must be considered if treatment with medical devices such as catheters is to be improved.

Complications related to catheters can arise during positioning or during the therapy period where the device is implanted in the body. Malpositioning can occur in up to 85 % of cases according to recent clinical studies.[8] There are two commonly used techniques for insertion of catheters. The first requires the patient to be in the radiology department, so that position can be tracked in real time using fluorescence microscopy. Alternatively, if real time tracking of insertion is not an option, clinicians must insert the device into the area and confirm correct positioning later using imaging techniques.

In 2015, Stevenson *et al* reported the fabrication of catheters with near-infrared (NIR) visible dye incorporated, as a safer alternative to commercially available catheters.[9] This was a successful study, where catheters were fabricated by firstly mixing dye with the PU matrix polymer, followed by processing *via* extrusion to form hollow tubes. It was found that the addition of NIR dye increased the visibility of the device by 14 times in comparison to the matrix PU alone. Biocompatibility was not compromised by the addition of the dye, although the material is not yet Food and Drug Administration (FDA) approved. However, a downfall of this type of device is the requirement to use an imaging modality not as widely used in hospitals and clinics such as X-ray and US. Fluorescence microscopes are used in some medical procedures but US and X-ray are much more common.[10] Additionally, it was found that the imaging depth was a

limiting factor, with image quality deteriorating at around 5 cm making it potential unsuitable for some applications.

3.2.2 Dispersants

Solid particles have a tendency to agglomerate. Dispersants are designed to prevent flocculation of solids particles in a liquid medium. They are interfacial additives which are used to overcome the attractive forces that exist between solid particles and separate them.[11] Dispersants typically contain a moiety with an affinity for the surface of the particle (the head group), and a tail group which ensures repulsion between particles *via* electrostatic or steric stabilisation.[12]

Dispersants for electrostatic stabilisation of particles typically contain a formal charge in their structure.[13] These charged species can form a strong adsorption onto the surface, which results in separation of particles due to repulsion between like charges. Generally, these dispersants are negatively charged, so this type of stabilisation is commonly referred to as anionic stabilisation.

Colloidal stability can also be achieved by the use of steric dispersants. This group of dispersants often contain oligomeric/polymeric tail groups which protrude away from the surface and are soluble in the surrounding solvent or matrix material.[14] When particles approach each other, the increase in the concentration of tail group causes the flow of matrix/solvent, separating the particles.

3.2.3 Phosphate based glass

Phosphate based glass (PBG) microspheres have been recently recognised to have promising potential in the field of biomedical applications.[15] Their most common

biomedical application uses currently are within drug delivery and the regeneration of tissue and bone.[16–18]

PBGs can be doped with a number of metal oxides, to affect material properties and degradation profile. The relative amounts of P and O have an effect on the structure of the glass, as shown in figure below. The number of bridging oxygen-phosphorus bonds affects the 3D glass structure and hence its properties (Figure 3-1).[19]

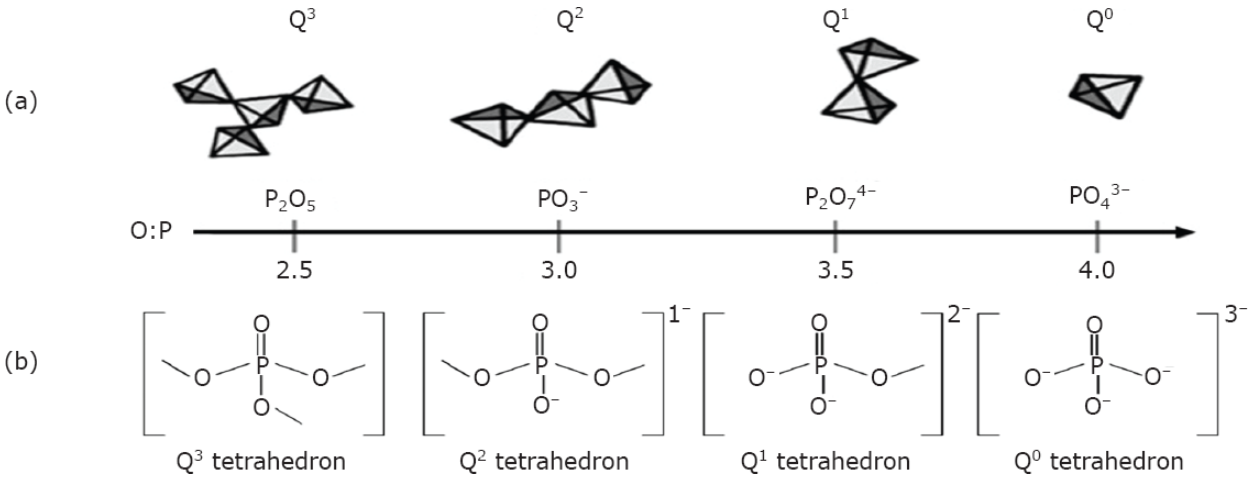


Figure 3-1. Structures of various phosphates.

PBG microspheres can be made *via* a flame spheroidisation process, and by carefully controlling processing parameters, the size/morphology and properties of the microsphere can be modified.[20] The addition of TiO_2 and other dopants can influence the degradation activity of the microspheres.[21,22]

It was noticed that glass spheres of a certain size could be detected using ultrasound radiation due to the emission of a twinkling signal, which was described as a scattering of signal. A group researching the micro-calcification of soft tissue discovered the twinkling phenomenon when using glass microspheres as a mimic for calcified

tissue.[23,24] They noticed that when the glass spheres were present in a sample, scattering of the ultrasound signal (twinkling) was seen. Thus far, the use of PBG microspheres has been for mimetic purposes.[25]

3.2.4 X-ray photoelectron spectroscopy (XPS)

XPS is a surface sensitive technique capable of detecting the molecular environment of atoms. Analysis obtained from this technique provides information on the atomic environments within a sample. XPS is often referred to as electron spectroscopy for chemical analysis (ESCA). XPS analysis is typically conducted under ultra-high vacuum (UHV) conditions.[26]

During XPS analysis, the sample is irradiated with X-rays, causing electrons to be excited and emitted. These electrons are detected by an electron analyser which measures their kinetic energy and records the number of electrons at each energy.[27] Each element (except hydrogen and helium) can be identified by a characteristic binding energy (BE), which can also provide information about the chemical environment it is in within the sample.[28] Quantitative information is obtained by XPS, whereby elemental composition of the sample and therefore empirical formula, can be determined by measuring the peak area at specific binding energies.[29] Wide scan spectra are obtained over a large range of binding energies to obtain elemental composition. In addition, high-resolution spectra are used to indicate the chemical environments of particular elements.

The binding energy (BE) of emitted electrons is calculated using the energy of the X-ray source ($h\nu$) and the measured kinetic energy (KE), using the following equation;

$$BE = h\nu - KE$$

The high-resolution spectra for specific elements can be mathematically deconvoluted to provide information on the atomic environment. Reference data, such as the NIST database, can be used to compare to spectra obtained to identify bonding within sample.[30]

3.2.5 Ultrasound imaging

Ultrasound waves have a frequency of above 20000 Hz, which is above the upper limit of the typical human hearing range. It is a type of non-ionising sound wave with a wavelength equal to or less than 1.9 cm.

The use of ultrasound as a means for imaging the body, such as the unborn baby or internal organs, has been implemented for years.[31] During a sonogram or ultrasound scan, the reflection of ultrasonic waves is detected and visualised as a monochromatic image. Different types of structures i.e. tissue, bone and blood vessels produce different ultrasound responses and can typically be differentiated between. Hyperechoic refers to a strong ultrasound response, in contrast hypoechoic and anechoic which refer to a sparsity and absence of echogenicity respectively. Bone is an example of an anechoic material, but the edges are detected and characterised by a hyperechoic response.

Ultrasound scans are widely regarded to be much safer than other imaging techniques, such as X-ray and computerised tomography (CT) scans.[7] The radiation is non-ionising and so is unlikely to cause damage to the surrounding tissues in the long or short term. However, its capabilities are limited to materials which contain enough interfaces or phases boundaries to reflect the ultrasound to be visible.

3.2.5.1 Principles of US imaging

To obtain US images, a probe containing piezoelectric elements called a transducer is used. The piezoelectric crystals inside the transducer expand and contract when a voltage is applied, generating an ultrasound wave. The transducer also detects the US signal which is returned from the body; the piezoelectric crystals expand and contact, generating a voltage which is used to produce the image. US waves travel at approximate velocities of 1540 m/s (in tissue) and 1570 m/s (in blood). 2D images can be obtained using this information by measuring the time taken for signals to be returned and detected.[31]

Absorption, reflection, refraction, and scattering are all processes which contribute to the reduction in amplitude of US signal, which is called attenuation. This is considered undesirable as it can reduce the information gained from images. Resolution is the minimum distance that can be differentiated between two objects. Typically, resolution is determined by the transducer and is dependent on the US beam properties such as direction and wavelength.[32]

3.2.5.2 Ultrasound imaging of medical devices

As discussed in section 3.2.1, the monitoring of medical devices is important, both during placement and whilst being used to deliver treatment. Ultrasound is rapidly becoming a preferred imaging modality due to its advantages over X-ray or fluorescence microscopy. However, some medical devices need to be modified in order for them to be US visible. Studies by Yang et al reported the development of an US activated film, which contained hollow microparticles.[33,34] This film was applied to needles and implantable medical devices. The US visibility of these devices was

attributed to the air in the particles acting as a contrast agent. Imaging was performed *in vitro* and *in vivo* (live animal) and good quality images were obtained in both cases. Additionally, they could also detect surgical equipment (such as tape and clips) left in the body that were coated with the film, showing US response was not deteriorated by the surrounding tissue.

Some of the most significant progress towards US visible medical devices has been carried out commercially and many patents have been obtained in the recent years. Companies such as Encapson have pioneered research into echogenic coatings for needles and catheters. The coating is comprised of acoustically reflective microspheres capable of returning ultrasound signal back to the detector providing an image of the medical device *in situ,* in real time. Other techniques of making echogenic medical devices involve the physical surface modification, to form a slightly rough surface which can be detected.[35]

3.3 Results and discussion

3.3.1 Dispersants for contrast agents

It was known from previous research by Ahmed et al, that dispersants or compatibilising agents, should contain a group with a strong affinity for the phosphate based glass such as a hydroxyl or diacid moiety.[36,37] This is due to the likely surface chemistry of the microsphere which comprises of a high density of oxygen containing groups. The selected commercially available dispersant for the initial compatibilisation of the PBG microspheres was dodecenylsuccinic anhydride (DDSA), which was ring-opened and then attached with a multi-step coating procedure. The microspheres

were soaked in a solution of the dispersant as described in Chapter 2. This procedure was adapted from that described in Ahmed et al's previous work.[38] The structure of DDSA and subsequent ring-opened species, dodecenylsuccinic diacid (DDSD) is shown in Figure 3-2.

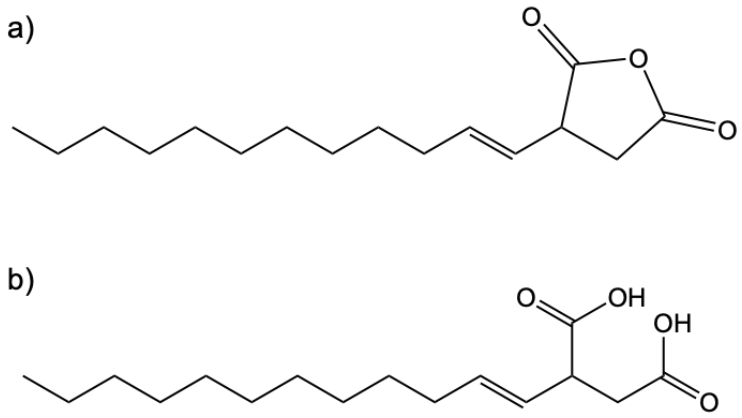


Figure 3-2. Structures of a) DDSA and b) DDSD.

In order to be a suitable dispersant, the anhydride group was opened to form a diacid (described in Chapter 2), which is assumed to be the head group that associates with the glass microsphere. The alkyl chains should induce repulsion between particles and associate with the polymer matrix of the medical device, behaving as a steric dispersant. The ring opening reaction was efficient and used very simple reaction conditions. No solvent was used and therefore no purification of the products was required. Residual water not consumed in the reaction was not considered to be significant since the relative quantity was very low.

3.3.2 Biphasic suspension test

To confirm attachment of dispersant to microsphere in a quick easy way, a biphasic suspension test was devised. To a vial containing 2 mL toluene and 2 mL deionised water, approx. 10 mg of microspheres was added. Based on an extraction efficiency

test, which is typically used on nanoparticulate systems, the hypothesis is that coated and uncoated microspheres will have a propensity to reside in either the organic or aqueous phase. This is dependent on the chemical groups present which can form many types of interaction with solvents.

Figure 3-3 shows images of a biphasic suspension test carried out on coated and uncoated microspheres.

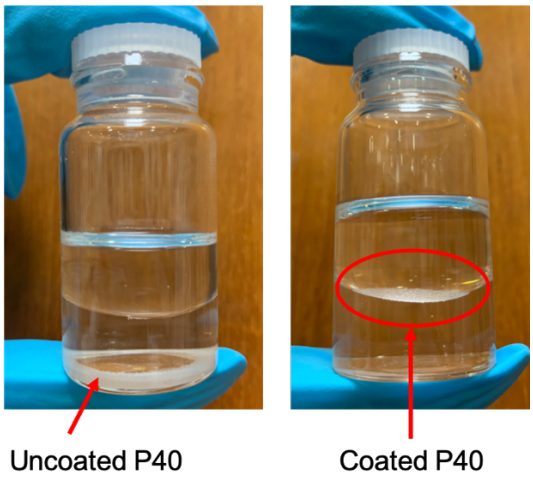


Figure 3-3. Biphasic suspension test.

When added to the biphasic mixture, the uncoated microspheres dropped and settled immediately at the bottom of the water phase as seen on the left image. However, the dispersant-coated microspheres tended to settle in the interface between the organic and aqueous layers forming a thin layer. This suggests their surface chemistry is different to the uncoated microspheres. Additionally, a control group of microspheres that had been subjected to the coating procedure in the absence of dispersant were tested. The control group were found to behave as uncoated microspheres did and sunk to the bottom of the aqueous phase indicating no change in surface chemistry had occurred.

3.3.3 Thermogravimetric analysis (TGA)

Thermogravimetric analysis (TGA) was performed in order to provide an indication of percentage of surface coating achieved. Initially, uncoated microspheres and dispersants were analysed separately to determine the onset temperature of degradation for each component. The thermal stability of starting materials is an important factor when considering composite processing parameters. All parts of the composite must be stable at the processing temperature. The thermograms for the composite are shown in Figure 3-4 below.

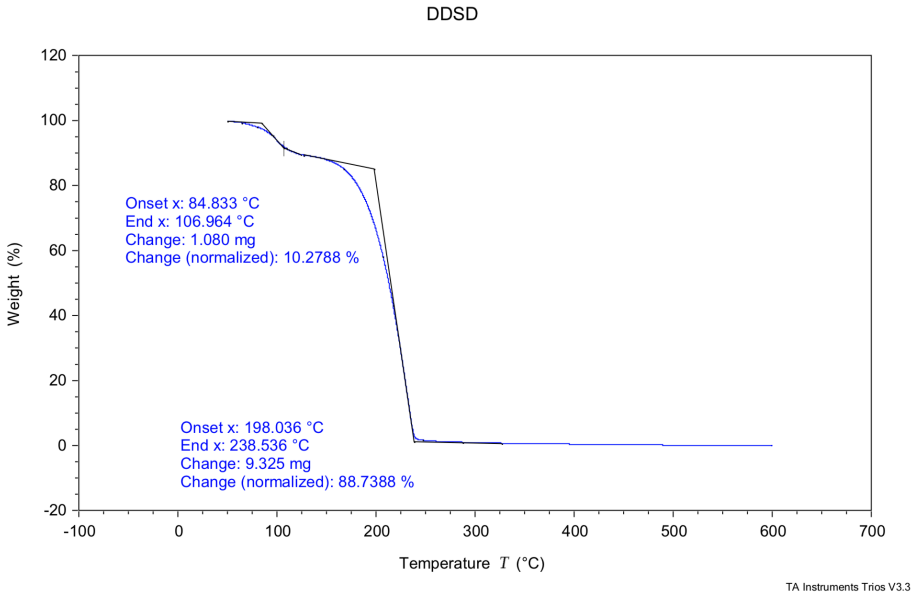


Figure 3-4. Thermogram of DDSD.

Figure 3-4 shows DDSD possessed two decomposition transitions; the first (onset temperature 85 ºC) is attributed to residual water that was not removed after the ring opening of the anhydride. The second is attributed to the thermal decomposition of the ring opened diacid species.

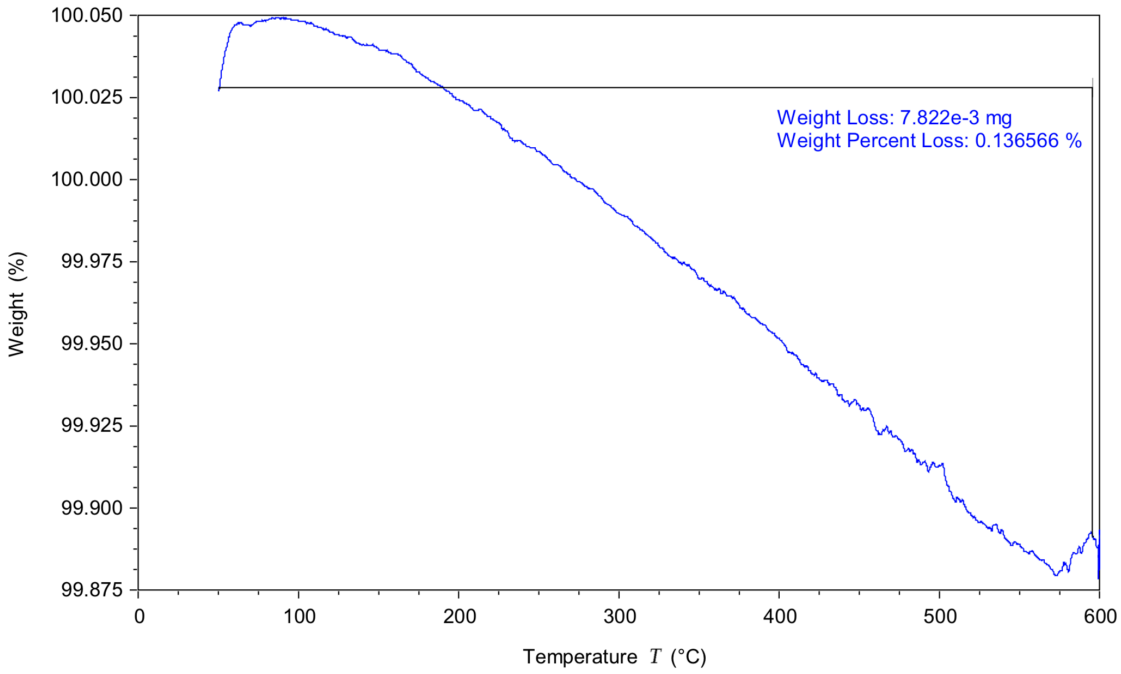


Figure 3-5. Thermogram of P40 microspheres.

The thermogram obtained for the microspheres (Figure 3-5) showed they possess very high thermal stability, with no significant weight loss of the sample observed at temperatures from ambient up to 600 ºC. The percentage weight loss value was reported to be 0.14 %, which is within error of the equipment. From this it was concluded that any weight loss observed for coated samples could be attributed to the dispersant coating. Therefore, TGA was performed on P40 samples that appeared (from observations in the biphasic suspension test) to have dispersant attached, an example is shown in Figure 3-6.

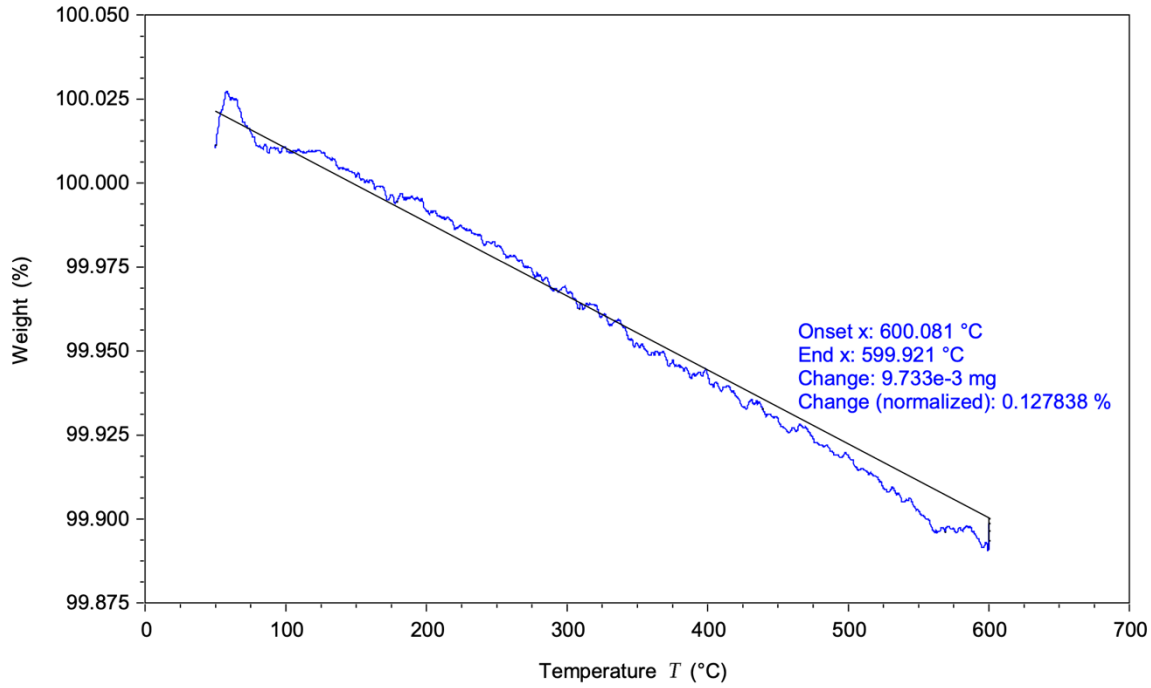


Figure 3-6. Example thermogram for P40-DDSD.

Five samples of P40-DDSD were analysed. There was not any significant weight loss observed for any of the samples, with an average of 0.28 %, which is within error of the measurement. This indicates the quantity of coating is very low, below the detection limit of the TGA equipment. Despite not being able to obtain the percentage coating of dispersant for these samples, the TGA did show that the thermal stability of the microspheres remained unaffected after the coating procedure.

The chosen polymer matrix for the composite devices was medical grade PU (RxT90A). TGA was performed to indicate suitable processing parameters for the material and is shown in Figure 3-7.

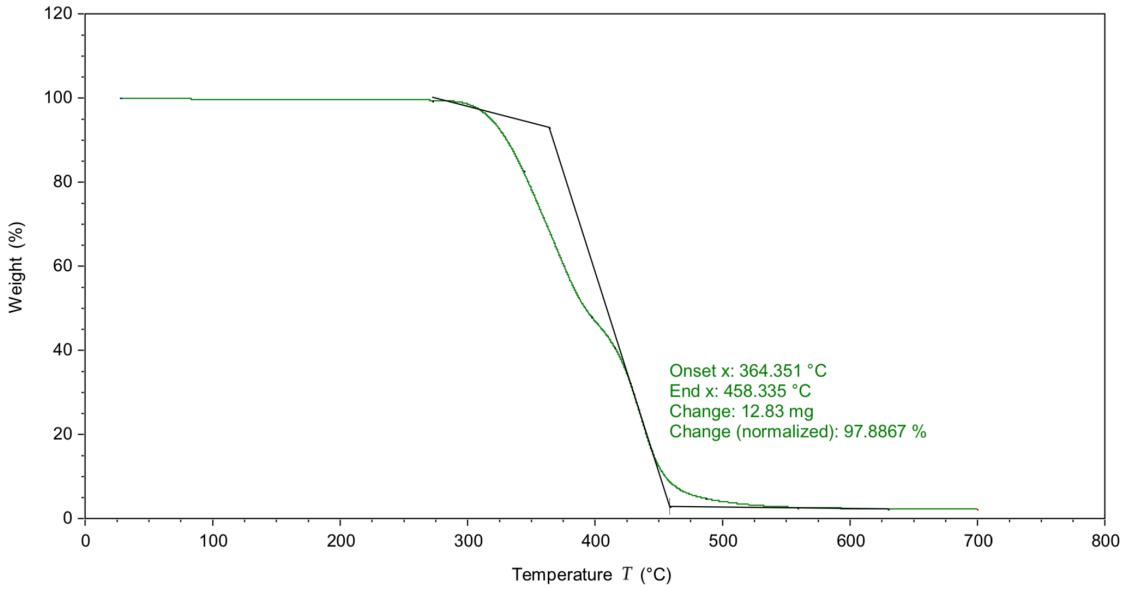


Figure 3-7. Thermogram of polyurethane.

The onset of degradation for PU was found to be approximately 365 ºC (Figure 3-7), meaning that processing of the polymer must be carried out at a temperature lower than this. The reported softening point of this particular PU is 180 ºC so there is a large processing window available.[9]

3.3.4 Scanning electron microscopy (SEM)

SEM images were obtained (Figure 3-8) to observe the surface of the microspheres before and after coating, and to determine the average particle size and morphology.

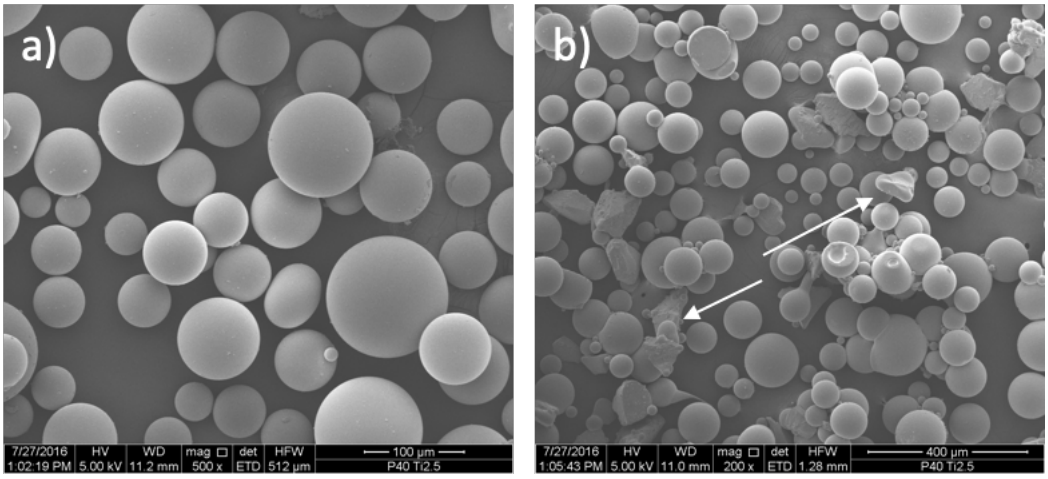


Figure 3-8. SEM images of P40 at varying magnification with arrows indicating non spherical particles.

The SEM images show that the P40 samples were predominantly comprised of spherical particles, with a varying size distribution. Some debris was observed, as non-spherical flakes and grains (Figure 3-8, b). Average particle size and standard deviation was determined using the diameter of at least 100 particles using ImageJ software. The uncoated P40 particles were found to be 67 μm with a standard deviation of ±25 μm. Flakes and non-spherical particles were not included when determining average particle size. After the coating procedure, P40-DDSD were imaged again (Figure 3-9) and visually appeared unchanged when compared to P40.

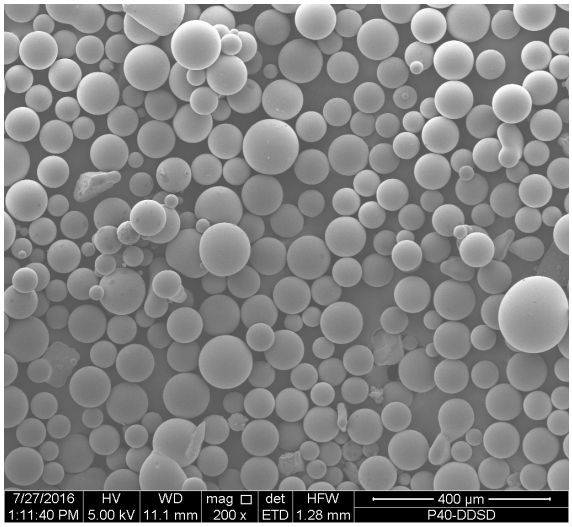


Figure 3-9. SEM image of P40-DDSD.

The average particle size of coated P40 was 74 μm (standard deviation ±20 μm). This increase of 7μm is not considered particularly significant given the standard deviation and any other errors. However, it was promising that the surface of the microspheres still appeared smooth and no aggregation of the dispersant was observed.

Further analysis of the P40 size, for example by dynamic light scattering (DLS) was not carried out as the particles were not stable in solution and could not be analysed due to sedimentation.

3.3.5 XPS

XPS was performed to investigate the surface chemistry of the microspheres, both uncoated and dispersant coated. An example wide-scan spectra is shown in Figure 3-10. Each peak corresponds to a signal from a particular element.

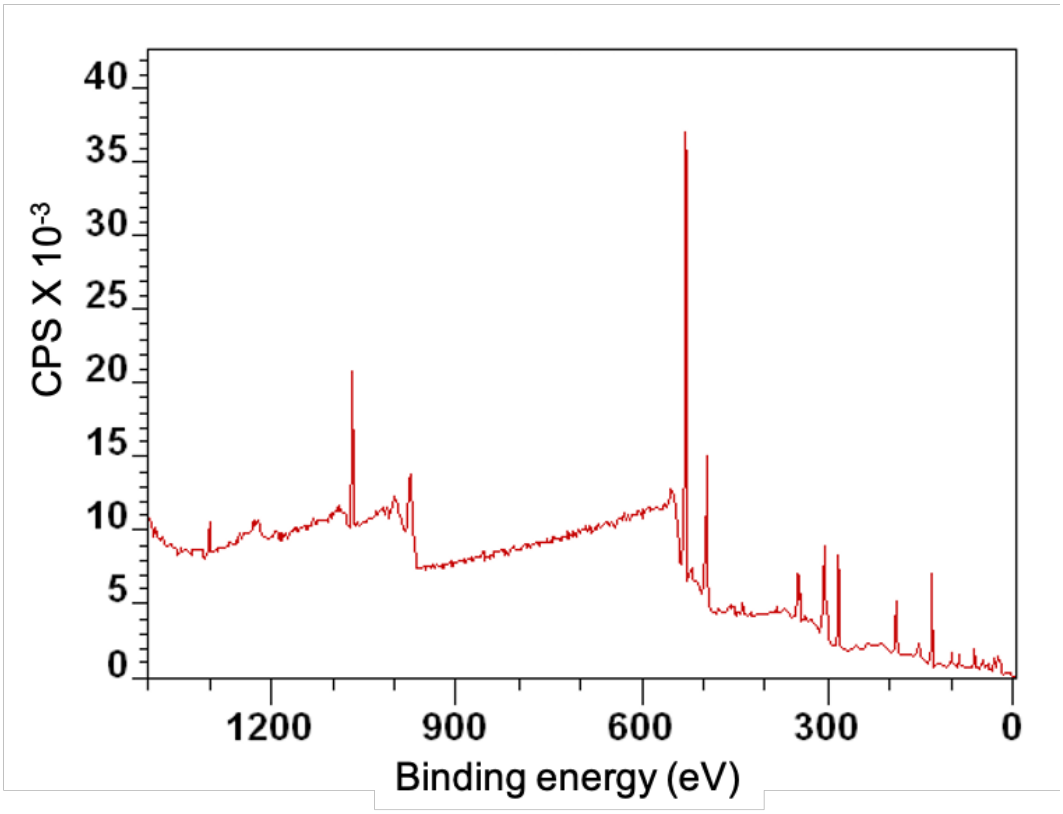


Figure 3-10. Example wide scan XPS spectra of uncoated P40.

The elemental composition of three samples of P40 is displayed in Table 3-1. The percentages shown are averages obtained from the analysis of 6 wide scan spectra.

Table 3-1. Elemental composition of P40 samples determined by XPS.

	Elemental composition (mol%)						
	C	**O**	**P**	**Ca**	**Na**	**Mg**	**Si**
P40	20.6	49.3	14.8	3.6	6.4	3.9	1.4

The composition of the P40 microspheres according to their preparation is $40P_2O_5$–$24MgO$–$16CaO$–$17.5Na_2O$–$2.5TiO_2$. However, the XPS analysis showed there was a significant amount of carbon (~21 %) present in the sample. This is termed 'adventitious carbon' and is most likely due to environmental debris, which could

become attached to the sample during preparation or storage. The remainder of the composition of P40 was as expected, comprising of oxygen, phosphorous, calcium, sodium and magnesium. However, titanium was not detected in any of the samples. It is the least abundant element in the P40 at a loading of 2.5 mol% TiO_2. Additionally, a small amount (~1 %) of silicon was detected, however this is another typical artefact of XPS and can be introduced during sample preparation.

3.3.5.1 P40-DDSD

Wide scan spectra were obtained for P40-DDSD samples.

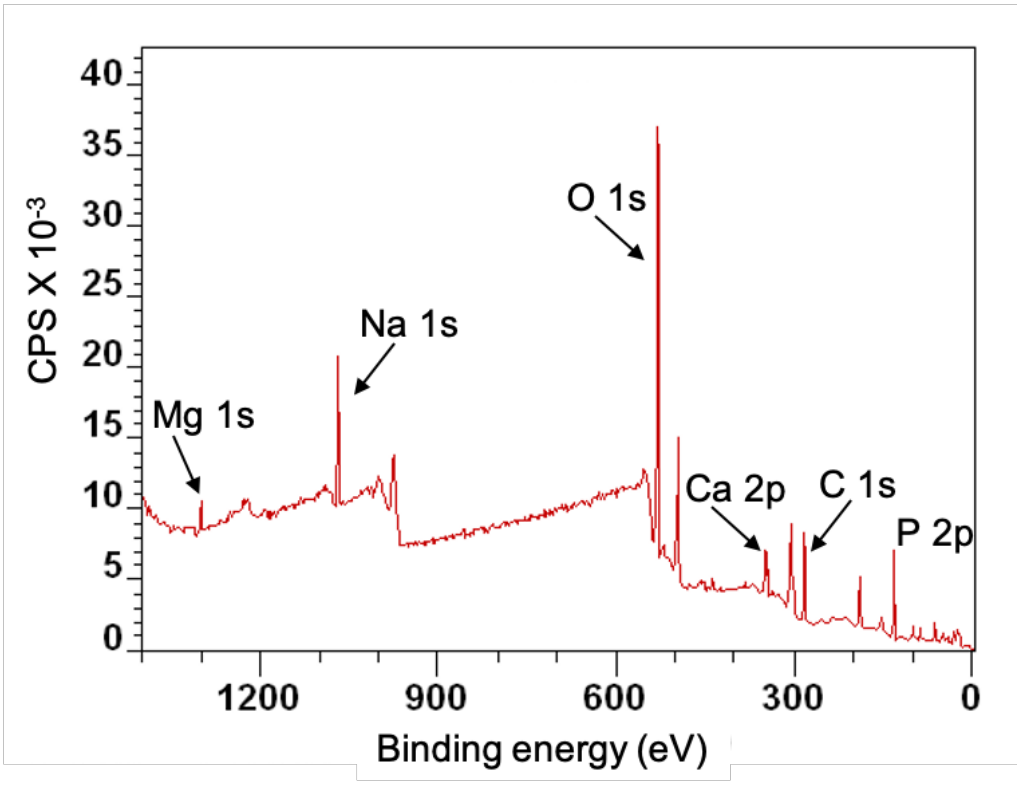


Figure 3-11. Example wide scan spectra of P40-DDSD with peaks assigned to elements.

Using averages obtained from five wide scan spectra, the elemental composition was determined for P40-DDSD samples and is shown in Table 3-2 with the previous results for P40 for comparison.

Table 3-2. Elemental composition of P40 and P40-DDSD samples determined by XPS.

	Elemental composition (mol%)						
	C	**O**	**P**	**Ca**	**Na**	**Mg**	**Si**
P40	20.6	49.3	14.8	3.6	6.4	3.9	1.4
P40-DDSD	31.6	43.7	11.3	2.9	3.4	4.3	3.2

The percentage composition of carbon in P40-DDSD is higher than the uncoated P40 microspheres (Table 3-2). This is expected as the coating, DDSD, is a carbon and oxygen containing molecule. Some of the carbon detected will be adventitious carbon, but unlike the uncoated microspheres, there are components that can be fitted in the high-resolution carbon scan, owing to the different environments present. The amounts of phosphorous, magnesium, calcium and sodium are all lower than the uncoated microspheres, which is also expected as an additional species is present in this sample, changing the relative percentages.

High resolution scans were obtained for some of the elements identified in the sample. To gain information about the dispersant coating, which is a hydrocarbon, carbon (C 1s) high resolution scans were analysed in detail, an example obtained spectra is shown in Figure 3-12.

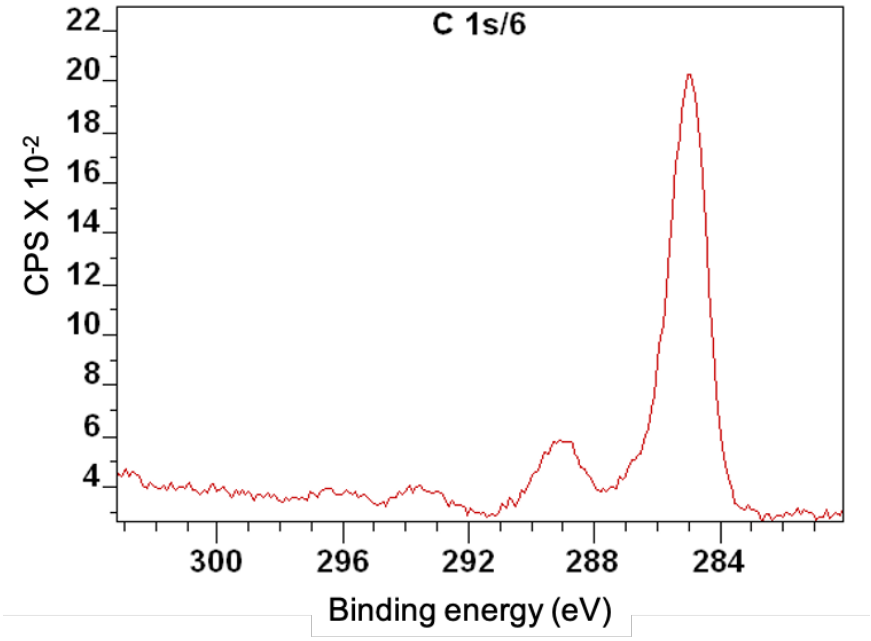


Figure 3-12. High-resolution C 1s scan P40-DDSD.

By applying mathematical fittings, the peaks detected in the high-resolution carbon scan can be deconvoluted into their component parts as shown in Figure 3-13. These components all correspond to particular molecular environments. These carbon environments are labelled in Figure 3-14.

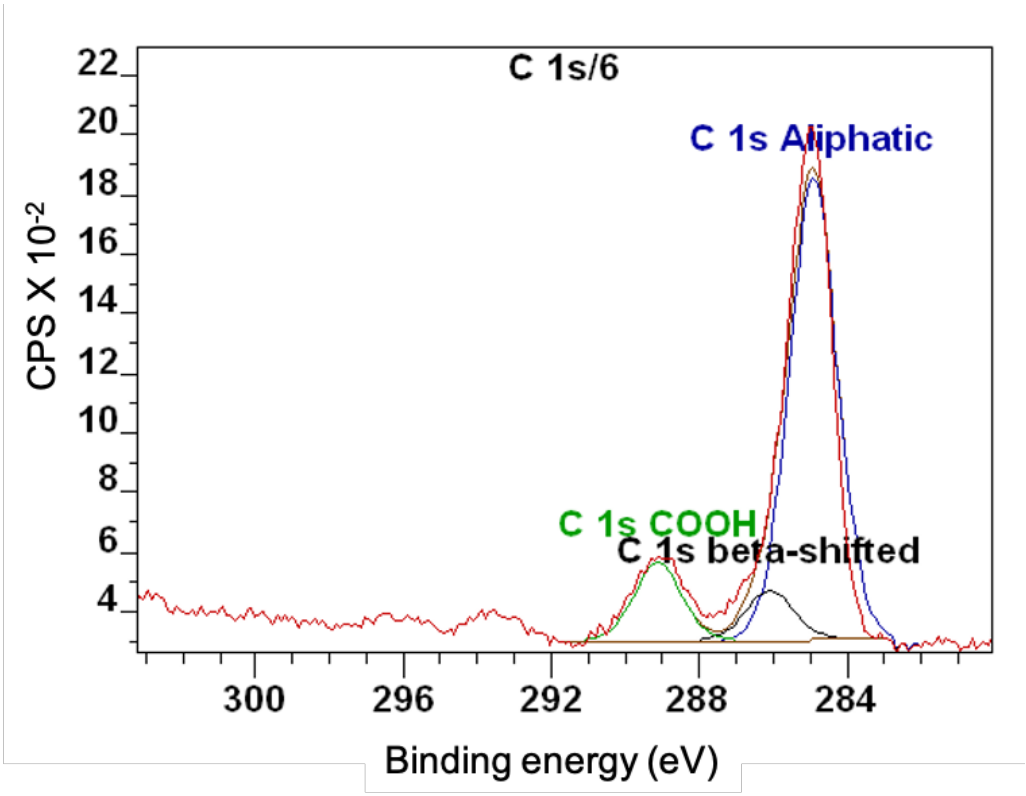


Figure 3-13. C 1s high-resolution scan P40-DDSD with environments fitted

Red – original spectra, blue – aliphatic component, green – COOH component, black – β-shifted component.

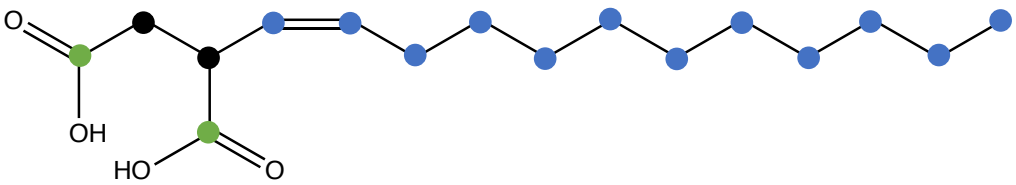


Figure 3-14. Structure of DDSD with carbon environments labelled in accordance to Table 3-3.

The data from the high-resolution scan in Figure 3-13 and assignments is shown in Table 3-3. The area under the peak is used to obtain the carbon composition (%). The peak position quoted in the table is taken from the centre of the fitting.

Table 3-3. High-resolution C 1s scan data and comparison with theoretical composition.

Environment	Key	Carbon (#)	Carbon composition theoretical (%)	Carbon composition experimental (%)	Peak position of fitting (eV)
O=C–OH		2	12.5	13	289
'β-shifted'		2	12.5	9	286
Aliphatic		12	75	78	285

The initial elemental composition values obtained (Table 3-2) showed that adventitious carbon is present in the samples, which is almost unavoidable and has the same chemical shift as aliphatic carbons. The structure of DDSD with components labelled is shown in Figure 3-14. 'β-shifted' carbons are those in the next nearest neighbour position to the carboxylic acid carbons. This carbon component is still part of the aliphatic carbon peak, as the shift is not significant enough to be a defined peak. The experimental values for the percentage composition of carbons in each environment differ from the predicted values (Table 3-3). The composition values for the aliphatic carbon (centred on 285 eV) include the adventitious carbon which has the effect of decreasing the intensity of the β-shifted carbons (centred at 286 eV) and increasing the intensity of the aliphatic carbons. Despite deviation from the theoretical ideal

values (detailed in Table 3-3), the experimental values do support the idea that there are 3 distinct carbon environments present in the sample, indicating there is a coating of DDSD present on the microspheres.

3.3.6 Extrusion of composites

Samples were extruded using a tabletop twin-screw mini extruder, with a 5 g capacity. A custom die was designed in order to produce hollow tubes. PU pellets were used as received and glass microspheres were physically mixed with the pellets before being added to the hopper. The chosen processing temperature was 185 ºC due to the softening point of PU. Additionally, this temperature is lower than the decomposition temperatures of the matrix and dispersant. The speed of extrusion was varied to find optimal conditions for producing consistent, transparent tubes. At higher temperatures, up to 195 ºC, the resulting samples obtained were slightly darker and some yellow in colour, attributed to burning of the polymer. Burning of the polymer also occurred when the composite mixture was held in the extruder before processing. A further observation was that during extrusion the tube diameter could vary depending on the pressure used to push the starting materials into the hopper.

It was determined that the melting of PU pellets was relatively slow so for future samples, the PU pellets were ground up to decrease the particle size. Smaller particles melted more quickly in the extruder, decreasing the time held at elevated temperature which could reduce burning and inconsistencies in the tubes. Additionally, smaller PU pellets were more easily mixed with the glass microspheres, meaning the starting materials mixture was more homogeneous. The cavity inside the extruder does not facilitate good mixing so the feed materials were combined before being added. This

should result in a good distribution of glass microspheres throughout the tube, particularly the dispersant coated ones.

After processing the composite, backscatter ESEM was performed (Jerry Contreras, Virginia Tech). Defects arising from the extrusion procedure can be seen in Figure 3-15.

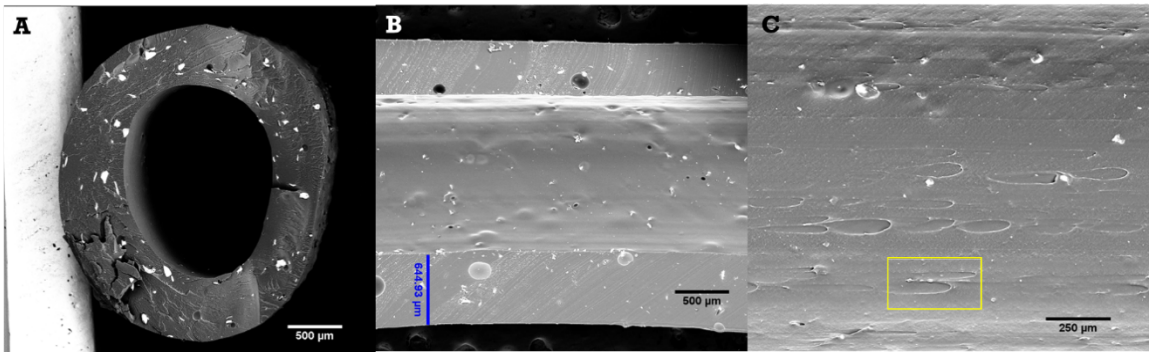


Figure 3-15. Backscatter ESEM images of extruded tube samples showing common defects. A – cross section of tube after cryofracture, showing fractured particles. B – inner lumen of tube after blade sectioning, showing shear defects. C – tube sample after sectioning, showing air pockets in the wall. Data collected by Jerry Contreras (Virginia Tech) and used with permission.

In Figure 3-15 image A, it can be seen that some glass microspheres have been crushed or fractured during processing. This reduces the density of the echogenic particles and is likely to result in a reduced US response. Image B shows air bubbles and shear marks in the polymer matrix. After exiting the extruder, the tube is still molten and can be pulled or stretched to decrease the lumen size. However, inconsistent force can lead to an inconsistent, varying tube diameter and wall thickness and can cause defects as shown here. The thickness of the wall is inconsistent across the tube. Image C shows voids in the wall of the tube. These are

attributed to the speed of processing – in this case it is thought the precursors were forced through the extruder too quickly, allowing air bubbles to become trapped in the molten polymer. Air voids, particularly on the surfaces of the tube, are not desirable. These contribute to increased surface roughness and could also provide a potential site for bacterial biofilm formation which needs to be avoided. The defects described were particularly pertinent in samples containing uncoated glass microspheres. The presence of air bubbles could actually contribute to the echogenicity of the tubes. However, they were not consistent or evenly distributed so are not considered advantageous in this study.

An SEM image of an optimal extruded sample containing no obvious defects is shown in Figure 3-16. Optimal samples showed no crushed particles, rather that they are intact and not agglomerated. Additionally, there should be a good dispersion of P40 throughout the tube.

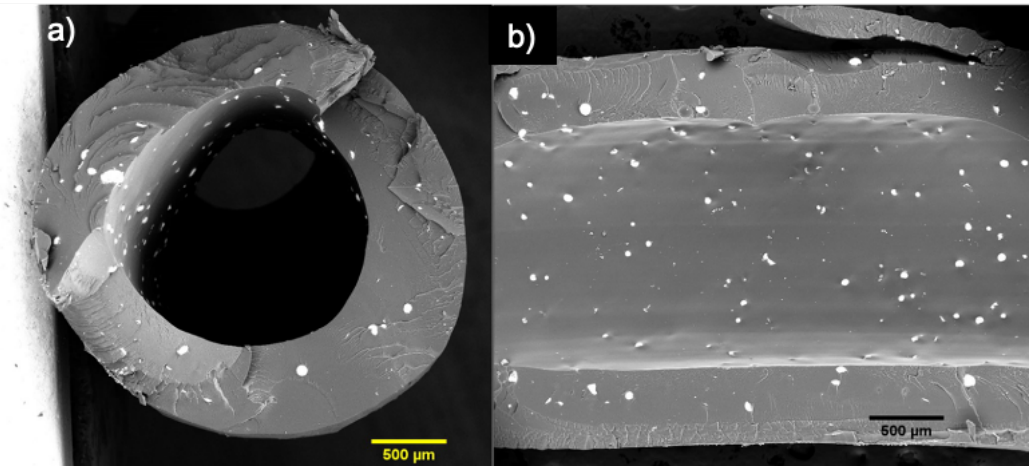


Figure 3-16. Backscatter ESEM images of optimal extrusion sample. a) - cross section and b) - lengthwise views of sample after cryofracture. Data collected by Jerry Contreras (Virginia Tech) and used with permission.

It can be seen from the SEM images that there is little agglomeration of particles in the tube sample. The outer wall of the tube is a uniform thickness and does not appear to contain air bubbles or other defects described previously such as shear marks.

3.3.6.1 TGA of composites

Tube samples containing 0, 1, 3 and 5 wt% of uncoated P40 microspheres were fabricated and sectioned according to Figure 3-17.

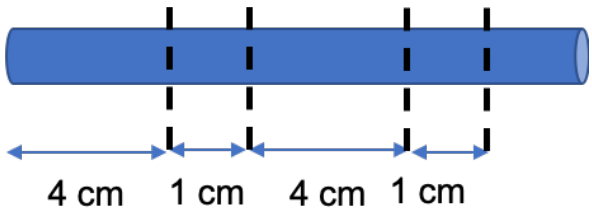


Figure 3-17. Sectioning of extruded tubes for analysis.

The smaller sections of the tube (1 cm) were analysed using TGA, the hypothesis being the weight loss could be attributed to the polyurethane matrix only, as the glass was found to be stable up to 600 ºC. If dispersion of glass microspheres was optimal, each section of the tube should exhibit the same decomposition behaviour. The 4 cm sections of tube were for ultrasound imaging (section 3.3.7).

Firstly, PU tubes containing no added P40 microspheres were analysed. Theoretically, there should be 100 % weight loss attributed to degradation of polyurethane. An example of a thermogram obtained for a sample of extruded PU tube is shown in Figure 3-18.

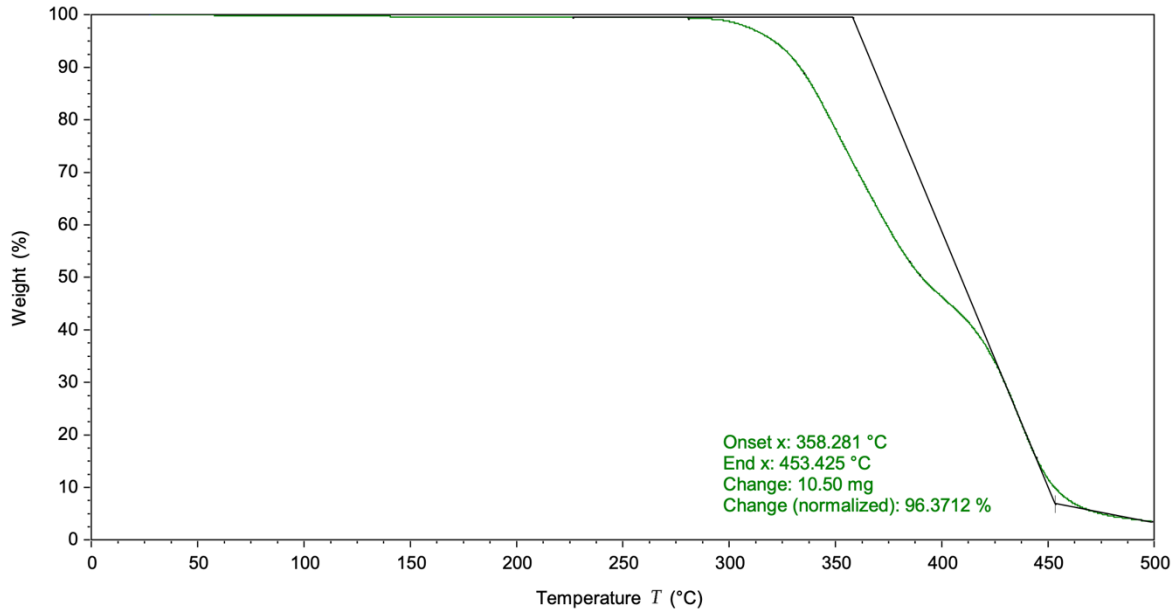


Figure 3-18. Example thermogram for extruded PU tube sample.

The onset temperature of degradation was found to be approx. 360 ºC, which is similar to previously determined value for a sample of the matrix polymer pellets as-received (section 3.3.3). The TGA results for six 1 cm PU tube sections were analysed and the average weight loss for these samples was determined to be 96 %.

TGA was then performed on tube samples containing P40 microspheres and compared to the plain PU tubes. The average weight loss for six samples at each P40 loading was obtained and is summarised in Table 3-4.

Table 3-4. TGA results of extruded tube samples.

wt% P40	Theoretical wt loss (%)	Average wt loss (%)	Discrepancy (%)	Standard deviation
0	100	96	4	1.2
1	99	94	5	1.2
3	97	94	3	1.0
5	95	93	2	1.4

The average weight loss for the 1 wt % samples was hypothesised to be 99 %, since the P40 particles are thermally stable up to 600 ºC. However, since the initial results showed that PU matrix does not fully decompose, the predicted weight loss estimate was adjusted to 95 %. The experimental average weight loss of these samples was found to be 94 % with a standard deviation of 1.2 %.

For the tube samples containing 3 wt% P40, the average weight loss *via* TGA was found to be 94 %, the same value as was found in the 1 wt% samples. The standard deviation in this case was determined to be ±1.0 %. Samples containing 5 wt% P40 showed an average weight loss of 93 %, which is the closest to predicted values but still has some deviation.

It is clear that in this case, TGA is not a sensitive enough technique to provide information on the composition of small tube sections. All results obtained were within error of each other and cannot be considered significant.

3.3.7 Imaging of composites

The US imaging of hollow tubes with varying wt% of dispersant coated microspheres was performed at Children's National Medical Center (Washington DC, USA). Imaging was performed using clinical US machines with handheld wands. To imitate the conditions in the body, a tube sample was placed in a water-filled latex tube (artery mimic) and put into a tissue mimic. The device will be implanted inside the body so it's important that it can be imaged through a few cm of tissue. The mimic also causes noise or scattering of the US signal which is more realistic and comparable to the body environment. Tube samples of approx. 4 cm length and 3 mm diameter were imaged and compared. Firstly, a plain PU tube was extruded, without any glass microspheres

to confirm a contrast agent was required for these to be US visible. This image is shown in Figure 3-19.

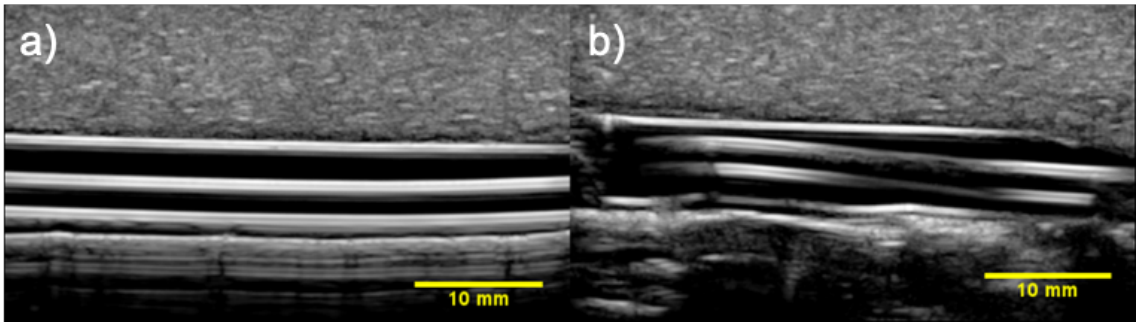


Figure 3-19. B-mode ultrasound images of a) commercially available catheter and b) extruded polyurethane tube.

The PU control tube can be distinguished from the soft tissue mimic, however the image is not clear and defined and may not be beneficial for diagnostic US purposes. The white lines represent the tube walls and black indicates the interior. Extrusion defects, such as air bubbles or roughness, may also contribute to the imaging artefacts observed. An image of a commercially used catheter is shown on the left for comparison. Again, this can be differentiated against the surrounding tissue, but the image contains shadowing, dark and bright areas, which could make determining position inaccurate.

To determine the optimum loading of glass microspheres, various samples were fabricated with different loadings. The addition of too many glass microspheres could increase surface roughness issues and prevent the device being transparent. A high loading of glass microspheres could also be detrimental to the mechanical properties of the device. Additionally, higher loadings of P40 were found to produce more defects in tube samples. Tubes which contained both uncoated and coated microspheres

were fabricated to determine whether the addition of dispersant has an effect on the image obtained i.e. whether the presence of dispersant reduced the contrast of images.

Firstly, tube samples containing 1, 3 or 5 wt% contrast agents were imaged in the same way as above Figure 3-20.

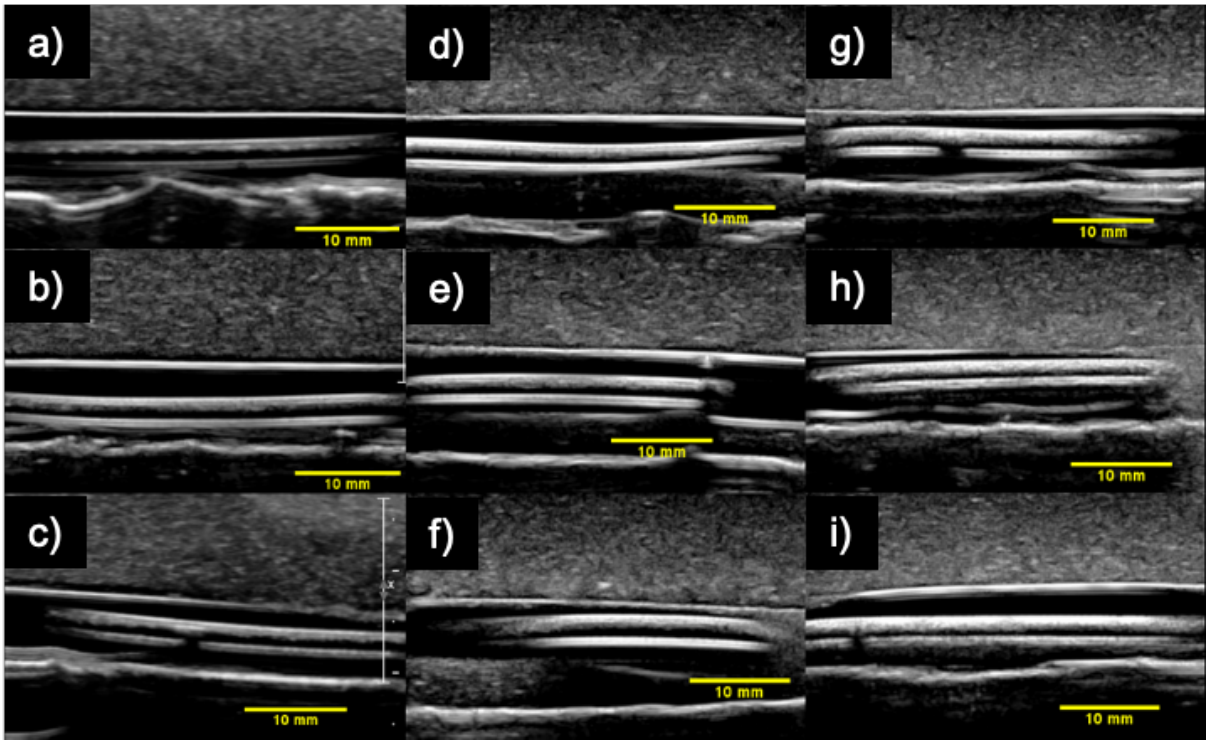


Figure 3-20. B-Mode US images of tubes with varying wt% of P40 microspheres. a, b, c - 1 wt%. d, e, f – 3 wt%. g, h, i – 5 wt%.

For the 1 wt% sample (Figure 3-20, a, b & c), the tube can be differentiated from the soft tissue surrounding it. White spots appear in the walls of the tube, which look different to the white signal caused by the PU. However, the shape is not clearly defined at the bottom of the image which could be attributed to attenuation of US signal due to defects. For the 3 wt% sample (d, e & f) the tube appears brighter and is more easily defined in comparison to the surrounding tissue. The white spots from P40 are

brighter in these samples compared to the 1 wt% tubes. The 5 wt% samples (g, h & i) are quite comparable to the 3 wt% samples, with the tube being clearly visible and distinguishable from the tissue mimic. There are some inconsistencies in the images, where dark spots appear, which can arise from attenuation of the US signal for example due to surface defects or air pockets. Another reason for these image artefacts is due to agglomeration of the contrast agent, which could cause increased scattering of US signal.

The next samples fabricated contained dispersant coated contrast agents, to overcome the unfavourable effects of agglomeration. The US images of samples containing 5 and 10 wt% DDSD coated P40 is shown in Figure 3-21.

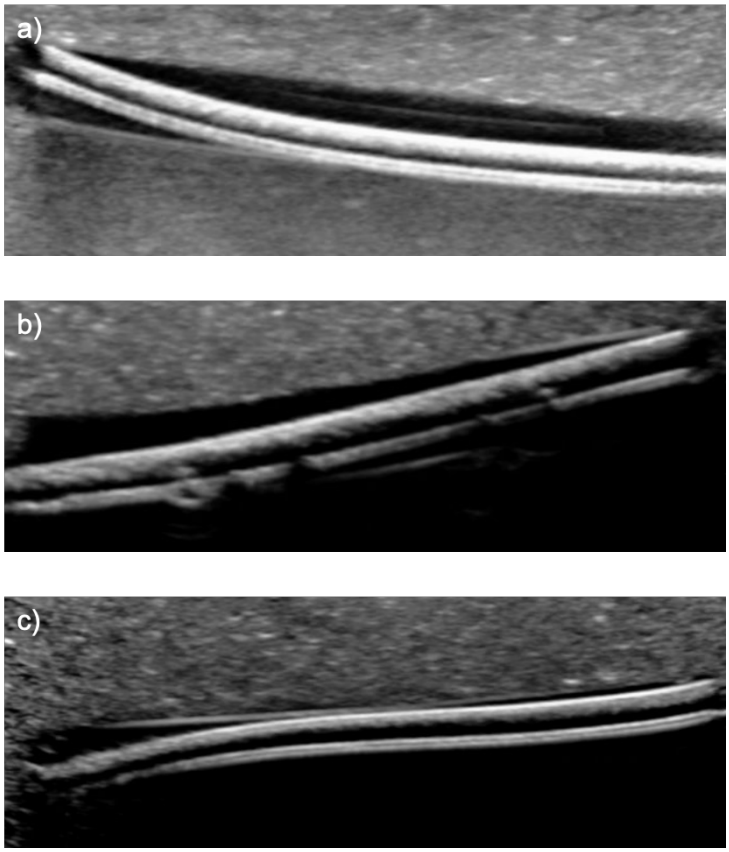


Figure 3-21. B-mode US images of extruded tubes containing P40-DDSD at a) 1 wt%, b) 5 wt% and c) 10 wt%.

The images obtained for the P40-DDSD tube samples indicate the contrast agent response was not drastically reduced by the presence of dispersant. Bright white features are clearly visible in each of the images and the tube can be differentiated from the surrounding tissue and artery mimics. In image b), there is some inconsistency in the signal observed where a dark spot is seen. This could be due to defects in the tube such as an air bubble.

3.4 Conclusions

The design and fabrication of an US visible, prototype medical device has been reported. A suitable method for applying a dispersant coating, comprised of a

commercially available material, to contrast agents was developed. In addition, a quick and simple test to confirm the attachment of commercially available dispersant was devised. The biphasic suspension test showed whether coating had been successful, then XPS was used to further confirm this.

Prototype medical devices containing echogenic contrast agents were fabricated *via* extrusion. TGA was explored as a method for determining dispersion of P40 microparticles throughout extruded tube samples but was not successful. The sensitivity of this technique was not good enough to differentiate between samples. Extruded tubes were imaged using SEM and US and compared to control devices. The SEM images showed the presence of defects in the matrix polymer and the microparticles that can arise during processing. For the US images, it was observed that the devices containing contrast agents were able to be visualised more clearly than the control devices. However, we still noticed imaging artefacts that were attributed to sub-optimal dispersion of contrast agent. It was concluded that addition of dispersant did not reduce ultrasound response significantly as tubes containing both uncoated and coated P40 both produced images with characteristic signals. The commercially available dispersant (DDSA) chosen was suitable for initial studies but to optimise the device to obtain better quality ultrasound images, it was decided to design bespoke dispersants that would have enhanced compatibility with the polymer matrix. The design and synthesis of these dispersants is discussed in Chapter 4.

3.5 References

1. Amerasekera, S. S. H., Jones, C. M., Patel, R. & Cleasby, M. J. Imaging of the complications of peripherally inserted central venous catheters. *Clinical*

Radiology **64**, 832–840 (2009).

2. Harrod, M. *et al.* Challenges for Nurses Caring for Individuals with Peripherally Inserted Central Catheters in Skilled Nursing Facilities. *J. Am. Geriatr. Soc.* **64**, 2059–2064 (2016).
3. Álvares, B. R. *et al.* Normal findings on chest x-rays of neonates NORMAL FINDINGS ON CHEST X-RAYS OF NEONATES*. *Radiol Bras* **39**, 435–440 (2006).
4. Cotogni, P. *et al.* Peripherally inserted central catheters in non-hospitalized cancer patients: 5-year results of a prospective study. *Support. Care Cancer* **23**, 403–409 (2015).
5. Kleinerman, R. A. Cancer risks following diagnostic and therapeutic radiation exposure in children. *Pediatr. Radiol.* **36**, 121–125 (2006).
6. Land, C. E. Estimating cancer risks from low doses of ionizing radiation. *Science* **209**, 1197–1203 (1980).
7. Ron, E. Cancer risks from medical radiation. in *Health Physics* **85**, 47–59 (2003).
8. Trerotola, S. O., Thompson, S., Chittams, J. & Vierregger, K. S. Analysis of Tip Malposition and Correction in Peripherally Inserted Central Catheters Placed at Bedside by a Dedicated Nursing Team. *J. Vasc. Interv. Radiol.* **18**, 513–518 (2007).
9. Stevenson, A. T. *et al.* Fabrication and characterization of medical grade polyurethane composite catheters for near-infrared imaging. *Biomaterials* **54**, 168–76 (2015).
10. Marshall, M. V *et al.* Near-Infrared Fluorescence Imaging in Humans with Indocyanine Green: A Review and Update. *Open Surg. Oncol. J.* **2**, 12–25 (2010).

11. Chapter 10 Dispersion of particles in liquids. in *Studies in Interface Science* **20**, 517–558 (Elsevier, 2005).

12. Clayfield, E. J. & Lumb, E. C. A theoretical approach to polymeric dispersant action I. Calculation of entropic repulsion exerted by random polymer chains terminally adsorbed on plane surfaces and spherical particles. *J. Colloid Interface Sci.* **22**, 269–284 (1966).

13. Boisvert, J. P., Persello, J., Castaing, J. C. & Cabane, B. Dispersion of alumina-coated TiO2 particles by adsorption of sodium polyacrylate. *Colloids Surfaces A Physicochem. Eng. Asp.* **178**, 187–198 (2001).

14. Hirtzei, C. S. & Rajagopalan, R. Invited review stability of colloidal dispersions. *Chem. Eng. Commun.* **33**, 301–324 (1985).

15. Abou Neel, E. A., Pickup, D. M., Valappil, S. P., Newport, R. J. & Knowles, J. C. Bioactive functional materials: a perspective on phosphate-based glasses. *J. Mater. Chem.* **19**, 690–701 (2009).

16. Knowles, J. C. Phosphate based glasses for biomedical applications. *J. Mater. Chem.* **13**, 2395 (2003).

17. Ahmed, I., Lewis, M., Olsen, I. & Knowles, J. C. Phosphate glasses for tissue engineering: Part 2. Processing and characterisation of a ternary-based P2O5–CaO–Na2O glass fibre system. *Biomaterials* **25**, 501–507 (2004).

18. Ahmed, I. *et al.* Composites for bone repair: phosphate glass fibre reinforced PLA with varying fibre architecture. *J. Mater. Sci. Mater. Med.* **22**, 1825–1834 (2011).

19. Hossain, K. M. Z., Patel, U. & Ahmed, I. Development of microspheres for biomedical applications: a review. *Prog. Biomater.* **4**, 1–19 (2014).

20. Brow, R. K. Review: the structure of simple phosphate glasses. *J. Non. Cryst.*

Solids **263**–**264**, 1–28 (2000).

21. Ahmed, I., Shaharuddin, S. S., Sharmin, N., Furniss, D. & Rudd, C. Core/Clad Phosphate Glass Fibres Containing Iron and/or Titanium. *Biomed. Glas.* **1**, (2015).
22. Ahmed, I., Ready, D., Wilson, M. & Knowles, J. C. Antimicrobial effect of silver-doped phosphate-based glasses. *J. Biomed. Mater. Res. Part A* **79A**, 618–626 (2006).
23. Liang, J. Z. & Li, R. K. Y. Measurement of Dispersion of Glass Beads in PP Matrix. doi:10.1106/EJRE-YF61-YNY9-70X3
24. Liu, L., Funamoto, K., Tanabe, M. & Hayase, T. Microscopic observation of glass bead movement in soft tissue-mimicking phantom under ultrasound PW mode scanning. *J. Med. Ultrason.* **42**, 59–63 (2014).
25. Funamoto, K., Yamashita, O. & Hayase, T. Poly(vinyl alcohol) gel ultrasound phantom with durability and visibility of internal flow. *J. Med. Ultrason.* **42**, 17–23 (2014).
26. Andrade, J. D. X-ray Photoelectron Spectroscopy (XPS) BT - Surface and Interfacial Aspects of Biomedical Polymers: Volume 1 Surface Chemistry and Physics. in *Surface and Interfacial Aspects of Biomedical Polymers* 105–195 (Springer US, 1985). doi:10.1007/978-1-4684-8610-0_5
27. Fadley, C. S. X-ray photoelectron spectroscopy: Progress and perspectives. *J. Electron Spectros. Relat. Phenomena* **178**–**179**, 2–32 (2010).
28. X-ray Photoelectron Spectroscopy: An introduction to Principles and Practices - Paul van der Heide - Google Books.
29. *Surface and Interfacial Aspects of Biomedical Polymers*. *Surface and Interfacial Aspects of Biomedical Polymers* (Springer US, 1985). doi:10.1007/978-1-4684-

8610-0

30. NIST X-ray Photoelectron Spectroscopy (XPS) Database Main Search Menu. Available at: https://srdata.nist.gov/xps/main_search_menu.aspx.

31. Ihnatsenka, B. & Boezaart, A. P. Ultrasound: Basic understanding and learning the language. *Int. J. Shoulder Surg.* **4**, 55–62 (2010).

32. Ng, A. & Swanevelder, J. Resolution in ultrasound imaging. *Contin. Educ. Anaesth. Crit. Care Pain* **11**, 186–192 (2011).

33. Yang, J. *et al.* Silica Shells/Adhesive Composite Film for Color Doppler Ultrasound Guided Needle Placement. *ACS Biomater. Sci. Eng.* **3**, 1780–1787 (2017).

34. Yang, J. *et al.* Ultrasound responsive macrophase-segregated microcomposite films for in Vivo biosensing. *ACS Appl. Mater. Interfaces* **9**, 1719–1727 (2017).

35. Nakagawa, K., Kamiya, T., Arakawa, K., Akiyama, S. & Sakai, K. Objective and subjective comparison of the visibility of three echogenic needles and a nonechogenic needle on older ultrasound devices. *Acta Anaesthesiol. Taiwanica* **53**, 1–6 (2015).

36. Chen, M. *et al.* In-situ polymerisation of fully bioresorbable polycaprolactone/phosphate glass fibre composites: In vitro degradation and mechanical properties. *J. Mech. Behav. Biomed. Mater.* **59**, 78–89 (2016).

37. Hossain, K. M. Z., Hasan, M. S., Felfel, R. & Ahmed, I. Development of phosphate-based glass fibers for biomedical applications. in *Hot Topics in Biomaterials* 104–115 (Future Science Ltd, 2014). doi:10.4155/ebo.13.352

38. Haque, P. *et al.* Interfacial properties of phosphate glass fibres/PLA composites: Effect of the end functionalities of oligomeric PLA coupling agents. *Compos. Sci. Technol.* **70**, 1854–1860 (2010).

Chapter 4 - The design and synthesis of dispersants for ultrasound visible medical devices.

4.1 Aims and objectives

The aim for this section of work was to build on successful prototype medical devices fabricated and reported in Chapter 3, whereby it was found that commercially available materials could be used as suitable dispersants. However, we noticed that small voids or air pockets were forming around the glass microsphere contrast agent after extrusion processing, which affected the quality of ultrasound images and suggested optimal dispersion throughout the device was not obtained. In an attempt to overcome this issue, dispersants which had a similar structure to the matrix polymer were designed. These were termed second-generation dispersants and were employed in the same coating and extrusion procedures as described in Chapter 3 to form hollow tubes.

4.2 Introduction

4.2.1 Thiols as chain transfer agents

The use of thiols as CTAs is well known, they can be considered the most commonly used CTAs for radical polymerisations.[1] Reported C_s values for common thiols range from 0.1 – 2.7 for polymerisation of MMA.[2] Their chain transfer ability is attributed to the weak S–H bond, which can readily dissociate by terminating a propagating polymer chain and in turn produce a thiyl radical species. This radical species can be used to initiate monomers and thus some polymer products will contain CTA

functionality. For this reason, this method can be utilised to obtain end-functionalised polymer products. The proportion of CTA-capped polymers can vary based on reaction conditions. Analysis of end group functionality can be assessed by techniques such as NMR and mass spectrometry.

4.2.2 Thiol-ene

Thiol-ene click chemistry is the reaction between a thiol (S-H) and an 'ene' molecule containing C=C double bond.[3] The criterion for click reaction were proposed by Sharpless and include; a reaction that is high yielding, generates inoffensive by-products and has a simple experimental set-up.[4] There are two types of thiol-ene chemistry commonly used; radical initiated and Michael addition.[5] A simple reaction scheme for radical initiated thiol-ene is shown in Figure 4-1.

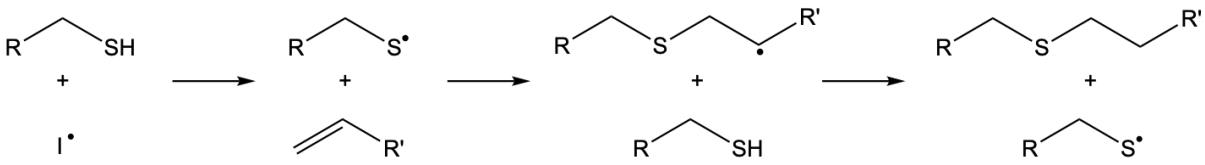


Figure 4-1. General thiol-ene scheme.

The radical initiator forms a thiyl radical, which attacks the ene-molecule, transferring the activity. Finally, a hydride is abstracted from the chain transfer agent to form another initiated CTA and terminate the thiol capped ene-molecule. Thiol-ene has reported as a good post-functionalisation route for vinyl-terminated polymers.[6]

4.2.3 Oligomers as dispersants

Polymers and oligomers can be used as dispersants provided they possess suitable head and tail groups. The head group is typically an anchor point to the particle to be

dispersed. The tail group protrudes away from the particle and prevents particles agglomerating *via* steric repulsion between chains. The use of oligomers as dispersants is widely employed commercially, with numerous patents obtained.[7–9] Industries such as automotive, personal care and laundry all employ polymeric molecules as lubricants, surfactants and detergents.

4.3 Results and discussion

To build on the previous results obtained in Chapter 3 where commercially available materials were determined to be suitable dispersants for contrast agents, the next stage was to design and synthesise tailored dispersants. The criteria for dispersants was as follows:

- Head group with affinity for glass microspheres
- Tail group to provide steric dispersion between particles.

4.3.1 MMA_2-3MPA

The first oligomeric dispersant was based on MMA, due to its relatively simple structure it is a suitable model monomer to base further studies on. Firstly, MMA_2 was synthesised *via* CCTP, using PhCoBF as a catalytic chain transfer agent (see Chapter 2 for reaction conditions and methodology). PhCoBF is a very efficient CTA for the polymerisation of MMA, further CCTP explanation and results are discussed in Chapter 5. After synthesis and purification of MMA_2, radical initiated thiol-ene click chemistry was attempted as a post-functionalisation method (Figure 4-2).

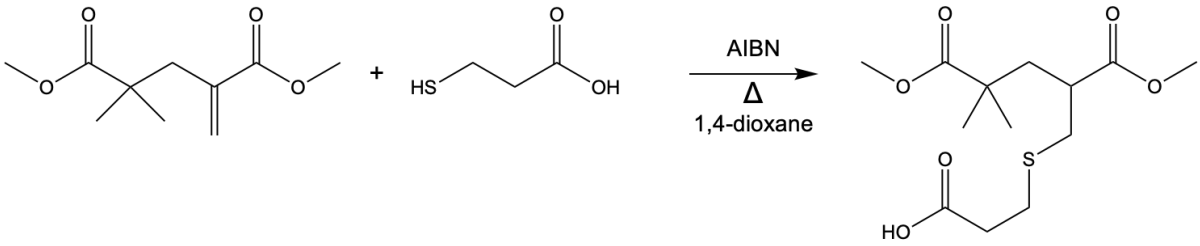


Figure 4-2. Thiol-ene reaction between MMA_2 and 3MPA.

3-mercaptopropionic acid (3MPA) was the thiol CTA chosen for this study (**Error! R eference source not found.**) as it contains a carboxylic acid group which could be a suitable head group for the P40 microparticle contrast agents.

Table 4-1. Thiol-ene reactions of MMA_2 (3 mmol) and 3MPA (3 mmol) with AIBN (0.6 mmol) in 1,4-dioxane (10 mL) at varying temperatures.

Entry	Temperature (ºC)	Conversion product (%)[a]	Conversion alkene (%)[a]
1	60	7	9
2	70	8	13
3	80	11	29
4	90	12	31

[a] determined by ^{1}H NMR

mol equivalents MMA_2:3MPA:AIBN 1:1:0.2

5 hours

The highest conversion to product reached by any of these reactions was 12 %. There is a very weak correlation between the conversion and temperature although no definitive conclusions can be drawn. When contrasting Entry 1 (60 ºC) to Entry 4 (90 ºC) it is seen that the higher temperature reaction yields

a slightly higher conversion. However, these values are all within error of ^{1}H NMR (±5 %) and cannot be considered significant.

The following series of reactions were carried out using microwave heating (MWH) techniques instead of conventional heating (CH) i.e. oil bath, methods. The use of microwaves as an alternative heating method is discussed in Chapter 5.

Table 4-2. Thiol-ene reactions of MMA_2 (3 mmol) and 3MPA (3 mmol) with AIBN (0.6 mmol) in 1,4-dioxane (10 mL) at varying temperatures using microwave heating.

Entry	Temperature (ºC)	Conversion product (%)[a]	Conversion alkene (%)[a]
1	60	9	12
2	70	6	11
3	80	10	23
4	90	25	33

[a] determined by ^{1}H NMR

mol equivalents MMA_2:3MPA:AIBN 1:1:0.2

5 hours

In these reactions, an increase in temperature resulted in an increase in conversion as previously seen and expected. A conversion difference of 16 % between reactions performed at 60 ºC and 90 ºC was observed. In comparison to the analogous CH reactions, this is a larger and more significant change. This tentatively shows that the application of MWH could increase the yield of the thiol-ene product formed. However, thiol-ene reactions are typically much higher yielding since they are considered to be ‘click’ reactions.

Using the conditions described for MMA_2, a further set of reactions was carried out to determine the reason behind the low conversions obtained. These reactions used 1-heptene as the 'ene' molecule instead of MMA_2. At temperatures ranging from 60 ºC – 90 ºC, the reaction between 1-heptene and 3MPA proceeded to 100% conversion to product. This suggests the conditions are suitable to promote the thiol-ene reaction in this case and confirmed that conditions for MMA_2 need to be further optimised. It is possible that the reason the conversions are not as high as those in the 1-heptene reactions is due to the higher steric bulk around the double bond of MMA_2, making it less susceptible to thiyl insertion.

Conditions were modified and the following series of reactions were carried out to obtain MMA_2-3MPA (**Error! Reference source not found.**).

Table 4-3. Bulk (no solvent) thiol-ene reactions between MMA2 (11 mmol) and 3MPA (11 mmol) with varying AIBN concentration and reaction time.

Entry	AIBN (mmol)	Temperature (ºC)	Reaction time (hours)	Conversion (product)[a]	Conversion (alkene)[a]
1	0.11	80	5	10	14
2	0.58	80	5	34	39
3	0.11	65	24	60	60
4	0.58	65	24	60	70

[a] determined by ^{1}H NMR

mol equivalents for entries 1 & 3 MMA_2:3MPA:AIBN 1:1:0.01

mol equivalents for entries 2 & 4 MMA_2:3MPA:AIBN 1:1:0.05

Firstly, reactions were carried out at 80 ºC, with the loading of initiator AIBN varied from 0.01 to 0.05 mol eq. wrt MMA_2 and thiol. The conversion reached in these two

reactions is higher than the previous reaction conditions yielded but is nevertheless still low. The difference between conversion to product and alkene bond is 4 % in both cases, which is not considered to be significant although could indicate some side reactions are also occurring. When the reaction temperature was decreased to 65 ºC, the time was increased to 24 hours due to the temperature dependent half-life of AIBN.

Table 4-4. Thiol-ene reactions between MMA2 (10 mmol) and 3MPA (10 mmol).

Entry	AIBN (mol eq.)	Temperature (ºC)	Conversion (%)[a]		Solv/bulk
			5 hours	24 hours	
1	0.01	80	32	48	5 ml solv
2	0.01	80	43	59	bulk
3	0.02	80	64	77	bulk
4*	0.02	80 (MWH)	64	-	bulk

[a] determined by ^{1}H NMR

* denotes MWH reaction, mmol quantities 25:25:0.61

mol equivalents for entries 1 & 2 MMA_2:3MPA:AIBN 1:1:0.01

mol equivalents for entries 3 & 4 MMA_2:3MPA:AIBN 1:1:0.02

When considering the reactions in this series, it is further confirmed that the presence of solvent does not have a beneficial effect. When comparing both the 5 hour and 24 hour conversions for entries 1 & 2, it can be seen that the bulk reaction yielded a higher amount of product over the duration of the reaction. A difference of 16 % conversion was observed, with the bulk reaction reaching 59 % product. For the subsequent reactions, the AIBN loading was increased from 0.01 to 0.02 mol eq. Firstly, for the conventional heated reaction, entry 3, a high conversion of 77 % was reached after 24 hours, with 64 % conversion after 5 hours. Using the same conditions but employing microwave heating instead, entry 4, the reaction reached the same

conversion after 5 hours. Due to safety reasons, MWH reactions could not be performed for the same duration as CH reactions and so only the 5 hour conversion was obtained.

4.3.2 Synthesis of oligomers

Thiol-ene reactions on vinyl terminated oligomers were difficult to optimise and were not high yielding. The initial results obtained were for MMA_2, so optimisation of the reaction would be required for each new oligomer. Furthermore, a research project run within the group aimed to use CCTP to synthesise oligomers of interest to this project. It was decided that it would be advantageous to pursue using thiols as CTAs, as a suitable one-step method to end functionalised oligomers. Therefore, the next results presented are attempts at synthesising a suitable oligomeric dispersant *via* the use of thiols as chain transfer agents. It was decided to employ thiols as CTAs because the mechanism of this control method leaves a functional group attached to some of the product end groups. By changing the thiol CTA, the end functionality can be changed. It was decided to use two thiols that contained carboxylic acid moieties. The acid group was thought to be a suitable head group for attachment to the glass microsphere contrast agents. 3-mercaptopropionic acid (3MPA) and mercaptosuccinic acid (MSA) (Figure 4-3) were used to control the polymerisation of meth/acrylate monomers of interest.

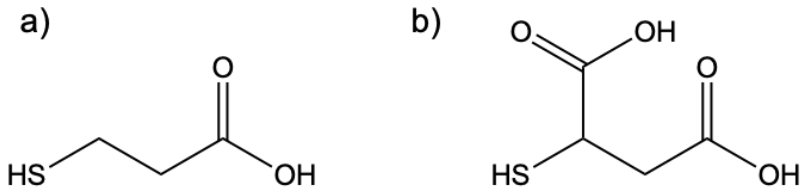


Figure 4-3. Structures of thiol CTAs a) 3-mercaptopropionoic acid and b) mercaptosuccinic acid.

4.3.2.1 MMA oligomers

Initial reactions were conducted using MMA as the monomer to determine the approximate concentration of thiol required to produce oligomers. MMA is a useful 'model monomer' and further studies can be based upon results obtained with the simple methacrylate. A series of reactions was carried out to find optimal conditions for using 3MPA as a CTA to produce oligomers (Table 4-5).

Table 4-5. Polymerisation of MMA using varying concentrations of 3MPA as CTA.

Entry	Thiol (mol eq)	Conversion (%)[a]	M_n (g mol^{-1})[b]	Đ[b]
1	1.2	90	4500	1.3
2	2.3	91	1200	1.4
3	3.5	85	1100	1.3
4	4.6	95	1200	1.4
5	5.8	93	1400	1.3

Reaction conditions – MMA (2 mL, 1.89 mmol), cyclohexanone (2mL), 3MPA (mol eq. relative to MMA) AIBN (0.5 wt% wrt MMA), 80 ºC, 5 hours

[a] determined by ^{1}H NMR [b] determined by GPC

3MPA performed as a good CTA in the conditions described. A trend was observed in which as the CTA concentration was increased, the molecular weight of product

obtained decreased. However, the M_n values for entries 2, 3, 4 & 5 were all relatively similar and ranged between 1100 and 1400 g mol^{-1} suggesting there is no need to increase the concentration of thiol above 2.3 (entry 2) as there is not a significant difference. The dispersity values obtained were between 1.3 –1.4, indicating 3MPA controlled the reaction well in all cases.

The next group of reactions employed mercaptosuccinic acid (MSA) as a CTA for the polymerisation of MMA (Table 4-6).

Table 4-6. Polymerisation of MMA using varying concentrations of MSA as CTA.

Entry	Thiol (mol)	Conversion (%)[a]	M_n (g mol^{-1})[b]	Đ[b]
1	1.2	95	400	6.4
2	2.3	96	700	4.2
3	3.5	95	600	3.7

Reaction conditions – MMA (2 mL, 1.89 mmol), cyclohexanone (2mL), MSA (mol eq. relative to MMA), AIBN (0.5 wt% wrt MMA), 80 ºC, 5 hours

[a] determined by ^{1}H NMR [b] determined by GPC

These results show MSA is less efficient as a CTA than the previous results obtained with 3MPA. There could be a number of reasons for this; firstly, MSA is a solid which is insoluble in MMA monomer and due to the high concentrations trialled in these experiments it was only partially soluble in the cyclohexanone solvent. It is clear from the high dispersity values that the reactions were not controlled. High dispersity values also affect M_n value obtained, since it is a number average measurement and can be skewed by polymers of widely varying chain lengths.

4.3.2.2 DEGMA oligomers

Di(ethylene glycol) methacrylate (DEGMA) was the next selected monomer for dispersant synthesis. This is due to the molecular structure of its pendent group, which is similar to that of polyurethane, the polymer matrix for medical device fabrication. A summary of DEGMA polymerisation results using 3MPA as a CTA is shown in Table 4-7.

Table 4-7. Polymerisation of DEGMA using varying concentrations of 3MPA as CTA.

Entry	Thiol (mol eq)	Conversion (%)[a]	M_n (g mol^{-1})[b]	Đ[b]
1	1.2	96	3000	1.4
2	2.3	95	1600	1.4
3	3.5	97	1300	1.4
4	4.6	96	1100	1.3
5	5.8	95	1000	1.3

Reaction conditions – DEGMA (2 mL, 1.09 mmol), cyclohexanone (2mL), 3MPA (mol eq. relative to DEGMA), AIBN (0.5 wt% wrt DEGMA), 80 ºC, 5 hours

[a] determined by ^{1}H NMR [b] determined by GPC

At all concentrations of 3MPA utilised in reactions in Table 4-7, oligomers were produced with narrow molecular weight dispersity values. The dispersity values ranged from 1.3 – 1.4 and all reactions reached over 95 % conversion. For comparison, reactions were performed with MSA as a CTA. This is shown in Table 4-8.

Table 4-8. Polymerisation of DEGMA using varying concentrations of MSA as CTA.

Entry	Thiol (mol)	Conversion (%)[a]	M_n (g mol^{-1})[b]	Đ[b]
1	1.2	97	4000	1.5
2	2.3	95	2700	1.3
3	3.5	96	2200	1.2

Reaction conditions – DEGMA (2 mL, 1.09 mmol), cyclohexanone (2mL), MSA (mol eq. relative to DEGMA), AIBN (0.5 wt% wrt DEGMA), 80 ºC, 5 hours

[a] determined by ^{1}H NMR [b] determined by GPC

In comparison to the previously obtained results in section 4.3.2.1 for MMA, it can be seen that MSA is a better CTA for the polymerisation of DEGMA. The dispersity values obtained in these reactions are below 1.5 which is considered typical of a controlled reaction. Conversion was not compromised by the high concentration of thiol, with values of 95 – 97 % obtained in this series.

4.3.2.3 PEGMA

Following results obtained for MMA and DEGMA, the next monomer selected for dispersant synthesis was poly(ethylene glycol) methacrylate (PEGMA). Its molecular structure is similar to that of the soft block of the matrix PU and thus should be compatible and a suitable tail group. A low degree of polymerisation was targeted and was achieved by utilising thiols as chain transfer agents and by using a 2:1 ratio of solvent:monomer. This data is shown in Table 4-9.

Table 4-9. Polymerisation of PEGMA using thiols as CTA.

Entry	Thiol (mol eq.)	Conversion (%)[a]	M_n (g mol^{-1})[b]	DP (approx.)	Đ[b]
1	3MPA (0.75)	93	800	2	1.7
2	3MPA (0.4)	96	1500	4	1.9
3	MSA (0.75)	95	1800	5	1.4
4	MSA (0.56)	96	2600	7	1.4

Reaction conditions – PEGMA (M_n = 360 g mol^{-1}, 6 mL, 1.84 mmol), cyclohexanone (12mL), 3MPA or MSA (mol eq. relative to PEGMA), AIBN (0.5 wt% wrt PEGMA), 80 ºC, 5 hours

[a] determined by ^{1}H NMR [b] determined by GPC

Both thiols performed as excellent chain transfer agents for the reactions with PEGMA, with narrow dispersity values of 1.4 – 1.9 and low molecular weight oligomer products obtained. The conversion values obtained ranged from 93 – 96 %. At the same molar equivent, 3MPA performed morfe efficiently in these conditions, with a bigger reduction in molecular weight obtained.

4.3.2.4 EGDPE(M)A

Polymers and oligomers based on ethylene glycol dicyclopentenyl ether acrylate (EGDPEA) have been identified as possessing microbial anti-attachment properties.[10] This means films containing poly(EDGPEA) were shown to prevent accumulation of microorganisms, by creating an uninhabitable surface where bacteria cannot attach and hence multiply. Medical devices are often locations for biofouling. EGDPEA was chosen as a dispersant precursor in this study because of its interesting properties that are being investigated at UoN. Despite most of the contrast agents being embedded into the polymer matrix, some may reside near the surface of the inner or

outer wall. If it was decided to include a coating on the medical device, the compatibility between materials could be beneficial.

Reactions were performed using EGDPEA with 3MPA as CTA, the results of these are shown in Table 4-10.

Table 4-10. Polymerisation of EGDPEA using varying concentrations of 3MPA as a CTA.

Entry	Thiol (mol eq)	Conversion (%)[a]	M_n (g mol^{-1})[b]	Đ[b]
1	0.13	85	3000	1.5
2	0.26	96	1500	1.4
3	0.53	95	3100	2.66

Reaction conditions – EGDPEA (2 mL, 0.87 mmol), cyclohexanone (4 mL), 3MPA (mol eq. relative to EGDPEA), AIBN (0.5 wt% wrt EGDPEA), 80 ºC, 5 hours

[a] determined by ^{1}H NMR [b] determined by GPC

3MPA was a suitable CTA for producing low molecular weight oligomers of EGDPEA. These reactions were carried out in solvent at a ratio of 1:2 (monomer:solvent v:v) because it was found at lower solvent ratios the increase in viscosity during the reaction was drastic and cross linking was occurring. At the highest thiol concentration for this series, Table 4-10 entry 3, the dispersity value obtained is quite high. This means the distribution of molecular weights in the sample is varied and could be resulting in a high calculated M_n (3100 g mol^{-1}). The products obtained in reactions with lower thiol concentrations, entries 1 & 2, are suitable for the intended application.

For comparison, the methacrylate analogue of EGDPEA was also selected as a monomer to compare to the efficiency 3MPA in acrylate polymerisations (Table 4-11).

Table 4-11. Polymerisation of EGDPEMA using varying concentrations of 3MPA as CTA.

Entry	Thiol (mol eq)	Conversion (%)[a]	M_n (g mol^{-1})[b]	Đ[b]
1	0.14	94	3200	1.6
2	0.28	98	1600	1.4
3	0.57	88	1000	1.4

Reaction conditions – EGDPEMA (2 mL, 0.81 mmol), cyclohexanone (4 mL), 3MPA (mol eq. relative to EGDPEMA), AIBN (0.5 wt% wrt EGDPEMA), 80 ºC, 5 hours

[a] determined by ^{1}H NMR [b] determined by GPC

The results presented in Table 4-11 show that 3MPA is a good CTA for the polymerisation of EGDPEMA. All reactions reached high conversions, ranging from 88 – 98 %. Oligomeric products were obtained and all reactions had a narrow dispersity. The results obtained in this case were very similar to the analogous acrylate monomer indicating the efficiency of 3MPA is similar in both cases.

4.3.2.5 Overview of suitable dispersants

Results obtained so far have shown that chosen monomers can be successfully polymerised using thiol CTAs to produce oligomers in high yields. An overview of the structures of these oligomers is shown in Figure 4-4.

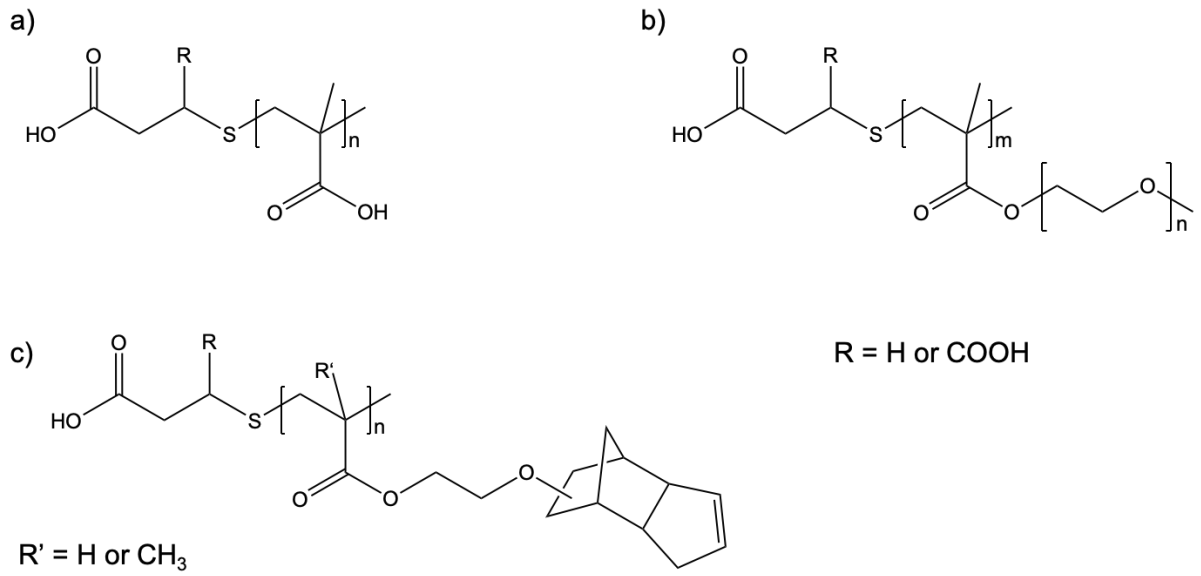


Figure 4-4. Structures of oligomers used as second-generation dispersants.

The oligomers chosen as second-generation dispersants shown in Figure 4-4 were based on the following monomers: a) MMA, b) If n = 2 – DEGMA, if n = 8 – PEGMA (M_n = 360), c) if R' = H – EGDPEA, if R' = CH_3 – EGDPEMA. For further investigation, certain reaction conditions for these monomers were selected and scaled up to produce larger quantities of dispersants.

Table 4-12. Overview of second-generation dispersants.

Entry	Monomer	Thiol (mol eq.)	M_n (g mol^{-1})[a]	Đ[a]
1	MMA	3MPA (0.06)	1700	1.5
2	EDGPEA	3MPA (0.13)	2500	1.5
3	EDGPEMA	3MPA (0.14)	2000	1.6
4	PEGMA	3MPA (0.75)	800	1.7
5	PEGMA	3MPA (0.40)	1500	1.9
6	MMA	MSA (0.10)	3700	1.2
7	EDGPEA	MSA (0.19)	3400	1.5
8	EDGPEMA	MSA (0.21)	4400	1.6
9	PEGMA	MSA (0.75)	1800	1.4
10	PEGMA	MSA (0.40)	2600	1.4

Reaction conditions – monomer (6 mL), cyclohexanone (12mL), 3MPA or MSA (mol eq. relative to monomer), AIBN (0.5 wt% wrt monomer), 80 ºC, 5 hours

[a] determined by GPC

These reactions were performed in a higher volume of solvent than those described in the previous sections (4.3.2.1 – 4.3.2.4). This was partly due to increasing the scale of the reaction, additional solvent would mitigate a thermal runaway. As a result of this, reactions were re-optimised to alter thiol concentrations to produce oligomers of the desired molecular weight. The ten dispersants shown in Table 4-12 were all produced in high conversions, above 90 %. For this reason, crude reaction mixtures were used for coating of P40 microparticles.

4.3.3 Coating of P40

The ten second-generation dispersants were used to coat P40 microparticles in a simple soaking procedure as described in Chapter 2. As mentioned in the previous

section, reactions to produce these dispersants all reached high conversion and as a result of this, the crude reaction mixtures were used in the P40 coating step. It is thought that the small amount of residual monomer did not affect the attachment of oligomers to P40 since the monomers did not contain the desired head group. To probe this, a solution of MMA monomer was made in cyclohexanone and coating procedure was carried out. The P40 obtained in this case did not pass the biphasic suspension test, i.e. the P40 settled to the bottom of the aqueous layer as was observed for uncoated P40. This further confirmed that purification of crude polymerisation solution was not necessary for successful coating.

4.3.4 XPS

XPS was performed on dispersant coated P40 samples to determine if the dispersant coating procedure had been successful.

4.3.4.1 P40-(MMA_2-3MPA)

The simplest dispersant based on molecular structure was used for XPS analysis. A sample of P40-(MMA_2-3MPA) was analysed to determine elemental composition and confirm presence of dispersant on the microparticle. The elemental composition obtained was from an average of six wide-scan spectra, which is shown in Table 4-13 with P40 for comparison.

Table 4-13. Elemental composition of P40-(MMA_2-3MPA) and P40 for comparison determined by XPS.

	Elemental composition (mol%)							
	C	**O**	**P**	**Ca**	**Na**	**Mg**	**Si**	**S**
P40	20.6	49.3	14.8	3.6	6.4	3.9	1.4	0
P40-(MMA_2-3MPA)	32.0	37.5	9.8	3.4	2.0	11.2	2.2	1.9

The difference in elemental composition indicates there is MMA_2-3MPA present in the samples. The coated samples contained more carbon, 32 % in comparison to 21 %, which is due to the structure of the dispersant. Its molecular formula is $C_{13}H_{22}O_6S$. In the uncoated P40 there was no sulfur peak detected. However, the composition of the coated samples contains 1.9 % sulfur, further confirming the attachment. High-resolution scans were obtained for C 1s to probe the carbon environments within the sample (Figure 4-5).

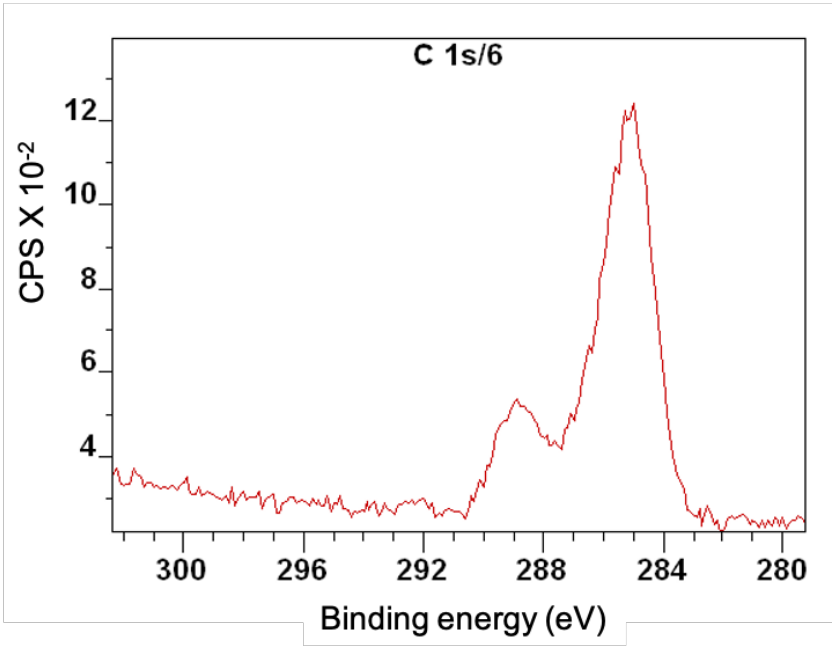


Figure 4-5. High resolution C 1s scan P40-(MMA_2-3MPA).

The high-resolution spectra showed there were multiple carbon environments present in the sample. The peaks were deconvoluted and mathematical fittings were applied to find the relative composition.

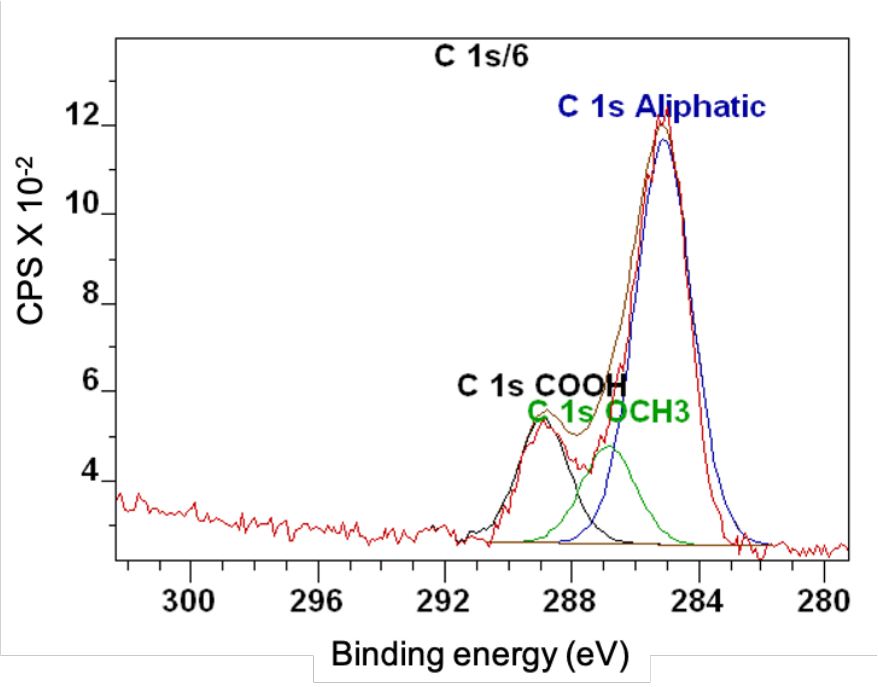


Figure 4-6. High-resolution C1s scan with components fitted. Red – original spectra, blue – aliphatic component, green – OCH_3 component, black – COOH component.

The high-resolution scan peaks can be deconvoluted into three peaks as shown in Figure 4-6. The most intense is attributed to the aliphatic carbons, centred at 285 eV. The other two distinct environments were a carboxylic acid component (COOH) and alkoxy group (CH_3). To determine the intensity of each type of carbon environment, the structure of the dispersant was considered, and its carbon environments assigned as shown in Figure 4-7.

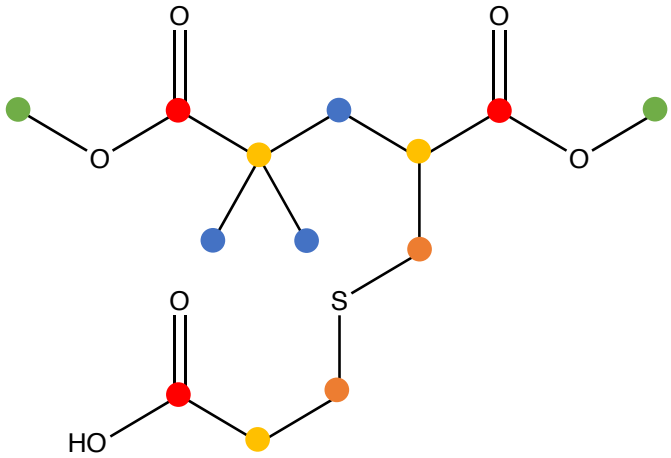


Figure 4-7. Structure of MMA_2-3MPA with different carbon environments labelled in accordance with Table 4-14.

The five different carbon environments present in MMA_2-3MPA are indicated by solid coloured dots. These environments are assigned in Table 4-14.

Table 4-14. High-resolution C 1s scan data and theoretical composition.

Environment	Key	Carbon (#)	Carbon composition theoretical (%)	Carbon composition experimental (%)	Peak position of fitting (eV)
O=C–OH	●	3	23	18	288.9
H_3C–O	●	2	15	15	286.8
'β-shifted'	●	3			
C–S	●	2	62	66	285.0
Aliphatic	●	3			

The reported binding energies for each component were found and related to the deconvoluted peaks in the high-resolution scan. For 'β-shifted', C-S and aliphatic, the BE values were all within the region of the peak assigned for aliphatic, so the intensity of this was taken to represent 3 different environments and was found to be 66 %. It should be remembered that adventitious carbon can contribute to the intensity of the aliphatic carbon and when considering this, there is a good agreement with theoretical values. The intensity calculated from the COOH peak is slightly lower than the theoretical composition. However, this is probably due to the increased aliphatic carbon intensity. Overall, XPS analysis supports the conclusion that MMA_2-3MPA was successfully attached to P40 microspheres.

4.3.5 Extrusion of tubes

To determine the performance of the bespoke second-generation dispersants, summarised in section 4.3.2.5 (Table 4-12), composite devices were fabricated. Extrusion of hollow tubes containing dispersant coated P40 microspheres was carried out as described previously in Chapter 2. The loading of P40 was 1, 3 or 5 wt% so that comparisons can be drawn against tubes fabricated in Chapter 3 and imaged using US.

4.3.6 Imaging of composites

It was previously found the addition of commercially available dispersant did not reduce the US response emitted as a result of P40. However, as dispersion of P40 was not optimal, imaging artefacts appeared as a result of tube defects. The second-generation dispersants should promote a more uniform distribution of contrast agents and reduce agglomeration. These dispersants are more complex than DDSD used

previously, so it is important to determine that they also do not dampen the intensity of the US signal emitted by P40. Due to time constraints and equipment availability, ultrasound imaging has not yet been performed on the second-generation dispersant devices described in this chapter. However, this action is a priority for future work and US and SEM images obtained will be analysed in a similar way to the first prototype devices containing DDSD as a dispersant. Dispersion of contrast agents will be assessed and the visibility of the device *via* ultrasound will be determined.

4.4 Conclusions

The design and synthesis of bespoke dispersants for echogenic contrast agents has been carried out. Thiols containing carboxylic acid moieties were utilised as CTAs for the polymerisation of methacrylate and acrylate monomers. These thiols (3MPA and MSA) performed well under conditions described and reactions produced end-functionalised oligomers with narrow dispersity values in high yields. These oligomers were all successfully attached to P40 microparticles, which was confirmed by a biphasic suspension test and XPS in a specific case. Oligomer dispersant coated P40 were fabricated into PU tubes *via* extrusion for comparison with previous composites made in Chapter 3. The second-generation dispersants were tailored to be more compatible with the matrix polymer than commercially available dispersants trialled initially and hence promote better dispersion throughout extruded tubes. This should reduce tube inconsistencies and imaging artefacts and hence improve US images obtained. Unfortunately, US imaging was not performed on these samples due to time constraints.

4.5 References

1. Matyjaszewski, K. & Davis, T. P. *Handbook of radical polymerization*. (Wiley-Interscience, 2002).
2. O'brien, J. L. & Gornick, F. *Chain Transfer in Polymerization of Methyl Methacrylate Chain Transfer in the Polymerization of Methyl Methacrylate. I. Transfer with Monomer and Thiols. The Mechanism of the Termination Reaction at 6001*. **20**, (1955).
3. Hoyle, C. E. & Bowman, C. N. Thiol-ene click chemistry. *Angew. Chem. Int. Ed. Engl.* **49**, 1540–73 (2010).
4. Kolb, H. C., Finn, M. G. & Sharpless, K. B. Click Chemistry: Diverse Chemical Function from a Few Good Reactions. *Angew. Chem. Int. Ed. Engl.* **40**, 2004–2021 (2001).
5. Mather, B. D., Viswanathan, K., Miller, K. M. & Long, T. E. Michael addition reactions in macromolecular design for emerging technologies. *Prog. Polym. Sci.* **31**, 487–531 (2006).
6. Lowe, A. B. Thiol–ene "click" reactions and recent applications in polymer and materials synthesis: a first update. *Polym. Chem.* **5**, 4820 (2014).
7. Marie Pearson, A. & Xiao Sun, J. *Pigmented inks with polymeric dispersants*. **138**, (1995).
8. Zerby, W. & Miller, S. W. *OLIGOMERIC HYDROPHOBIC DISPERSANTS AND LAUNDRY DETERGENT COMPOSITIONS COMPRISING OLIGOMERiC DISPERSANTS*. **753**, (2002).
9. Leister, N. A., Valley, H., Piccolini, R. J. & Assignee, P. *United States Patent PROCESSES OF PREPARING OLIGOMERS*.
10. Adlington, K. *et al.* Application of Targeted Molecular and Material Property

Optimization to Bacterial Attachment-Resistant (Meth)acrylate Polymers. *Biomacromolecules* **17**, 2830–2838 (2016).

Chapter 5 - An investigation into the use of iron-α-diimine complexes as catalytic chain transfer agents and alternative routes to functional materials

5.1 Aims and objectives

The initial objective of this section of research was to make progress towards finding alternatives to cobalt based catalysts for catalytic chain transfer polymerisation (CCTP). This is due to the benchmark catalyst's inherent toxicity and thus the potential limitations that this would have on the commercialisation of the production of materials for medical applications. A strategy was adopted to investigate potential catalysts with iron centres, as complexes containing this metal centre are generally regarded to be more acceptable in the fabrication of medical devices.

5.2 Introduction

Polymerisations can proceed in an uncontrolled manner, leading to potentially dangerous reaction conditions and undesirable, high molecular weight and polydisperse products.[1,2] This phenomena is known as the Trommsdorff-Norrish effect and can be prevented in a number of ways such as: using a polymerisation solvent, terminating the reaction at low conversion or keeping the molecular weight of the polymers low.[3,4] The addition of chain transfer agents (CTA), such as thiols is an industrially applicable method of promoting the control of free radical polymerisations by keeping molecular weight low.[5] However, difficulties can arise when attempting to synthesise very low molecular weight or oligomeric products, which are one of the key molecular targets of this study. This is difficult, in the case of industrial non-catalytic CTAs, due to the stoichiometric quantities of chain transfer agent required.[6] One of

the key attractions of CCTP is to overcome this barrier by reducing the required levels of control agent to as low as parts per million (ppm).

5.2.1 Catalytic chain transfer polymerisation

In 1975, Smirnov and Marchenko reported a method of controlling the polymerisation of methyl methacrylate (MMA) by adding catalytic quantities of cobalt-based complexes.[6] A significant reduction in molecular weight was observed in polymerisations containing cobalt-porphyrins, without compromising the conversion of monomer to polymer or the dispersity of the final product. This technique was termed CCTP and has since become a commercially exploited technique used for controlling polymerisations on an industrial scale.[7–9] One of the most notable advantages of CCTP over traditional chain transfer techniques is the low concentration of catalyst required to obtain very low molecular weight polymers. Additionally, the accepted mechanistic cycle for the technique produces polymers terminated with a carbon-carbon (C=C) double bond as opposed to a chain transfer agent moiety. The latter mechanistic feature means that: no additional heteroatoms are added to the structure as a result of the chain transfer reaction, which is of particular interest in biological or medical applications; and the oligomers/polymers can be involved in either secondary polymerisation or post-functionalisation processes to make more complex structures such as comb-graft polymers or end-functional materials.

The structure of the first viable cobalt-porphyrin catalyst used in the polymerisation of MMA is shown in Figure 5-1.

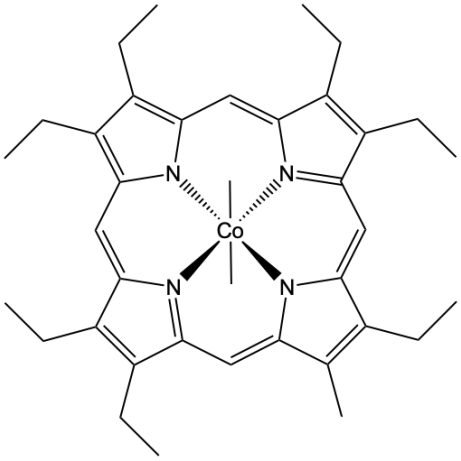


Figure 5-1. Structure of cobalt-porphyrin CCTP catalyst. Axial ligands are not shown in structures as there are a variety of groups available that form active catalysts.

While exhibiting high activity as chain transfer agents, and despite the natural occurrence of porphyrin derivatives, cobalt-porphyrins were considered expensive, largely attributed to the fact that the synthesis of these structures is problematic. The use of cobalt-porphyrins also typically gave rise to highly coloured polymerisation solution and as a result, final polymers. For these reasons, alternatives to the first generation of cobalt-based catalyst were quickly investigated. Cobalt-phthalocyanines are similar complexes which would have been expected to behave in a similar way due to the molecular similarities (Figure 5-2), but these were found to be very poor in the presence of certain solvents or monomers.

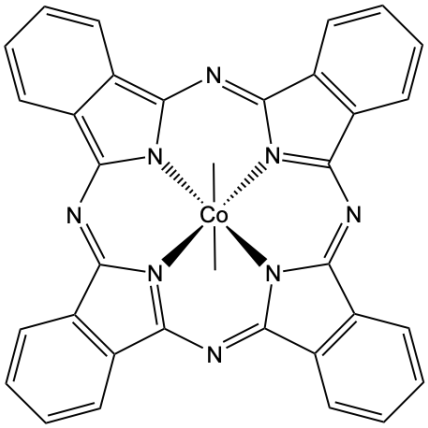


Figure 5-2. Structure of cobalt-phthalocyanine.

This observation was attributed to catalytic inhibition of radical polymerisation (CIRP). It was found to be related to the catalysts' low solubility in most organic solvents which required the polymerisations to be conducted in aprotic solvents such as dimethylformamide (DMF).[10] As a result of this, it was suggested that in this case a competing reaction to CCT takes place. Typically, hydride transfer occurs exclusively between propagating polymer and cobalt species. However in the case of cobalt-phthalocyanine, the radicals produced do not initiate monomers, but preferentially react with the Co(III) species, preventing polymerisation occurring.

One successful strategy applied to control agent design was to develop organometallic derivative structures based on the corrin ring centre of co-vitamin B-12, which was known to be a key species which mediates free radical processes in the body.[11] This strategy gave rise to the cobaloxime type CCT agents such as shown in Figure 5-3.

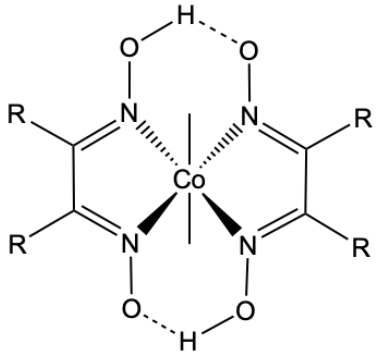


Figure 5-3. General structure of cobaloxime CCT agent.[12]

Cobaloxime catalysts are, to date, considered the most efficient group of CCTP catalysts. Dependent on the ligand system, they can have a chain transfer constant (C_s) value of up to 100,000.[13,14] Gridnev proposed the following requirements for an efficient CCT catalyst:[15]

- Cobalt (II) centre
- Surrounded by multidentate or chelating ligand system which contains conjugated π-electrons
- Two or more nitrogen atoms coordinated to cobalt in the macrocyclic ligand(s).

Typically, the complexes are low spin and have octahedral geometry. Chain transfer activity is higher if the macrocyclic ring is closed, for example by bridging hydrogen bonds between oxime ligands as shown in Figure 5-3. A readily accessible and reversible redox change of ±1 is also required.[6]

In 1984, two groups of researchers reported the use of cobalt (II) dimethylglyoxime ($[Co(dmg)_2]$) as an efficient CCT catalyst.[10,12] Commercialisation of CCTP was pioneered by DuPont, who facilitated research into CCT agents. It was found that

complexes containing BF_2 bridges, formed from the reaction of $[Co(dmg)_2]$ with BF_3OEt_2, in which the bidentate ligands are converted to a tetradentate ligand, were excellent catalysts. The catalyst, bis[(difluroboryl) diphenylglyoximato] cobalt(II), (Figure 5-4) subsequently referred to as PhCoBF was developed as it was shown the phenyl groups had a favourable stabilising effect on the complex without compromising catalytic activity.

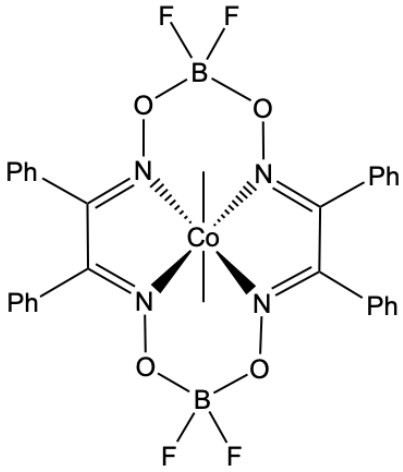


Figure 5-4. Structure of bis[(difluoroboryl) diphenylglyoximato] cobalt (II) (PhCoBF).

The proposed and most generally accepted mechanistic cycle of PhCoBF mediated CCTP of MMA is shown in Figure 5-5.[6]

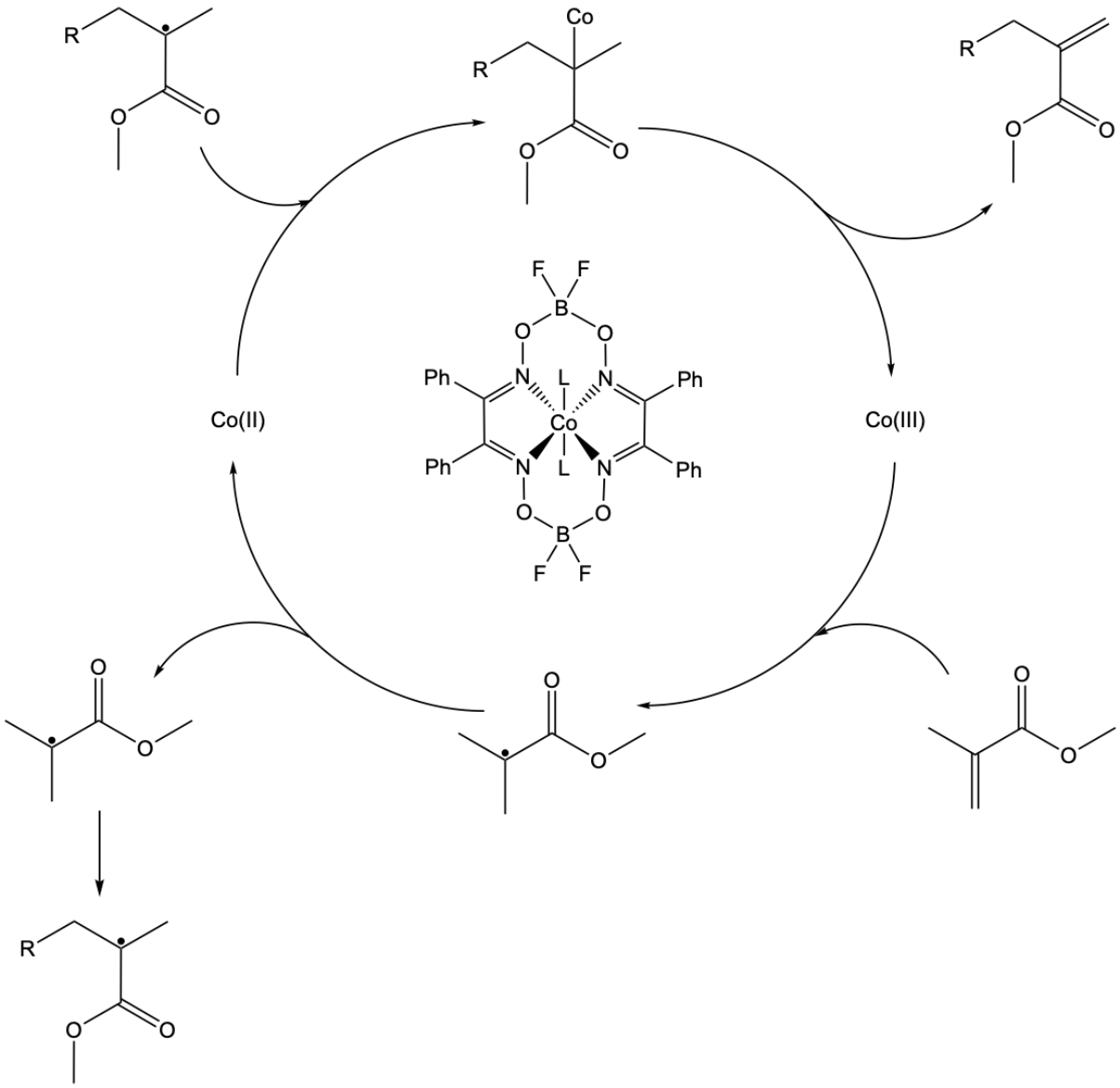


Figure 5-5. Mechanism of CCTP cycle of MMA mediated by PhCoBF.

In CCTP, initiation of monomer and propagation proceeds as in uncatalysed free radical polymerisation (FRP, Chapter 1). The mechanism shows the action of the Co(II) complex, which reversibly binds with a propagating polymer to form a polymer-cobalt adduct. Hydride abstraction occurs from the α-methyl group of the polymer to the Co(II) complex, which results in a polymer terminated with a vinyl group and Co(III)-H complex being formed. The β-hydride transfer is the rate limiting step of the polymerisation cycle.[16] Subsequently, the catalyst is reformed to complete the

mechanistic cycle, when the Co-H bond dissociates, and in addition produces a hydride (H^-) which can be used to initiate a monomer or terminate a polymer. The cycle proceeds until there is an absence of reactive radicals in the reaction mixture. As previously stated, due to the nature of this mechanism, the polymer product contains no fragment of the chain transfer agent and theoretically all catalyst can be recovered. Additionally, the terminal vinyl group produced as a result of CCTP allows a facile route for post-functionalisation of the polymer/oligomer. This is achieved by techniques such as thiol-ene click chemistry (Chapter 4).[17]

It is widely accepted that CCTP is not an effective polymerisation control technique for monomers which do not have an α-methyl group next to the polymerisable double bond.[18] These are vinyl monomers such as acrylates and acetates. This is partially due to the stability of the C-Co bond formed by propagating acrylate species and the catalyst.[19,20] This results in a reduction in the amount of catalyst in the system that can be used for chain transfer reactions and therefore molecular weight obtained from the polymerisation can be too high for intended application. Furthermore, it has been reported that polymerisation occurs after an induction period, as a result of the reversible inhibition of catalyst.[21] For this reason, acrylate polymerisations that utilize CCTP conditions can be uncontrolled and subject to thermal runaway if not carefully monitored to ensure the system safely overcomes this initial induction period. Early studies did show that the polymerisation of methyl acrylate could be carried out in the presence of a cobalt-porphyrin but this followed a living radical polymerisation mechanism rather than CCTP.[18]

Figure 5-6 shows the proposed molecular structures of terminated polymers synthesised from CCTP of vinyl (acrylate) and vinylene (methacrylate) monomers respectively.

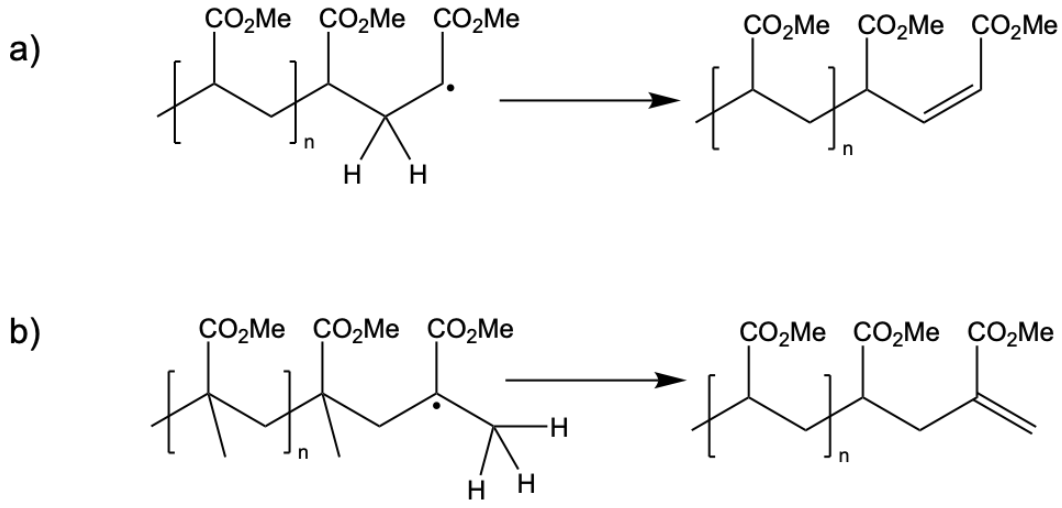


Figure 5-6. Proposed termination schemes of a) methyl acrylate and b) methyl methacrylate.[22]

In scheme a), the position of the abstractable hydrides is indicated, next to the secondary carbon radical. Hydride abstraction from a secondary carbon is harder than from a primary carbon, so other reactions are more favoured. For vinylene monomers, hydride abstraction occurs from a primary carbon (CH_3) to a tertiary radical centre, which is much more favourable and hence CCTP is typically more efficient with these monomers.

5.2.2 Alternatives to cobalt catalysts for CCTP

Whilst the advantages of CCTP are undeniable in terms of extending the potential range of polymer structures that are available *via* a commercially viable route, there are some undesirable aspects. These mainly originate from the toxicity and

sustainability issues related to the use of cobalt. Whilst only very small quantities (concentrations of ppm) of cobalt are used, which do not remain attached to the polymers molecular structure, there are concerns that there may be traces of the catalyst remaining in the polymer even after purification. This is a particularly pertinent concern in medical or food applications, due to the toxicity of cobalt and its complexes. The other consequence of residual catalyst is discolouration of the polymer, which would not be suitable for certain applications such as optical. Theoretically, any transition metal complex with an easily accessible ±1 redox change could be a suitable catalyst for CCTP.[6] However, there has not been extensive investigation into alternatives to cobalt based control agents as early studies reported low or no activity with Fe, Ni, V, Sn, Cu, Zn, Mg, Od, Pt and Mn complexes.[10,23,24] Chromium complexes do show some activity as CCT agents but their C_s values are orders of magnitude lower in comparison to cobalt and have had little research carried out as a result of this, in addition to the greater toxicological concerns over this metal centre.[25]

The desire to develop a catalyst based on abundant and toxicologically friendly metal is not limited to CCTP and has led to studies into the applicability of iron complexes.[26] With particular relevance to this study, an investigation into what were predicted to suitable ATRP chain transfer agents uncovered CCTP-type behaviour exhibited by certain four-coordinate iron complexes.[27] These complexes were pseudotetrahedral, Fe(II) centred complexes with α-diimine ligands. The study reported an investigation into the polymerisation of MMA in the presence of four different iron catalysts and characteristic properties of CCTP were observed with catalysts containing aryl substituted ligands rather than alkyl substituted. CCTP was accepted as the mechanism for two of these complexes, as halide analysis of the polymers confirmed the absence of halide functionality and instead a terminal vinyl group. Initially, these

complexes were used in the polymerisation of styrene as suggested ATRP agents. However, Gibson et al provided an explanation of their poor performance and attributed it to an outer sphere electron transfer (OSET) mechanism.[28] After further studies with MMA, they could conclude a CCTP mechanism was occurring under specific reaction conditions.[29]

5.2.3 Fundamentals of microwaves

The use of microwave heating (MWH) as an alternative to conventional heating (CH) methods has been widely explored and the effects debated over the years.[3031] CH methods such as the use of oil baths, heating mantles and heating jackets are arguably the most widely employed techniques of controlling reaction temperature. However, these can be energy and time intensive and for these reasons, the use of MWH has increased. Additionally, CH methods rely on heat transfer *via* convection currents generated as a result of heating the outside of the reaction vessel. In contrast to that, MWH reactions are heated much more efficiently and evenly, dependent on the reactants. This is because reaction vessels for MWH are typically not microwave sensitive, i.e. the reactions are not heated from the outside of the vessel. Instead, microwaves can couple with certain reactants and heat is generated by the movement of these microwave sensitive materials, which is then dissipated throughout the solution. A diagrammatic representation of the heat dissipation in CH and MWH reactions is shown in Figure 5-7.

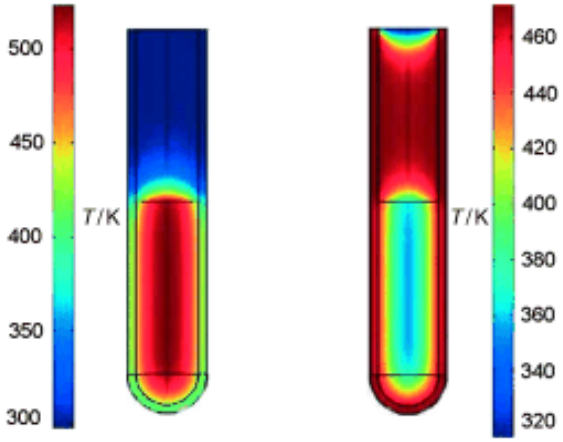


Figure 5-7. Comparison of heat dissipation between CH (RHS) and MWH (LHS).[32]

The use of MWH as an industrially applicable technique for large scale processing was in first reported in the 1960s, where it was implemented in the tyre industry for the vulcanisation of rubber.[33] Since then, the use of MWH has expanded to include control of organic chemical reactions, curing of resins and sintering of ceramics.[34–37] Many people claim the effect of MWH is a non-thermal, specific effect and boasted higher yields and improved reaction rate when employing this heating technique.[38] However, this was disputed by many including Strauss who reported in 2002 that the reason for apparent differences in MWH and CH reactions were purely due to thermal effects.[39] This was supported by Kappe et al who showed, with strict temperature controls, MWH had no effect on the rate of reactions and suggested differences were because of poor temperature control.[32] Despite this claim, many continue to use MWH because the strict temperature controls used in Kappe's study are not feasible to apply to all reactions. Additionally, the benefits of MWH are appealing; reduction in reaction time can be achieved, as well as the ability to increase reaction rates and hence obtain slightly different products. Due to these reasons, it can be thought to be more sustainable than CH methods.

5.2.3.1 The electromagnetic spectrum

Microwaves can be thought to consist of an electric field and a magnetic field, which travel as perpendicular sinusoidal waves. They have wavelengths of between 1 mm and 1 m, with corresponding frequencies of 0.3 – 300 GHz.[40] They are located between radio and infrared waves on the electromagnetic spectrum (Figure 5-8).

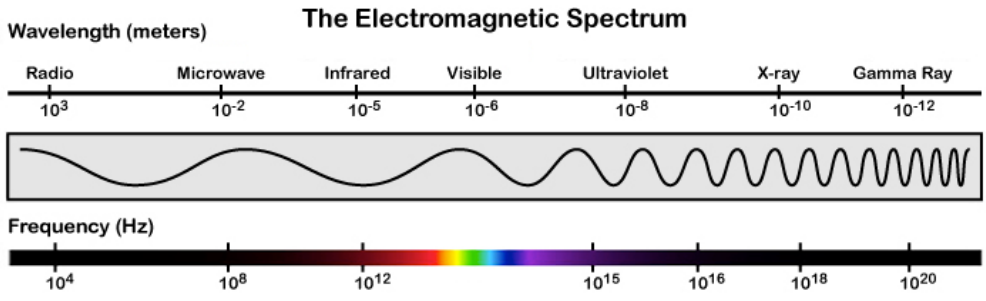


Figure 5-8. The electromagnetic spectrum.

General uses of microwaves are for radar, telecommunication and navigation purposes. There are particular frequencies which are defined for industrial, scientific and medical (ISM) purposes, which are dependent on geographical location.[41] ISM frequencies are identified so as not to cause interference with the general applications of microwaves. The most commonly used ISM frequency for microwave reactors is 2.45 GHz, which is a worldwide allowed frequency.

Microwaves are a non-ionising form of radiation, i.e. their energy (0.0016 eV) is not sufficient enough to initiate chemical reactions *via* bond cleavage. However certain molecules are more susceptible to MWH and this is due to their dielectric properties resulting from their structure.

5.2.3.2 Microwave heating mechanisms

There are thought to be two methods in which microwaves selectively heat molecules: dipolar polarisation and ionic conduction. A representation of these mechanisms is shown in Figure 5-9.

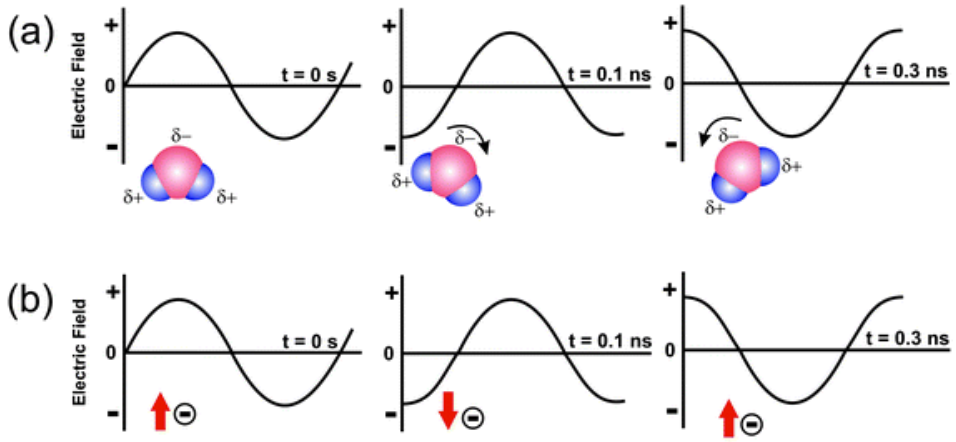


Figure 5-9. Mechanisms of microwave heating methods: a) dipolar polarisation and b) ionic conduction.

Dipolar polarisation relies on the molecule to be heated having a dipole moment, which is defined as partial opposite charges on neighbouring atoms, denoted by δ+ and δ-. Microwaves travel as sinusoidal waves; they have positive and negative phases. Molecules with partial charges are attracted to and repelled by these waves and move mainly by rotation to align with the changing phases. Rotation of the molecules results in collisions with other molecules in the medium, which in turn generates energy in the form of heat resulting from the conversion of kinetic energy. The frequency of the wave is evidently an important factor when considering the rotational velocity of molecules. A low frequency wave allows for more molecules to become aligned with the wave, hence less collisions occur and the resulting energy imparted to the system is low. Conversely, a high frequency wave can have the same effect because any rotation

will effectively be cancelled out because the phase changes too quickly for molecules to align. However, as previously mentioned, there are only certain frequencies that can be used for microwave reactors.

Ionic conduction requires molecules to have a formal charge, which move to align with the microwave phases as shown in Figure 5-9 (b). Similarly to dipolar polarisation, collisions between molecules cause energy to be dissipated in the form of heat.

5.2.3.3 Dielectric properties

As previously stated, the way in which reactions are heated using microwaves relies on materials having a permanent or induced dipole. Interaction of microwaves with certain molecules causes bulk heating of the reaction medium. The dielectric properties of a material can provide information about how susceptible to MWH it is.

$$tan\delta = \frac{\varepsilon''}{\varepsilon'}$$

Where tanδ is the loss factor (the ability of a material to convert electromagnetic energy into heat at a specific frequency and temperature), ε" is the dielectric loss (determines the material's efficiency at converting electromagnetic radiation into heat energy) and ε' is the dielectric constant (represents the polarisability of the material). Typically, if the value of tanδ is above 0.1, the material is said to be microwave absorbing. If tanδ is less than 0.1 then the material is considered microwave transparent.[32]

The other important parameters when considering the use of MWH is the penetration depth of the wave and the relaxation time of the molecule. The relaxation time can be

defined as the period of time a molecule requires to rotate back to its original conformation after it has been exposed to microwave radiation. If the relaxation time is short, then MWH will not be effective because the molecule will not generate heat energy as it can perfectly align with the microwave before the phase of the wave changes. Additionally, if the relaxation time is too long then the molecule will not have time to return to its original conformation before the phase of the wave changes again and thus MWH will not be effective. Theoretically, the frequency of the wave could be altered to allow for different relaxation times, however this is restricted by the allowed frequencies of microwave reactors.

5.3 Results and discussion

5.3.1 PhCoBF mediated polymerisations

The chosen monomer for this study was MMA due to the extensive body of literature available on the controlled polymerisation of this key monomer *via* CCTP. This monomer is commercially exploited in many different applications. Furthermore, it is a good model for other methacrylate monomers which may be used in the future research. Initial reactions were conducted to determine the efficiency of the benchmark catalyst, PhCoBF. This would allow the efficiency of some relatively unexplored iron-based chain transfer agents to be compared to put their effectiveness into context. Additionally, control reactions were carried out in the absence of any chain transfer agent to define the relative scale of the molecular weight reductions achieved with both types of catalyst. The data from these experiments is summarised in Table 5-1.

Table 5-1. Comparison of reduction in molecular weight obtained in PhCoBF mediated polymerisations of MMA.

Entry	PhCoBF (ppm)	Conversion (%) [a]	M_n (g mol^{-1}) [b]	Đ [b]
1	600	57	1000	1.51
2	6000	26	800	2.57
3	0	86	52000	1.76

Reaction conditions – MMA (10 mL), toluene (10 mL), AIBN (1 wt% wrt MMA), 80 °C, 3 hours.

[a] determined by ^{1}H NMR, [b] determined by GPC

PhCoBF is known to be an excellent CTA for the polymerisation of MMA, with reported chain transfer constants of up to 10,000.[42] The results obtained in the conditions described support this, with oligomers obtained in both cases (Table 5-1, entries 1 & 2). However, conversion was low, with the reaction containing 6000 ppm producing just 26 % conversion of monomer to polymer. This is a common side effect of using too much CTA and is referred to as catalytic inhibition. The high concentrations were chosen so that these reactions could be compared with subsequent iron mediated polymerisations. In contrast, the control reaction carried out without the addition of any CTA reached much higher conversion, 86 %. In uncontrolled reactions, where the Trommsdorff-Norrish effect occurs, viscosity increases dramatically due to the high molecular weight of polymer produced. The consequence of this is a reduction in the rate of termination reactions, which are diffusion controlled.

5.3.2 Iron mediated polymerisations

The next set of reactions use four coordinate iron α-diimine complexes like those described in section 5.2.2. Previous work has investigated the use of metal-chloride

and metal-bromide catalyst precursors so in this case, iron (II) chloride and iron (II) bromide were the centres of the complexes (Figure 5-10).[28] The two ligands chosen were because Gibson et al reported the effect of aryl substituents as promoting CCTP.

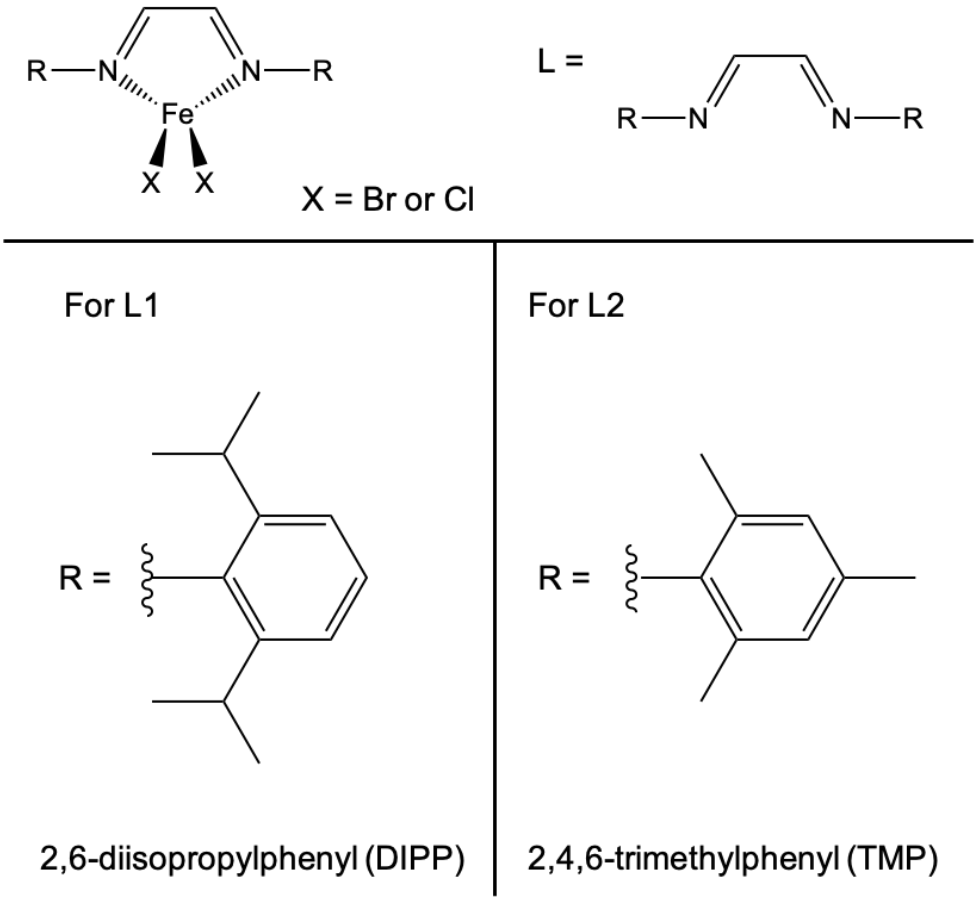


Figure 5-10. Structures of FeX_2L.

The above complexes were synthesised and isolated as described in Chapter 2. They were used in the polymerisation of MMA in the same conditions as the PhCoBF mediated reactions above (Table 5-1). The properties of the polymers obtained from these polymerisations is shown in Table 5-2.

Table 5-2. Iron-mediated polymerisation of MMA.

Entry	CTA	Conversion (%) [a]	Mn (g mol^{-1}) [b]	Đ [b]
1	$FeCl_2L1$	88	40000	1.51
2	$FeCl_2L2$	88	37000	1.65
3	$FeBr_2L1$	94	28000	1.70
4	$FeBr_2L2$	86	35000	1.64

Reaction conditions – MMA (10 mL), toluene (10 mL), CTA (600 ppm), AIBN (1 wt% wrt MMA), 80 °C, 3 hours.

[a] determined by ^{1}H NMR, [b] determined by GPC

As is evident from the molecular weight data obtained for the iron mediated polymerisations, the iron complexes are not as efficient as PhCoBF. However, a reduction in M_n is observed when comparing these reactions to the control polymerisation where PMMA of 52000 g mol^{-1} was obtained. Additionally, the dispersity values all indicate these polymerisations were controlled, with values ranging from 1.51 to 1.70, which is around the lowest that would be expected from CCTP. Conversion from monomer to polymer was relatively high in all reactions indicating little inhibition occurred.

The conditions described here were chosen because they are regularly used for CCTP. They differ from the conditions described by Gibson et al, who were initially investigating ATRP. Their study used ethyl-2-bromoisobutyrate which is typically used as an ATRP initiator. In our case, AIBN was used as the radical initiator for ease of comparison with prior PhCoBF mediated CCTP reactions. The volume of solvent added to the polymerisation was equivalent to the volume of monomer. This was to

maintain a low viscosity and prevent the Trommsdorff-Norrish effect in case the control of the reaction was poor. The original study reported the products to be PMMA of up to 3600 g mol $^{-1}$ with dispersity values of less than 1.60. Whilst we did not observe such a drastic reduction of molecular weight using conditions described, dispersity values were comparable, and conversion reached was consistently higher in shorter reaction times. Since the radical initiator was not a halide containing compound, halide analysis was not carried out on the products as we were not expecting to observe ATRP behaviour. However, examining the terminal group of the polymer was problematic due to the high molecular weight of polymer obtained. The product was not suitable for MALDI-TOF spectrometry and ^{1}H NMR is not accurate enough in this case.

5.3.3 Effect of catalyst generation method

After initial reactions using the four iron complexes showed that employing conditions suitable for the benchmark catalyst (PhCoBF) did not produce particularly low molecular weight polymers, further investigation was carried out into the catalyst generation method. It has been previously shown that transition metal catalysts can be generated *in situ*; i.e. the precursors (FeX_2 and α-diimine ligand) are added as reagents to the polymerisation reaction solution. For one *in situ* method, the complex is allowed to generate during a 'pre-stir' (ps) period where the reaction is stirred at room temperature for 1 hour before the polymerisation commences.[43] The other generation method has no pre-stir (nps) time allocated and polymerisation is started immediately after the starting materials are combined and degassed. For comparison, the final methodology used a pre-synthesised and isolated form of the complex as was

the case in section 5.3.2. During the *in situ* reactions, a colour change is observed which is assumed to be the catalyst forming.

As previously discussed, efficiency of chain transfer can be assessed by comparing the molecular weight and dispersity of the product and conversion of monomer to polymer to an uncontrolled free radical polymerisation of MMA. Subsequent reactions will also be compared to PhCoBF mediated and control (no CTA) reactions to investigate the efficiency of the iron complexes. The first comparison of the effect of catalyst generation method was determined using $FeCl_2L2$ and results are shown in Table 5-3.

Table 5-3. Effect of catalyst generation method on polymerisation of MMA with $FeCl_2L2$ as CTA.

Entry	Method	Conversion (%) [a]	M_n (g mol^{-1}) [b]	Đ [b]
1	Isolated	88	37000	1.65
2	*In situ* (pre-stir)	87	32000	1.62
3	*In situ* (no pre-stir)	91	22000	1.51

Reaction conditions – MMA (10 mL), toluene (10 mL), CTA (600 ppm), AIBN (1 wt% wrt MMA), 80 °C, 3 hours.

[a] determined by ^{1}H NMR, [b] determined by GPC

The highest molecular weight of PMMA obtained was 37000 g mol^{-1} (Table 5-3, entry 1). This is a lower molecular weight product than that obtained from the control reaction, so it was suggested that the iron complex is having an effect on the polymerisation since all other conditions are constant. On the other hand, in comparison to the analogous PhCoBF mediated reactions where oligomers of 1000 g

mol^{-1} were obtained, it is obvious that $FeCl_2L2$ is not as active as a chain transfer agent.

The generation method appeared to have an effect on the molecular weight of the polymer obtained in the above reactions. Both *in situ* methods produced lower molecular weight polymer than the isolated method, with 32000 and 22000 g mol^{-1} for pre-stir and no pre-stir reactions respectively. Dispersity was slightly lower in the no pre-stir reaction, with a value of 1.51 indicating a high level of control of the reaction. This is a value verging on the lowest of what would be expected from CCTP. However, when comparing the activity of the iron complexes to that of the benchmark cobalt complexes, it is noted that the molecular weights observed are much higher. Conversion ranged very slightly, between 87 and 91 %, although this is not particularly significant.

A suggestion as to why the three different generation methods produce polymer of such varied molecular weight could be attributed to the air sensitivity of the catalyst. Atmospheric oxygen or moisture can affect the oxidation state of the metal complex. The isolated catalyst was not stored in an inert atmosphere after it was synthesised, which allows time for potential or partial decomposition of the catalyst. If this decomposition occurred in a short time scale, this hypothesis could also explain the difference observed between the two *in situ* methods. Catalyst deactivation could occur due to reaction with residual air in the reaction vessel during the 60-minute pre-stir, which would mean the *in situ* (no pre-stir) methodology could be the most effective.

A similar trend to that above was observed when $FeCl_2L1$ was used in the polymerisation of MMA (Table 5-4).

Table 5-4. Effect of catalyst generation method on polymerisation of MMA with $FeCl_2L1$ as CTA.

Entry	Method	Conversion (%) [a]	M_n (g mol^{-1}) [b]	Đ [b]
1	Isolated	88	40000	1.51
2	*In situ* (pre-stir)	91	29000	1.66
3	*In situ* (no pre-stir)	93	27000	1.63

Reaction conditions – MMA (10 mL), toluene (10 mL), CTA (600 ppm), AIBN (1 wt% wrt MMA), 80 °C, 3 hours.

[a] determined by ^{1}H NMR, [b] determined by GPC

The highest molecular weight obtained was as a result of the isolated catalyst generation method (entry 1,Table 5-4). This supports the previous results observed and also provides more evidence that the isolated catalyst is the worst performing. Although not quite so pronounced as the previous trend, both *in situ* methodologies were shown to provide better control of the system, with the no pre-stir reaction producing slightly lower molecular weight polymer (27000 g mol^{-1}, entry 3,Table 5-4).

Bromide containing complexes were also investigated in this study. In the same method as described above, initially $FeBr_2L1$ was used as an isolated complex or generated *in situ* in the polymerisations of MMA (Table 5-5).

Table 5-5. Effect of catalyst generation method on polymerisation of MMA with $FeBr_2L1$ as CTA.

Entry	CTA (ppm)	Method	Conversion (%) [a]	M_n (g mol^{-1}) [b]	Đ [b]

1	600	Isolated	94	28000	1.70
2	6000	Isolated	74	22000	1.49
3	600	*In situ* (pre-stir)	92	26000	1.66
4	6000	*In situ* (pre-stir)	51	20000	1.26
5	600	*In situ* (no pre-stir)	91	27000	1.66
6	6000	*In situ* (no pre-stir)	53	26000	1.25

Reaction conditions – MMA (10 mL), toluene (10 mL), AIBN (1 wt% wrt MMA), 80 °C, 3 hours.

[a] determined by ^{1}H NMR, [b] determined by GPC

Comparable molecular weight data to that of reactions with the chloride containing complex was obtained, with M_n ranging between 20000 – 28000 g mol^{-1}. All polymers obtained had a relatively tight dispersity, particularly those from the reactions using a high concentration of chain transfer agent (Table 5-5, entries 2, 4, & 6). A dispersity value of 1.25 is lower than what would be expected of a polymerisation following a CCTP mechanism. The highest dispersity, 1.7, is very acceptable. It should be noted that when comparing these reactions with the PhCoBF mediated, a much higher molecular weight is obtained but dispersity is not compromised by this or a low conversion. In this case, the generation method has less of a pronounced effect than the $FeCl_2L$ but is still evident when comparing isolated and *in situ* methodologies. The reaction containing the isolated chain transfer agent (600 ppm) yielded a polymer of 28000 g mol $^{-1}$, which is not significantly higher than product obtained from either of the *in situ* reactions which were 27000 and 26000 g mol $^{-1}$ (Table 5-5, entries 1, 3 & 5). A slightly more pronounced trend emerged when considered the reactions containing a higher concentration of chain transfer agent, but this observation was not the same as that of the chloride containing complexes (iso > *in situ* ps > *in situ* nps wrt

product M_n). Instead, the method that produced the lowest molecular weight polymer was *in situ* with 1 hr pre-stir. PMMA of 20000 g mol $^{-1}$, with a dispersity of 1.26 was obtained *via* this method.

Unlike the previous group of reactions, using the higher loading of $FeBr_2L$ had a detrimental effect on the conversion, with values of approx. 50 % obtained. This suggests some form of radical inhibition may have occurred. Overall, this set of data provides some insight into the efficiency of $FeBr_2L2$ but trends were not as defined as previously observed.

The following group of reactions were carried out to determine the efficiency of $FeBr_2L2$ as a chain transfer agent and are summarised in Table 5-6.

Table 5-6. Polymerisation of MMA with $FeBr_2L2$ as CTA.

Entry	Catalyst (ppm)	Method	Conversion (%) [a]	M_n (g mol^{-1}) [b]	Đ [b]
1	600	Isolated	86	35000	1.64
2	6000	Isolated	62	20000	1.39
3	600	*In situ* (pre-stir)	78	32000	1.54
4	6000	*In situ* (pre-stir)	53	19000	1.71
5	600	*In situ* (no pre-stir)	91	23000	1.58
6	6000	*In situ* (no pre-stir)	88	27000	1.58

Reaction conditions – MMA (10 mL), toluene (10 mL), AIBN (1 wt% wrt MMA), 80 °C, 3 hours.

[a] determined by ^{1}H NMR, [b] determined by GPC

The trends observed for this set of data are similar to those previously discussed. A reduction in molecular weight is observed when comparing different catalyst loadings, with the higher concentration reactions yielding a lower molecular weight polymer. However, this is not the case for the in situ (nps) method (Table 5-6, entries 5 & 6). Notably, conversion for entry 6 is comparable to entry 5, indicating perhaps the concentration of $FeBr_2L1$ in the reaction was lower than intended and hence could be an anomaly.

Although typically, slightly lower molecular weight polymers were obtained using bromide containing complexes, the chloride containing complexes performed better in terms of conversion. Further investigation is needed into the stability of the complexes as this provide an explanation as to why there are different trends and some unreliable results observed.

5.3.4 The effect of MWH on MMA polymerisations

The next group of reactions were carried out to determine if the application of microwave heating would have an effect on the iron-mediated MMA polymerisations. In order to make direct comparisons, the reactions were performed in the same way, with the only difference being the method of heating utilised. It was hypothesised that the paramagnetic iron complex may have a favourable interaction with the microwave radiation. This could increase its catalytic/CTA activity. Data reported earlier in this chapter is recreated in Table 5-7 to compare the effect of the application of MWH.

Table 5-7. Effect of heating method on polymerisation of MMA with $FeBr_2$ based CTAs.

Entry	CTA (ppm)	Ligand	Method	Conversion (%)[a]	M_n (g mol^{-1})[b]	Đ[b]
1	600	L1	CH	59	27000	1.66
2	600	L1	MWH	93	51000	1.72
3	6000	L1	CH	53	26000	1.25
4	6000	L1	MWH	84	42000	1.60
5	600	L2	CH	91	23000	1.58
6	600	L2	MWH	94	46000	1.73
7	6000	L2	CH	88	27000	1.58
8	6000	L2	MWH	92	48000	1.67

Reaction conditions – MMA (10 mL), toluene (10 mL), AIBN (1 wt% wrt MMA), 80 °C, 3 hours, catalyst generated *in situ* (no pre-stir).

[a] determined by ^{1}H NMR, [b] determined by GPC

The products obtained from MWH reactions were significantly different in terms of molecular weight in comparison to the analogous CH reactions. A two-fold increase in molecular weight was observed when MWH was applied. The dispersity remains low, indicating no loss of control as a consequence. This suggests the catalyst is active and the increase in molecular weight observed is not due to thermal runaway or the Trommsdorff-Norrish effect. The increase in molecular weight could be attributed to an increase in the rate of propagation during polymerisation.

5.3.5 Iron-mediated polymerisation of methyl acrylate

Due to the aforementioned reasons, CCTP is not generally a suitable method of controlling acrylate polymerisations. However, the efficiency of the iron based complexes for methacrylates was not as high as what would be expected from a suitable CCT agent suggesting an alternative mechanism was occurring. Methyl acrylate was polymerised in the presence of the $FeBr_2L$ with interesting results observed. In the presence of PhCoBF, the polymerisation of MA in conditions described is subject to the Trommsdorff-Norrish effect after less than 25 minutes. The products from these reactions were not isolated but the crude mixture had a high molecular weight and a broad dispersity. Due to the reactivity of MA, a control reaction in the absence of any catalyst was not carried out.

Table 5-8. Effect of CTA generation method and concentration on polymerisation of MA with $FeBr_2L1$ as CTA.

Entry	CTA (ppm)	Method	Conversion (%)[a]	M_n (g mol^{-1})[b]	Đ[b]
1	600	Isolated	91	17000	2.37
2	6000	Isolated	30	26000	1.61
3	600	*In situ* (pre-stir)	74	17000	3.00
4	6000	*In situ* (pre-stir)	No peak	No peak	-
5	600	*In situ* (no pre-stir)	93	14000	2.52
6	6000	*In situ* (no pre-stir)	No peak	No peak	-

Reaction conditions – MA (10 mL), toluene (10 mL), AIBN (1 wt% wrt MA), 80 °C, 3 hours,

[a] determined by ^{1}H NMR, [b] determined by GPC

Entries 4 and 6 in Table 5-8 show that when 6000 ppm of iron complex was added to the polymerisation using the *in situ* methodology, the polymerisation was inhibited. No peak owing to the presence of polymer was observed in the ^{1}H NMR spectra so conversion could not be obtained, suggesting little or no polymerisation occured. The GPC trace also did not contain a polymer peak. Catalyst inhibition is a process in which free radicals are consumed by the catalyst instead of taking part in the polymerisation reaction resulting in little or no product, this appears to have happened. In the case above when 6000 ppm of the isolated complex was used, some inhibition was evident from the low conversion of 30 % obtained.

At lower concentration of catalyst (600 ppm), polymerisation of MA occurred and products were obtained and analysed. Conversion of these reactions was high at around 90 %. However, the dispersity values of the polymers do not indicate efficient control of the reaction. The dispersity values ranged from 2.37 – 3.00, much higher than would be expected from a reaction using CCTP conditions. The molecular weights of the products were between 14000 – 17000 g mol^{-1} but this is not likely to be a completely genuine representation due to the broad dispersity values observed.

If the iron complexes were behaving as CCT agents, the control over the polymerisation of MA would be low. Despite a potential lack of control indicated by the dispersity values, the molecular weight data suggests that the polymerisation is not proceeding as a FRP would. A much higher molecular weight polymer product would be expected as was the case in the PhCoBF mediated reactions. Additionally, the inhibition of reaction at higher catalyst loadings suggests that the iron complexes are having an effect as a completely uncontrolled reaction would still yield polymer. The Trommsdorff-Norrish effect was not observed for any of the iron mediated

polymerisations of MA. The iron complexes' activity with methyl acrylate further supports the idea that these CTAs are not promoting CCTP behaviour under the conditions employed, and rather favour an alternative mechanism.

5.3.6 Iron mediated hyperbranched polymer synthesis

Due to the rapid nature of the polymerisation of multifunctional monomers, controlling this type of reaction is important. The following group of reactions was carried out in order to find the efficiency of iron based complexes as chain transfer agents for the polymerisation of divinyl benzene (DVB). As a comparison, PhCoBF was also used as a catalytic chain transfer agent.

Since the polymerisation of difunctional monomers can progress to produce a cross-linked 3D network, an important property and an estimate of efficiency of CTAs is to prolong the gel point of the reaction. The gel point is defined as the time in the polymerisation where stirring ceases due to a rapid increase in viscosity, which can be accompanied by the appearance of bubbles in the solution. The appearance of the gel formed varies depending on factors such as the amount of solvent and volume of reaction mixture. The determination of the gel point is by visual inspection, and can be confirmed by attempting to dissolve the reaction solution in organic solvent (DCM, chloroform, THF). An increase in temperature, or exotherm, is often observed.

Table 5-9. Gel point determination.

Entry	CTA	Reaction time (mins)	M_n (g mol^{-1})[a]	Đ[a]
1	-	7 (gel point)	-	-

2	$FeBr_2L1$	44 (gel point)	-	-
3	$FeBr_2L1$	39	52000	3.66

Reaction conditions – DVB (10 mL), diphenyl ether (10 mL), CTA (600 ppm), 150 ^oC.

[a] determined by GPC

The gel point was determined to be 7 minutes for the self-initiated reaction at 150 ^oC (Table 5-9). The polymer produced could not be spectroscopically analysed, confirming the formation of a cross linked network. The inclusion of the isolated complex $FeBr_2L1$ resulted in a longer more controlled reaction, with a prolonged gel point of 44 minutes. The subsequent reaction was terminated at 39 minutes in order to obtain solvent soluble hyperbranched polymer. GPC analysis of the product showed a dispersity of 3.66 with a molecular weight of 53000 g mol^{-1}. The GPC trace was multimodal, which is characteristic of hyperbranched polymers, as the random nature of branching leads to a large distribution in molecular weight.

Following initial success using the isolated iron complex, the next reactions were carried out to determine whether using the CTA generated in situ was viable.

During the 1 hour pre-stir, the colour of the solution changed indicating the generation of the iron complex. The reaction reached its gel point after 68 minutes. The following reaction was terminated at 63 minutes to obtain polymer that could be spectroscopically analysed.

In preliminary studies, $FeBr_2L1$ has proved to be an efficient chain transfer agent for the polymerisation of DVB. Reaction time was prolonged by up to 1 hour in comparison

to the uncontrolled reaction. The polymer products obtained in these cases were in expected, acceptable yields and displayed the characteristic broad dispersity of a branched structure. It was shown again that the *in situ* generation method seemed to provide more control over the polymerisation, with longer reaction time observed.

5.4 Conclusions

In this chapter, the performance of iron-based complexes as catalytic chain transfer agents was investigated. In comparison to the benchmark catalyst PhCoBF, which can successfully be used to synthesise oligomers, their performance was poor. The range of molecular weights of PMMA obtained in the conditions described was from 22000 to 40000 g mol^{-1}. Additionally, the presence of double bond end groups could not be confirmed and an alternative mechanism may be occurring. The FeX_2L complexes cannot be described as catalytic chain transfer agents in this case. However, control was observed, indicated by the narrow dispersity values obtained for most of the reactions. Methacrylate polymerisation always occurred in the presence of the iron CTAs and typically in high conversion. It was soon realised this process using conventional heating methods was not suitable for synthesising oligomeric dispersants for the echogenic composite project but despite this, investigations into the effect of the use of MWH and the generation method of CTA was carried out. A significant increase in the molecular weight was observed, while dispersity remained narrow and conversion remained high. This increase in molecular weight is attributed to an increase in the rate of propagation during MWH reactions, which is an effect noted previously. It was found that an *in situ* methodology was a suitable way of forming these complexes during the reaction, removing a synthetic step in the process. The *in*

situ generated CTAs performed better than the isolated equivalents, which is attributed to the air sensitivity of the complexes. This is further supported by the two *in situ* methods, where complexes which were left to generate during a pre-stir did not provide as much control as those which were used in the reaction immediately.

An unexpected but interesting result was the control over methyl acrylate polymerisations. Although, this further backs up that we are not promoting CCTP in our reaction conditions. Despite dispersity being quite broad (above 2) in the iron mediated reactions, a decrease in molecular weight was observed when compared to PhCoBF mediated reactions where the Trommsdorff-Norrish effect occurred.

Overall, despite not achieving the initial objective of this section, we have shown that four-coordinate iron(II)-α-diimine complexes do exhibit activity as CTAs. A full investigation into these complexes, perhaps including conditions from Gibson et al's studies may provide a more comprehensive explanation of their behaviour.

5.5 Future work

Ideally, the mechanism in which the iron complexes control polymerisations should be determined. The chain transfer constants (C_s) were not obtained in this study, but it would be interesting to compare their activity to other commonly used CTAs such as thiols. Additionally, expanding the library of monomers in this study would provide information about the potential mechanism. The complexes' promising results with acrylate monomers could mean they are potentially suited for a wide class of reactive monomers.

We briefly investigated the performance of FeX_2L as CTAs for the synthesis of hyperbranched polymers, which would be an interesting route to investigate as promising initial results were obtained. They were comparable to PhCoBF mediated reactions, but were not pursued as the monomer was unsuitable for the intended potential applications.

Also very briefly investigated were the differences between analogous monomers which differed only in their absence or presence of an α-methyl group, such as vinyl acetate and isopropenyl acetate, styrene and α-methyl-styrene and so on. Understanding how these complexes provide control over such similar reactions could indicate what mechanism is occurring.

5.6 References

1. Carraher, C. E. & Jr. *Introduction to Polymer Chemistry,*. (Taylor & Francis, 2006).
2. Alger, M. S. M. *Polymer Science Dictionary*. (Springer Science & Business Media, 1997).
3. *IUPAC. Compendium of Chemical Terminology (the 'Gold Book')*. (Blackwell Scientific Publications, Oxford).
4. Mayo, F. R. Chain Transfer in the Polymerization of Styrene: The Reaction of Solvents with Free Radicals 1. *J. Am. Chem. Soc.* **65**, 2324–2329 (1943).
5. Matyjaszewski, K. & Davis, T. P. *Handbook of radical polymerization*. (Wiley-Interscience, 2002).
6. Gridnev, A. A. & Ittel, S. D. Catalytic Chain Transfer in Free-Radical

Polymerizations. *Chem. Rev.* **101**, 3611–3660 (2001).

7. Janowicz, A. H. & Inventor, D. *Bimetallic catalytic chain transfer agents for molecular weight control in free radical polymerization*. (1986).
8. Janowicz, A. H., Du, E. I. & Burcyzk, A. F. *Application Data 63 Continuation*. *Indian Journal of Chemistry* **367**, (1985).
9. *Star polymers made from macromonomers made by cobalt chain transfer process*. (1993).
10. Karmilova, L. V, Ponomarev, G. V, Smirnov, B. R. & Bel 'govskii, I. M. Metalloporphyrins as Catalysts of Chain Transfer in Radical Polymerisation and Stereoselective Oxidation. *Uspekhi Khimii Russ. Chem. Rev.* **53095**, (1984).
11. Pratt, J. M. Inorganic chemistry of vitamin B12. *Inorg. Chem. Vitam. B12.* (1972).
12. Burczyk, A. F., O'Driscoll, K. F. & Rempel, G. L. Cobaloxime as a catalytic chain transfer agent. *J. Polym. Sci. Polym. Chem. Ed.* **22**, 3255–3262 (1984).
13. Forster, D. J., Heuts, J. P. A. & Davis, T. P. Conventional and catalytic chain transfer in the free-radical polymerization of 2-phenoxyethyl methacrylate. *Polymer (Guildf).* **41**, 1385–1390 (2000).
14. Heuts, J. P. A., Davis, T. P. & Russell, G. T. Comparison of the Mayo and Chain Length Distribution Procedures for the Measurement of Chain Transfer Constants. *Macromolecules* **32**, 6019–6030 (1999).
15. Gridnev, A. A., Lampeka, Y. D., Smirnov, B. R. & Yatsimirskii, K. B. Structural features of macrocyclic cobalt complexes ?catalysts of chain transfer to a monomer in radical polymerization. *Theor. Exp. Chem.* **23**, 293–297 (1987).
16. Gridnev, A. A., Ittel, S. D., Wayland, B. B. & Fryd, M. Isotopic Investigation of Hydrogen Transfer Related to Cobalt-Catalyzed Free-Radical Chain Transfer. *Organometallics* **15**, 5116–5126 (1996).

17. Lowe, A. B. Thiol–ene “click” reactions and recent applications in polymer and materials synthesis: a first update. *Polym. Chem.* **5**, 4820 (2014).

18. Wayland, B. B., Poszmik, G., Mukerjee, S. L. & Fryd, M. Living Radical Polymerization of Acrylates by Organocobalt Porphyrin Complexes. *J. Am. Chem. Soc.* **116**, 7943–7944 (1994).

19. Woska, D. C. *et al.* Determination of organo-cobalt bond dissociation energetics and thermodynamic properties of organic radicals through equilibrium studies. *J. Am. Chem. Soc.* **118**, 9102–9109 (1996).

20. David C. Woska, † *et al.* Determination of Organo−Cobalt Bond Dissociation Energetics and Thermodynamic Properties of Organic Radicals through Equilibrium Studies. (1996). doi:10.1021/JA960002C

21. Evan Roberts, G., Heuts, J. P. A. & Davis, T. P. Direct observation of cobalt-carbon bond formation in thé catalytic chain transfer polymerization of methyl acrylate using matrix-assisted laser desorption lonization time-of-flight mass spectrometry. *Macromolecules* **33**, 7765–7768 (2000).

22. Chiefari, J. *et al.* Chain transfer to polymer: a convenient route to macromonomers. *Macromolecules* **32**, 7700–7702 (1999).

23. Abramo, G. P. & Norton, J. R. Catalysis by C5Ph5Cr(CO)3· of chain transfer during the free radical polymerization of methyl methacrylate. *Macromolecules* **33**, 2790–2792 (2000).

24. Enikolopyan, N. S., Smirnov, B. R., Ponomarev, G. V. & Belgovskii, I. M. Catalyzed chain transfer to monomer in free radical polymerization. *J. Polym. Sci. Polym. Chem. Ed.* **19**, 879–889 (1981).

25. David C. Woska, Yaping Ni, and & Wayland*, B. B. Thermodynamic and Activation Parameters for Dissociation of [CpCr(CO)3]2 and [Cp*Cr(CO)3]2 into

Paramagnetic Monomers from 1H NMR Shift and Line Width Measurements. (1999). doi:10.1021/IC990342+

26. *The Biological Chemistry of Iron*. (Springer Netherlands, 1982). doi:10.1007/978-94-009-7882-9

27. Gibson, V. C., O'Reilly, R. K., Wass, D. F., White, A. J. P. & Williams, D. J. Polymerization of Methyl Methacrylate Using Four-Coordinate (α-Diimine)iron Catalysts: Atom Transfer Radical Polymerization vs Catalytic Chain Transfer. *Macromolecules* **36**, 2591–2593 (2003).

28. Gibson, V. C. *et al.* Four-coordinate iron complexes bearing ??-diimine ligands: efficient catalysts for Atom Transfer Radical Polymerisation (ATRP). *Chem. Commun.* 1850–1851 (2002). doi:10.1039/b204510a

29. Shaver, M. P., Allan, L. E. N., Rzepa, H. S. & Gibson, V. C. Correlation of metal spin state with catalytic reactivity: polymerizations mediated by alpha-diimine-iron complexes. *Angew. Chem. Int. Ed. Engl.* **45**, 1241–4 (2006).

30. Hoogenboom, R., Leenen, M. A. M., Wiesbrock, F. & Schubert, U. S. Microwave Accelerated Polymerization of 2-Phenyl-2-oxazoline: Microwave or Temperature Effects? *Macromol. Rapid Commun.* **26**, 1773–1778 (2005).

31. Sinnwell, S. & Ritter, H. Microwave Accelerated Polymerization of 2-Phenyl-2-oxazoline. *Macromol. Rapid Commun.* **26**, 160–163 (2005).

32. Kappe, C. O. Controlled microwave heating in modern organic synthesis. *Angew. Chem. Int. Ed. Engl.* **43**, 6250–84 (2004).

33. Lidström, P., Tierney, J., Wathey, B. & Westman, J. Microwave assisted organic synthesis—a review. *Tetrahedron* **57**, 9225–9283 (2001).

34. Marand, E., Baker, K. R. & Graybeal, J. D. Comparison of reaction mechanisms of epoxy resins undergoing thermal and microwave cure from in situ

measurements of microwave dielectric properties and infrared spectroscopy. *Macromolecules* **25**, 2243–2252 (1992).

35. Caddick, S. Microwave assisted organic reactions. *Tetrahedron* **51**, 10403–10432 (1995).

36. Giguere, R. J., Bray, T. L., Duncan, S. M. & Majetich, G. Application of commercial microwave ovens to organic synthesis. *Tetrahedron Lett.* **27**, 4945–4948 (1986).

37. Agrawal, D. K. Microwave processing of ceramics. *Curr. Opin. Solid State Mater. Sci.* **3**, 480–485 (1998).

38. Lewis, D. A., Summers, J. D., Ward, T. C. & McGrath, J. E. Accelerated imidization reactions using microwave radiation. *J. Polym. Sci. Part A Polym. Chem.* **30**, 1647–1653 (1992).

39. Strauss, C. R. Microwave-Assisted Reactions in Organic Synthesis—Are There Any Nonthermal Microwave Effects? Response to the Highlight by N. Kuhnert. *Angew. Chemie* **114**, 3741–3743 (2002).

40. Wiesbrock, F. & Schubert, U. S. *Microwaves in chemistry: the success story goes on*. *chimica oggi • Chemistry Today* • **24**,

41. Thostenson, E. T. & Chou, T.-W. Microwave processing: fundamentals and applications. *Compos. Part A Appl. Sci. Manuf.* **30**, 1055–1071 (1999).

42. Heuts, J. P. A. *et al.* Reversible Cobalt-Carbon Bond Formation in Catalytic Chain Transfer Polymerization. (1999). doi:10.1021/ma981707x

43. Adlington, K., Green, A., Wang, W., Howdle, S. M. & Irvine, D. J. Direct ‘in situ’, low VOC, high yielding, CO2 expanded phase catalytic chain transfer polymerisation: towards scale-up. *Dalton Trans.* **42**, 127–36 (2013).

Chapter 6 - Conclusions and future work

A summary of conclusions from the research projects in this thesis is presented here.

6.1 Chapter 3 – the design and synthesis of novel composite for the improved monitoring of medical devices

The design and fabrication of an US visible, prototype medical device has been reported. A suitable method for applying a dispersant coating, comprised of a commercially available material, to contrast agents was developed. In addition, a quick and simple test to confirm the attachment of commercially available dispersant was devised. The biphasic suspension test showed whether coating had been successful, then XPS was used to further confirm this.

Prototype medical devices containing echogenic contrast agents were fabricated *via* extrusion. TGA was explored as a method for determining dispersion of P40 microparticles throughout extruded tube samples but was not successful. The sensitivity of this technique was not good enough to differentiate between samples. Extruded tubes were imaged using SEM and US and compared to control devices. The SEM images showed the presence of defects in the matrix polymer and the microparticles that can arise during processing. For the US images, it was observed that the devices containing contrast agents were able to be visualised more clearly than the control devices. However, we still noticed imaging artefacts that were attributed to sub-optimal dispersion of contrast agent. It was concluded that addition of dispersant did not reduce ultrasound response significantly as tubes containing both uncoated and coated P40 both produced images with characteristic signals. The commercially available dispersant (DDSA) chosen was suitable for initial studies but to optimise the device to obtain better quality ultrasound images, it was decided to

design bespoke dispersants that would have enhanced compatibility with the polymer matrix. The design and synthesis of these dispersants is discussed in Chapter 4.

6.2 Chapter 4 – the design and synthesis of dispersants for ultrasound visible medical devices

The design and synthesis of bespoke dispersants for echogenic contrast agents has been carried out and reported in Chapter 4. Thiols containing carboxylic acid moieties were utilised as CTAs for the polymerisation of methacrylate and acrylate monomers. These thiols (3MPA and MSA) performed well under conditions described and reactions produced end-functionalised oligomers with narrow dispersity values in high yields. These oligomers were all successfully attached to P40 microparticles, which was confirmed by a biphasic suspension test and XPS in a specific case. Oligomer dispersant coated P40 were fabricated into PU tubes *via* extrusion for comparison with previous composites made in Chapter 3. The second-generation dispersants were tailored to be more compatible with the matrix polymer than commercially available dispersants trialled initially and hence promote better dispersion throughout extruded tubes. This should reduce tube inconsistencies and imaging artefacts and hence improve US images obtained. Unfortunately, US imaging was not performed on these samples due to time constraints.

6.2.1 Future work

Based on results obtained and presented in Chapters 3 & 4, the recommendations for future work are based on optimising dispersion of contrast agent throughout extruded

tube. The US images of second-generation dispersant devices need to be analysed in comparison with the first prototype devices described in Chapter 3.

6.3 Chapter 5 – an investigation into the use of iron-α-diimine complexes as catalytic chain transfer agents and alternative routes to functional materials

In this chapter, the performance of iron-based complexes as catalytic chain transfer agents was investigated. In comparison to the benchmark catalyst PhCoBF, which can successfully be used to synthesise oligomers, their performance was poor. The range of molecular weights of PMMA obtained in the conditions described was from 22000 to 40000 g mol^{-1}. Additionally, the presence of double bond end groups could not be confirmed and an alternative mechanism may be occurring. The FeX_2L complexes cannot be described as catalytic chain transfer agents in this case. However, control was observed, indicated by the narrow dispersity values obtained for most of the reactions. Methacrylate polymerisation always occurred in the presence of the iron CTAs and typically in high conversion. It was soon realised this process using conventional heating methods was not suitable for synthesising oligomeric dispersants for the echogenic composite project but despite this, investigations into the effect of the use of MWH and the generation method of CTA was carried out. A significant increase in the molecular weight was observed, while dispersity remained narrow and conversion remained high. This increase in molecular weight is attributed to an increase in the rate of propagation during MWH reactions, which is an effect noted previously. It was found that an *in situ* methodology was a suitable way of forming

these complexes during the reaction, removing a synthetic step in the process. The *in situ* generated CTAs performed better than the isolated equivalents, which is attributed to the air sensitivity of the complexes. This is further supported by the two *in situ* methods, where complexes which were left to generate during a pre-stir did not provide as much control as those which were used in the reaction immediately.

An unexpected but interesting result was the control over methyl acrylate polymerisations. Although, this further backs up that we are not promoting CCTP in our reaction conditions. Despite dispersity being quite broad (above 2) in the iron mediated reactions, a decrease in molecular weight was observed when compared to PhCoBF mediated reactions where the Trommsdorff-Norrish effect occurred.

Overall, despite not achieving the initial objective of this section, we have shown that four-coordinate iron(II)-α-diimine complexes do exhibit activity as CTAs. A full investigation into these complexes, perhaps including conditions from Gibson et al's studies may provide a more comprehensive explanation of their behaviour.

6.3.1 Future work

To fully understand the mechanism of the iron-based catalysts would be useful, this would allow for optimisation of the polymerisation reaction, perhaps to form oligomers. The advantages of iron over the typically used cobalt are mainly based on its biocompatibility, which is especially relevant in the production of medical devices. Additionally, it would be interesting to complete the initial study on using these complexes as CTAs for hyperbranched polymerisations.